

UNCLASSIFIED

AD 414885

DEFENSE DOCUMENTATION CENTER

FOR

SCIENTIFIC AND TECHNICAL INFORMATION

CAMERON STATION, ALEXANDRIA, VIRGINIA



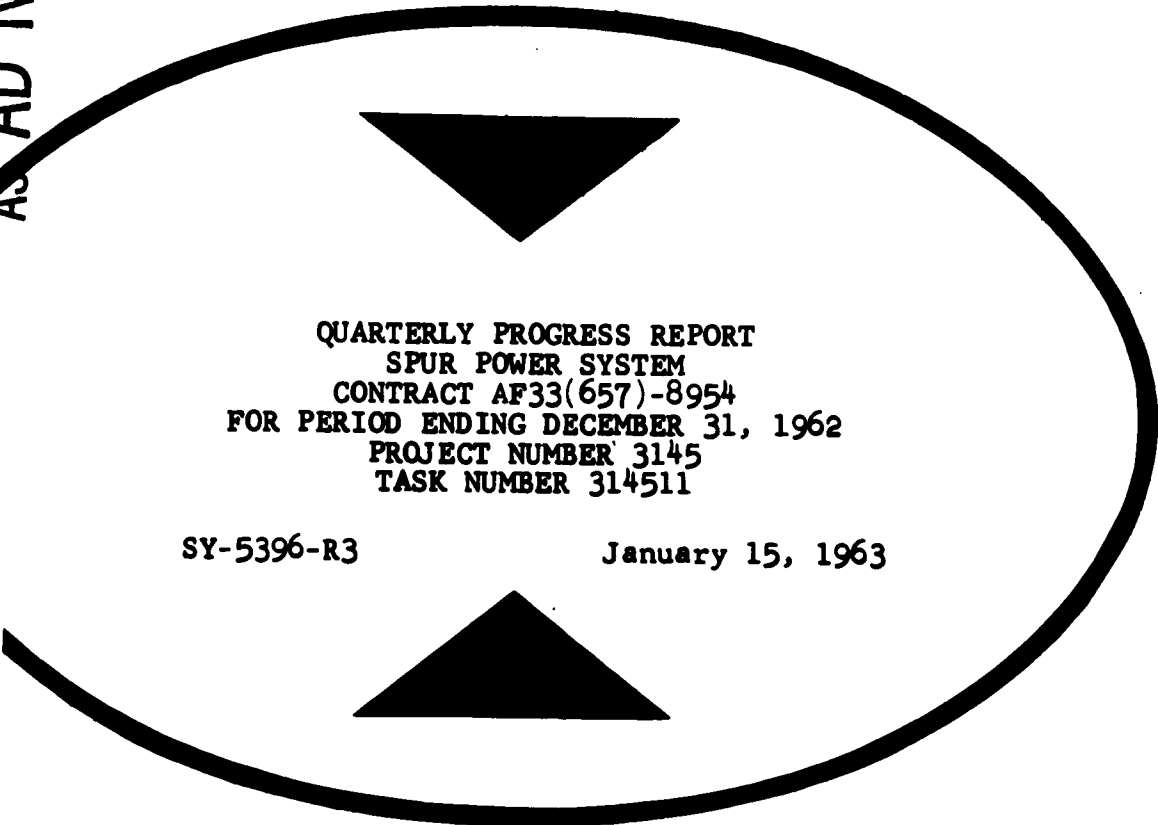
UNCLASSIFIED

NOTICE: When government or other drawings, specifications or other data are used for any purpose other than in connection with a definitely related government procurement operation, the U. S. Government thereby incurs no responsibility, nor any obligation whatsoever; and the fact that the Government may have formulated, furnished, or in any way supplied the said drawings, specifications, or other data is not to be regarded by implication or otherwise as in any manner licensing the holder or any other person or corporation, or conveying any rights or permission to manufacture, use or sell any patented invention that may in any way be related thereto.

12-4-62

CATALOGED BY DDC
AS AD NO. 414885

414885



QUARTERLY PROGRESS REPORT
SPUR POWER SYSTEM
CONTRACT AF33(657)-8954
FOR PERIOD ENDING DECEMBER 31, 1962
PROJECT NUMBER 3145
TASK NUMBER 314511

SY-5396-R3

January 15, 1963

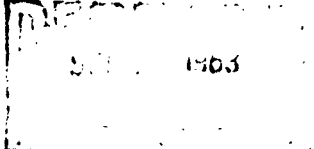


THE BARRETT CORPORATION

AiResearch Manufacturing Division

Phoenix, Arizona

DDC



QUARTERLY PROGRESS REPORT
SPUR POWER SYSTEM
CONTRACT #F33(c57)-8954
FOR PERIOD ENDING DECEMBER 31, 1962
PROJECT NUMBER 3145
TASK NUMBER 314511

SY-5396-R3

January 15, 1963

Prepared by F. B. Wallace

Initial Issue
Approved by

W. N. Blatt
W. N. Blatt, Supvr Pwr Turb Group

R. D. Gruntz
R. D. Gruntz, Supvr SPUR Conv Loop

J. H. Dannan
J. H. Dannan, SPUR Proj Engr

L. D. Six
L. D. Six, Chief, Advanced
Power Generation

REPORT NO. SY-5396-R3

TOTAL PAGES 190

NOTICE

To expedite dissemination of technical information this report is being made available prior to approval or review by ASD. Consequently this report does not necessarily represent the views of ASD or the USAF. Comments and/or suggestions regarding the information contained in this report are welcomed. Comments and/or suggestions should be directed to ASD (WWRMFP-1), Wright-Patterson Air Force Base, Ohio.

ATTACHMENTS:

REV	BY	APPROVED	DATE	PAGES AND/OR PARAGRAPHS AFFECTED



ABSTRACT

This report, submitted by the AiResearch Manufacturing Company of Arizona, Phoenix, Arizona, a division of The Garrett Corporation, describes work accomplished in the period from October 1, 1962 to December 31, 1962, under Phase II of the SPUR Program, in accordance with United States Air Force Contract AF33(657)-8954.

The Phase II contract provides for continued analytical and experimental studies in support of the Space Power Unit, Reactor (SPUR) Program. Progress is reported for a total of 32 tasks.

In addition to a discussion of the work accomplished by AiResearch, the prime contractor, this report contains a discussion of the work accomplished by Aerojet-General Nucleonics (reactor system), Westinghouse Electric Corporation, (electrical generator), and Battelle Memorial Institute (material support). The program progress on each of these tasks is discussed in Section II.



TABLE OF CONTENTS

	Page
ABSTRACT	i
TABLE OF CONTENTS	ii
LIST OF FIGURES	iv
I INTRODUCTION	1
II TECHNICAL DISCUSSION	4
A. Materials Testing	5
1. Creep-Rupture Properties of Mo + 1/2 w/o Ti	5
2. Fatigue Evaluation of Mo + 1/2 w/o Ti	13
3. Cantilever Bending Fatigue of Cb + 1 w/o Zr	15
4. Creep-Rupture of SAE 4340 Steel in 1000°F Potassium Vapor	19
5. Mass-Transfer Tests with Two-Phase Flow	22
6. Liquid-Potassium Mass-Transfer Tests	32
7. Capsule Tests	36
8. Fabrication Studies	36
B. Testing Techniques	42
1. High-Temperature Heater Evaluation	42
C. Bearing Development	45
1. Bearing Tests	45
2. Bearing Analysis	48
D. Turbine Development	51
1. Turbine Test Rig Design	51
2. Turbine Material Erosion Tests	79



TABLE OF CONTENTS (Cont'd)

	Page
E. Generator Development	83
1. Generator Design	83
2. Generator Test-Rig Design	92
3. Generator Stator Seal	99
4. Generator Insulation System Development	107
5. Generator Rigid Insulation	114
6. Hyperco 27-to-Columbium Joint Development	118
7. 50-KW Liquid-Metal Model Generator	128
F. Alternate Turbogenerator	133
G. Heat-Transfer Development	135
1. Single-Tube Boiling-Potassium Tests	135
2. Vapor-Liquid Separator	137
3. Multitube Water Boiler	139
4. Flow Visualization Studies	140
5. Stainless Steel Heat Transfer Components	143
6. Stainless Steel Heat-Transfer Loop	146
H. Controls Development	155
1. Steady-State Controls Analysis	155
2. System Start-Up Analysis	156
3. Controls Experiment	158
I. Reactor Loop	159
1. Reactor Loop Pump Bearing Test and Loop Simulation	159
2. Reactor Controls	169
3. Properties of Reactor Clad and Structural Materials	175



LIST OF FIGURES

<u>Figure Number</u>	<u>Title</u>	<u>Page Number</u>
1	Mo + 1/2 w/o Ti Creep-Rupture Test	8
2	Mo + 1/2 w/o Ti Creep-Rupture Test	9
3	Mo + 1/2 w/o Ti Creep-Rupture Test	10
4	Mo + 1/2 w/o Ti Creep-Rupture Test	11
5	Mo + 1/2 w/o Ti Creep-Rupture Test	12
6	Ivy Dynamic Creep Machine	14
7	Creep Specimen	16
8	Cantilever Bending Fatigue of Cb + 1 w/o Zr	18
9	Creep-Rupture of SAE 4340 at 1000°F	20
10	"I" Tube Test Chamber	23
11	"I" Tube Test Setup	25
12	Tantalum Heater Test Setup	26
13	Tantalum Heater Test Bus Bar Junction Check	27
14	Tantalum Heater Test Assembly	29
15	Tantalum Heater Test Assembly	30
16	Tantalum Heater Test Assembly After Test	31
17	Cb + 1 w/o Zr Two-Phase Loop, Argon Purification System	33
18	Cb + 1 w/o Zr Two-Phase Loop, Argon Purification System	34
19	Cb + 1 w/o Zr Two-Phase Loop, Argon Blower Box	35
20	Brazed "I" Specimen	40
21	Bearing Test Rig	49
22	Bearing Test Rig	50
23	Turbine Blade Surface Velocity Distribution	54



LIST OF FIGURES
 (Cont'd)

<u>Figure Number</u>	<u>Title</u>	<u>Page Number</u>
24	Turbine Blade Surface Velocity Distribution	55
25	Turbine Blade Surface Velocity Distribution	56
26	Turbine Blade Surface Velocity Distribution	57
27	Turbine Blade Surface Velocity Distribution	58
28	Turbine Blade Cross Sections	59
29	Aerodynamic Turbine Layout	61
30	Turbine Disc Stress Distribution	63
31	Turbine Disc Stress Distribution	64
32	Turbine Disc Stress Distribution	65
33	Turbine Test Rig Temperature Distribution	69
34	Turbine Test Rig Critical Speeds	72
35	Erosion Test Rig	80
36	Erosion Test Rig	81
37	Erosion Test Section	82
38	Generator No Load and Load Saturation Curves	90
39	Continuous Torque Rectiflow Drive	93
40	Generator Liquid-Metal Test Loop Instrumentation	95
41	Generator Liquid-Metal Test Loop Flow Schematic	96
42	Generator Nonmetallic Coolant Test Loop Flow Schematic	97
43	Construction of Ceramic Cup Samples	101
44	Ceramic Tube for Measurement of Gas Permeation	103
45	Ceramic Tensile Specimens with Test Capsule	104
46	Partially Wound Statorette	108



LIST OF FIGURES
(Cont'd)

<u>Figure Number</u>	<u>Title</u>	<u>Page Number</u>
47	Partially Encapsulated Statorette	110
48	Partially Wound Statorette	115
49	Fully Wound Statorette	116
50	Rigid Insulation Components	117
51	Typical Braze Wetting Tests	121
52	Typical Braze Wetting Tests	122
53	Typical Braze Wetting Tests	123
54	Typical Braze Wetting Tests	124
55	Cross Section of 50-KW Generator	131
56	Outline of 50-KW Generator	132
57	Vapor-Liquid Separator Components	138
58	Freon Blow-Down Test Loop	141
59	Quartz Tube Freon Boiling Section	142
60	Physical Properties of Candidate Radiator Materials	145
61	Heat-Transfer Loop, Sodium Piping Elevation	148
62	Heat-Transfer Loop, Secondary Loop Elevation	149
63	Heat-Transfer Loop, Plan View	150
64	External Appearance After Loop Rupture	161
65	Loop Rupture - Outlet of Thermionic Converter	163
66	Journal Bearing - Post Test	164
67	Journal Bearing - As Fabricated	165
68	Upper Pump Section - Post Test	167
69	Crack in Weld Zone - Lower Housing Expansion Tank	168
70	Temperature Perturbations in Primary Loop	174
71	Furnace Tube Assembly	181



LIST OF TABLES

<u>Table Number</u>	<u>Title</u>	<u>Page Number</u>
I	Creep-Rupture Tests on Mo + 1/2 w/o Ti at 2000°F	6
II	Cantilever Bending Tests on Cb + 1 w/o Zr at 800°F	17
III	Creep-Rupture of SAE 4340 at 1000°F	21
IV	Brazed "T" Specimens After 500-Hour Test	37
V	Brazed Cb + 1 w/o Zr "T" Specimens	39
VI	Turbine Disc Stresses at 24,000 RPM	67
VII	Summary of Generator Design Data	83
VIII	Summary of Generator Construction Materials	84
IX	Brazing Alloy Wetting Tests	119
X	Strength of Brazed Columbium to Hiperco 27 Joints	126



QUARTERLY PROGRESS REPORT
SPUR POWER SYSTEM
CONTRACT AF33(657)-8954
FOR PERIOD ENDING DECEMBER 31, 1962
PROJECT NUMBER 3145
TASK NUMBER 314511

I INTRODUCTION

The Space Power Unit, Reactor (SPUR) Program was initiated by the United States Air Force, in cooperation with the Atomic Energy Commission, in May of 1960. The ultimate objective of the SPUR Program is to develop a nuclear-dynamic space power system capable of supplying 300 kilowatts or more of electrical power, with a design life of 10,000 hours.

The power system will consist of a nuclear reactor as a heat source, the mechanical means of converting thermal energy to electrical energy, a radiator for rejection of waste heat, controls, and all other necessary auxiliary equipment. The thermodynamic conversion system will be a closed-cycle dynamic system, capable of operating unattended under the specified conditions. An electromagnetic-type generator is used to produce the electric power.

A description of the SPUR system and its components is included in the SPUR Phase I Final Report, ASD Technical Report ASD TR 61-656.



The objectives of the Phase II Program are to continue portions of the study and experimental program initiated under Contracts AF33(616)-7379 and AF33(616)-8322 and to investigate several additional areas through analysis and experiment. The major technical work areas are as follows:

Materials testing, including creep-rupture and fatigue evaluation of Mo + 1/2 w/o Ti and Cb + 1 w/o Zr.

Mass-transfer tests of Cb + 1 w/o Zr with two-phase potassium flow.

Fabrication studies, including evaluation of methods for joining refractory metals in heat exchangers and in the radiator

Liquid-potassium bearing tests and analysis

Turbine performance test-rig design.

Turbine material-erosion tests.

Complete generator and generator test-rig designs.

Continued development of the generator stator seal and insulation system.



Design and fabricate a 50-kw, liquid-metal-cooled, model generator.

Boiling potassium heat-transfer tests.

Study of flow stability and heat-transfer flow processes, including development tests on a separator.

Design of stainless steel heat-transfer components and a heat-transfer test loop.

Steady-state and load-change control analysis and a start-up control analysis and simulation test.

Reactor-loop pump analysis and bearing test, and loop dynamic simulation.

Reactor-loop control analog simulation.



II TECHNICAL DISCUSSION

The following paragraphs include a discussion of the program progress through December 31, 1962.

The various tasks are designated by the paragraph number from Contract AF33(657)-8954, and are discussed on subsequent pages.

Tasks accomplished under subcontract are listed below. The remaining tasks were accomplished by AiResearch, the prime contractor.

Battelle Memorial Institute: Four of the materials development tasks, pages 5 through 21.

Westinghouse Electric Corporation: Generator Development, pages 83 through 132.

General Electric: Alternate Turbogenerator, pages 133 and 134.

Aerojet-General Nucleonics: Reactor Loop, pages 159 through 183.



A. Materials Testing, Task 2.2.2

1. Creep-Rupture Properties of Molybdenum + 1/2
w/o Titanium at 2000°F in Potassium Vapor,
Task 2.2.2.1

This task was designed to extend the creep-rupture data on stress-relieved Mo + 1/2 w/o Ti in potassium vapor up to 2000°F. Tubular specimens, with potassium vapor sealed inside, are being tested in conventional vacuum-creep apparatus. The external environment is a dynamic vacuum of $<0.5\mu$.

Table I summarizes the conditions and results of the tests run to date.

The deformation-time curves for these tests are shown in Figures 1, 2, and 3, and Figure 4 shows stress versus minimum creep rate. Figure 5 presents the 2000°C design curves. Although final conclusions may not yet be drawn from these data, several tentative observations may be made.



TABLE I
CREEP-RUPTURE TESTS ON Mo + 1/2 w/o Ti AT 2000°F

Test No.	1	2	3	4	5	6
Type of specimen	Hollow	Solid bar	Hollow	Hollow	Hollow	Hollow
Stress, psi	35,000	35,000	35,000	48,000	25,000	25,000
Internal environment	Helium	--	K vapor	K vapor	K vapor	Helium
Estimated time to rupture, hrs	100	100	100	10	700	700
Actual time to rupture, hrs	101.1	116.2	140.6	9.2	b	b
Elongation at fracture, %	11.1	12.7	15.0	16.0	b	b
Reduction of area at fracture, %	90+ ^a	88.6	90+ ^a	90+ ^a	b	b
Minimum creep rate, %/hr.	0.017	0.016	0.016	0.36	0.0011	0.0015
Specimen appearance after test	Bright	Bright	Bright	Bright	b	b

a. Cannot make precise measurements on hollow specimen fractures.

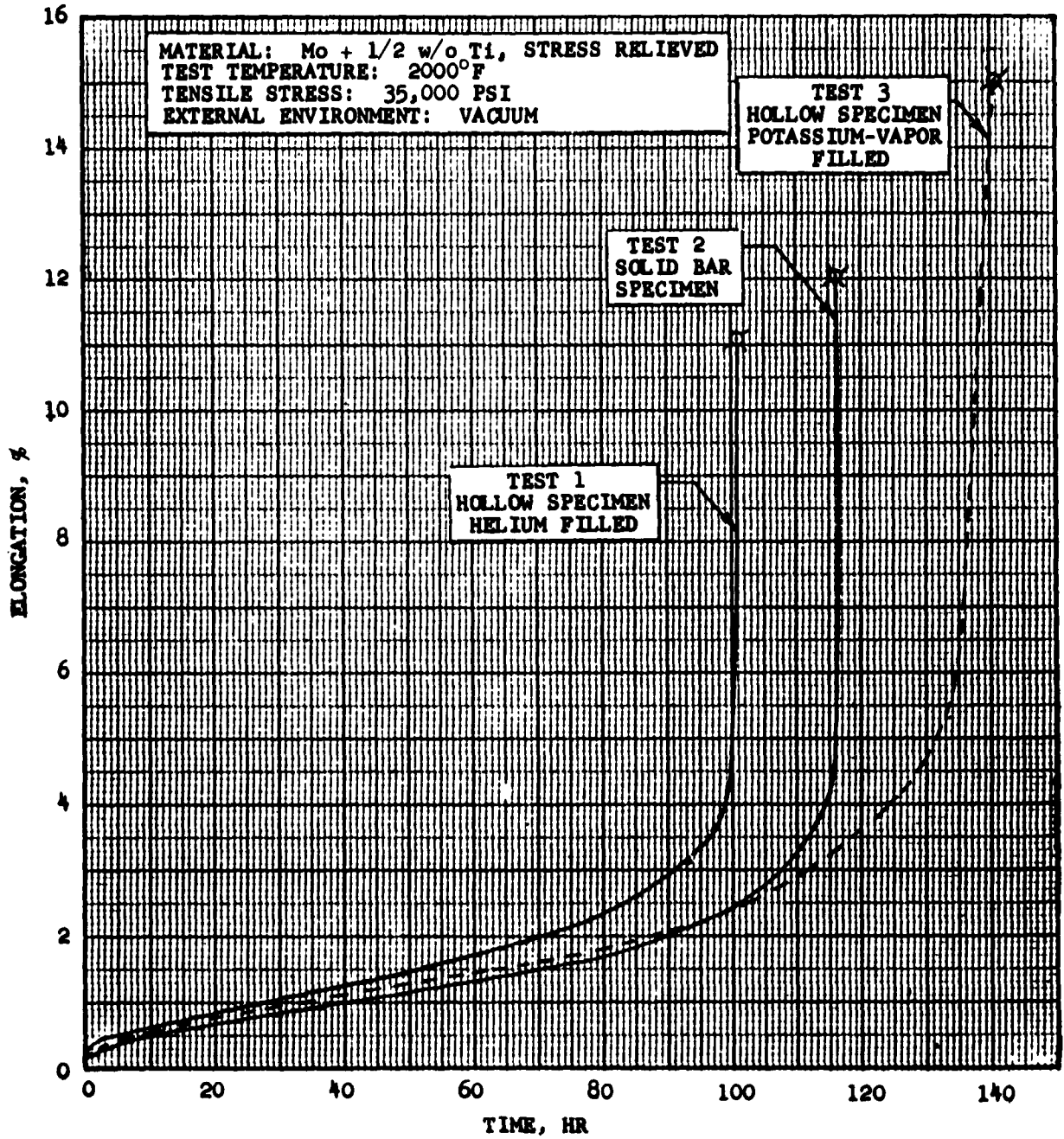
b. Test still in progress.



Considering the scatter normally encountered in creep-rupture data, the differences in rupture life among Tests 1, 2, and 3 are not deemed significant. However, as can be seen in Figure 1, the first and second stages of the creep curves are very nearly the same for all three tests. This evidence, then, suggests that (1) the hollow creep-rupture specimen gives results that are closely comparable to the solid-specimen results and (2) that exposure of the Mo + 1/2 w/o Ti to 2000°F potassium vapor has no adverse effect on its creep properties. The latter observation is substantiated by comparison of the two solid curves of Figure 3 (Test 5, with potassium vapor, and Test 6 without) wherein the agreement between the two curves is quite good.

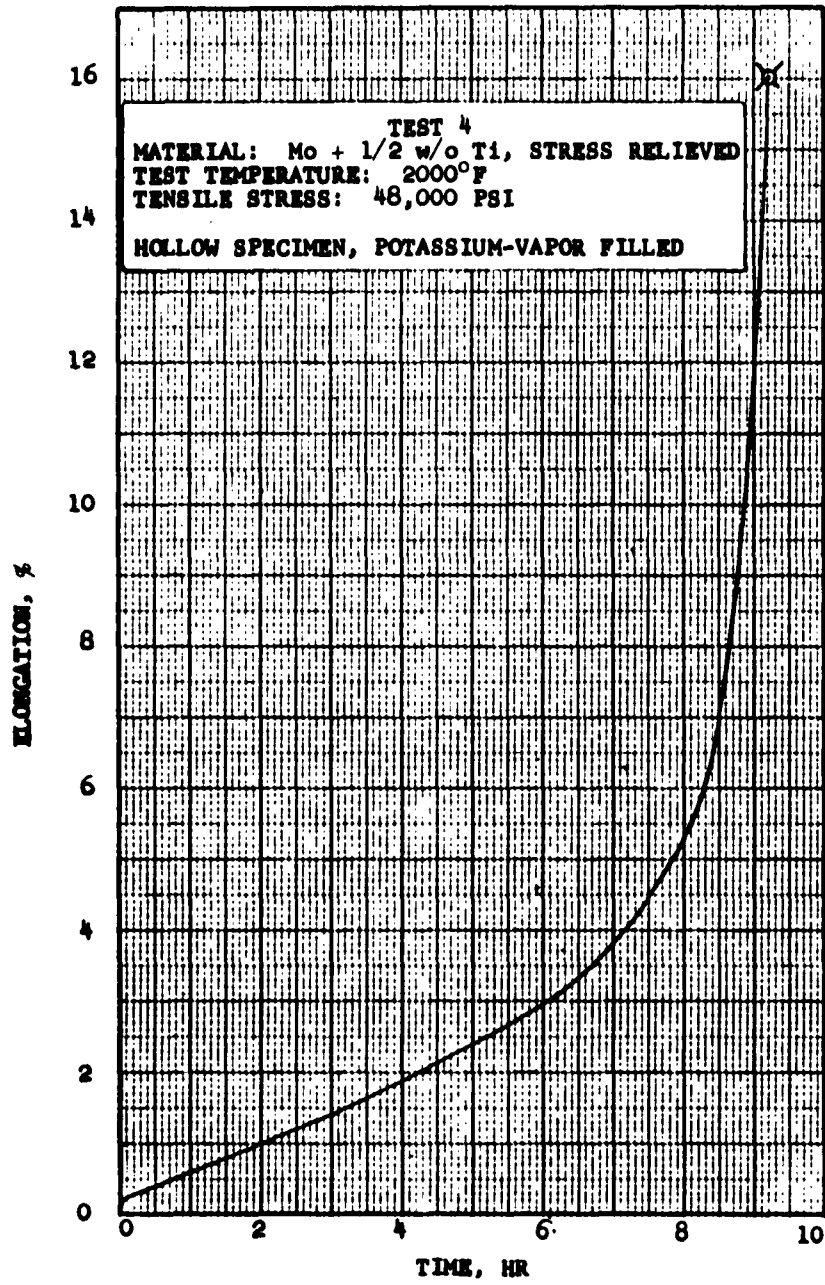
The apparent lack of influence of the potassium vapor on second-stage creep rate is illustrated in Figure 4. Here, it is observed that the points representing potassium-vapor tests appear to be randomly interspersed among those without potassium.

In Figure 5, the 1957 Climax data for 0.5 and 1.0 percent deformation and for rupture at 2000°F are drawn in as dotted curves. The rupture data are not too far apart, but the other two curves are substantially lower than the corresponding ones from the present research. Apparently, the material now being used is more creep-resistant, especially in the first and second stages, than that used in 1957, though the heat treatments were to be the same. This is illustrated by the dotted curves in Figures 3 and 4.



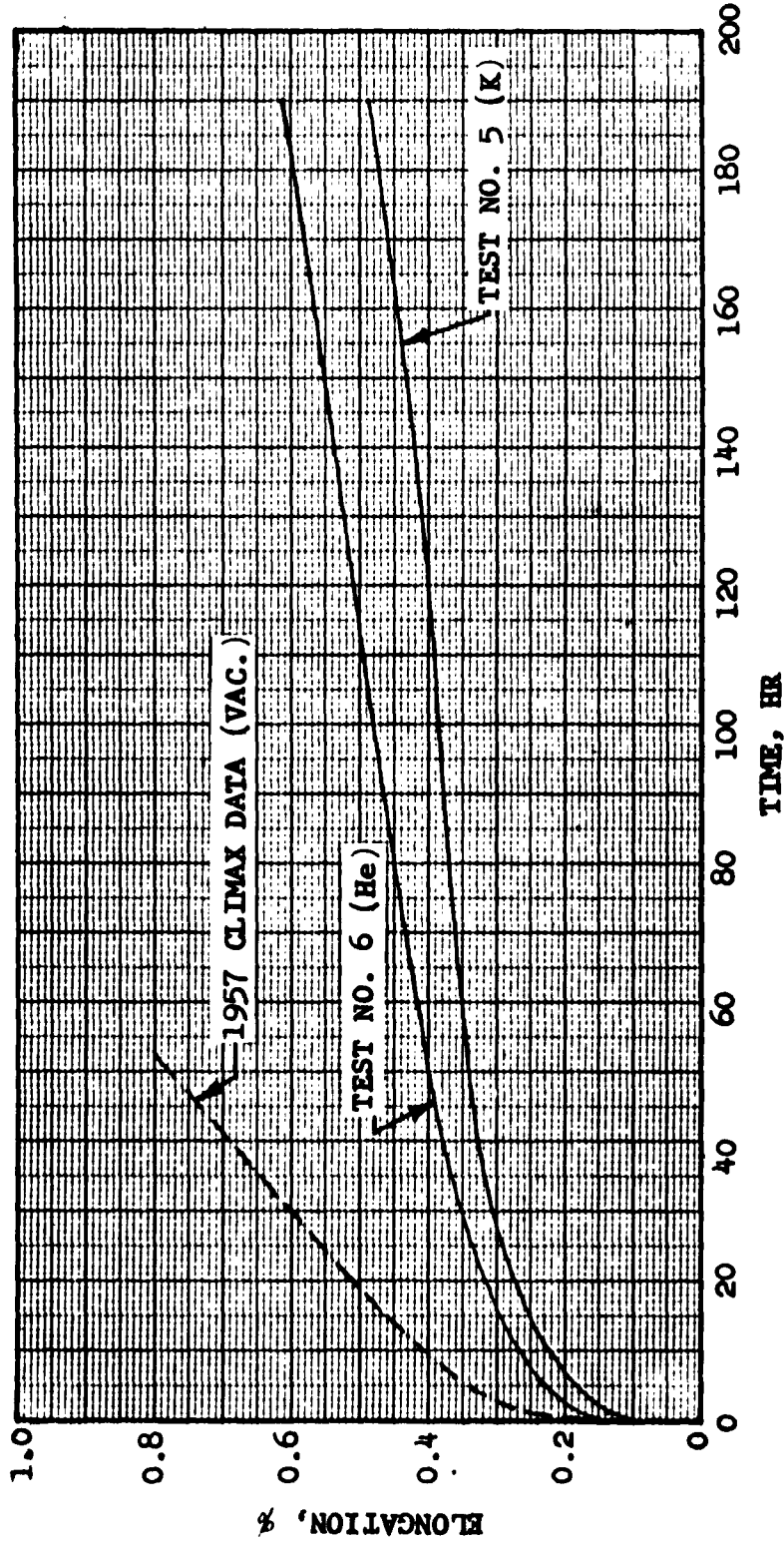
		DEFORMATION-TIME CURVES FOR 35,000-PSI CREEP-RUPTURE TESTS	FIGURE 1
PREPARED			
WRITTEN			
APPROVED			

FORM 2787A-1

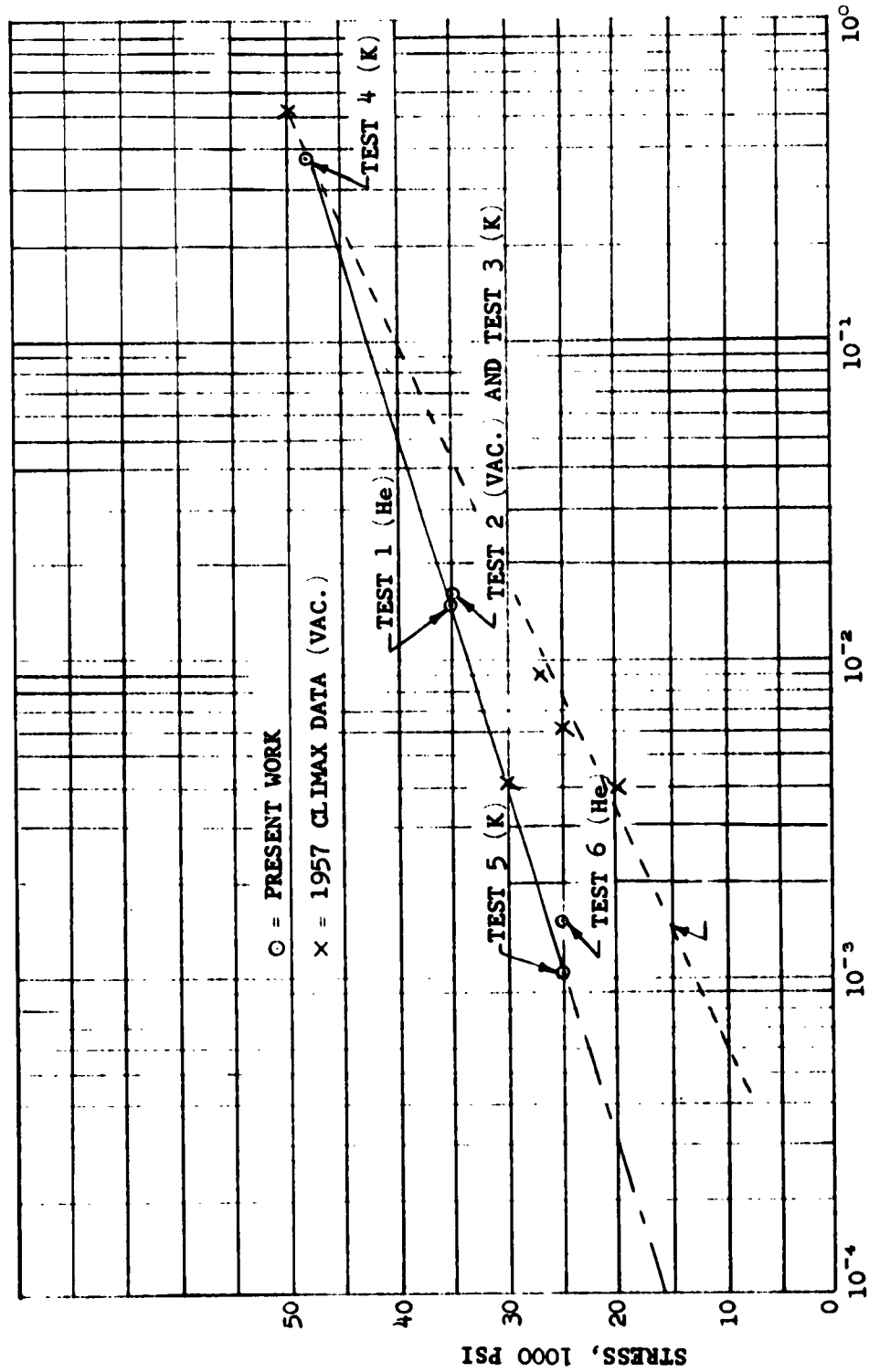


			DEFORMATION-TIME CURVE FOR 48,000-PSI CREEP-RUPTURE TEST	FIGURE 2
PREPARED				
WRITTEN				
APPROVED				

FORM 2787A-1



DEFORMATION-TIME CURVES FOR FIRST 190 HR OF 25,000 PSI CREEP RUPTURE TESTS		FIGURE 3	
_____	_____	_____	_____



MINIMUM CREEP RATE, %/HR

STRESS VS. MINIMUM CREEP RATE
 FOR Mo + 1/2 w/o Ti AT 2000°F
 WITH AND WITHOUT EXPOSURE
 TO POTASSIUM VAPOR

PREPARED	
WRITTEN	
APPROVED	

FIGURE 4



An as-received specimen of Mo + 1/2 w/o Ti and specimens from Tests 1, 2, 3, and 4 are being examined metallographically for evidences of recrystallization and interaction with the potassium vapor.

It will be noted from Table 1 that Tests 5 and 6 were still in progress at the time of preparation of this report. Actually, Test 6 was interrupted twice and Test 5 once by furnace failures. Experience has shown that creep experiments interrupted by power failures can be restarted with little or no loss in reliability of results, provided that the temperature drops quickly or the load is removed immediately.

Four additional tests are scheduled under this task. Conditions for these tests will be established upon completion of those now in process.

2. Fatigue of Mo + 1/2 w/o Ti in Potassium Vapor to 2000°F, Task 2.2.2.2

Work is in progress to adapt the Ivy Dynamic Creep Tester, shown in Figure 6, for use in evaluating the fatigue characteristics of Mo + 1/2 w/o Ti in contact with potassium vapor up to 2000°F. In the last Quarterly Progress Report, a layout of the components was presented and described. A hollow, axial-load specimen, as shown in Figure 7, will be used. A small charge of potassium will be sealed into the cavity so that, at temperature, the inner walls will be exposed to potassium vapor. The outer walls will be in a dynamic vacuum and will be protected from

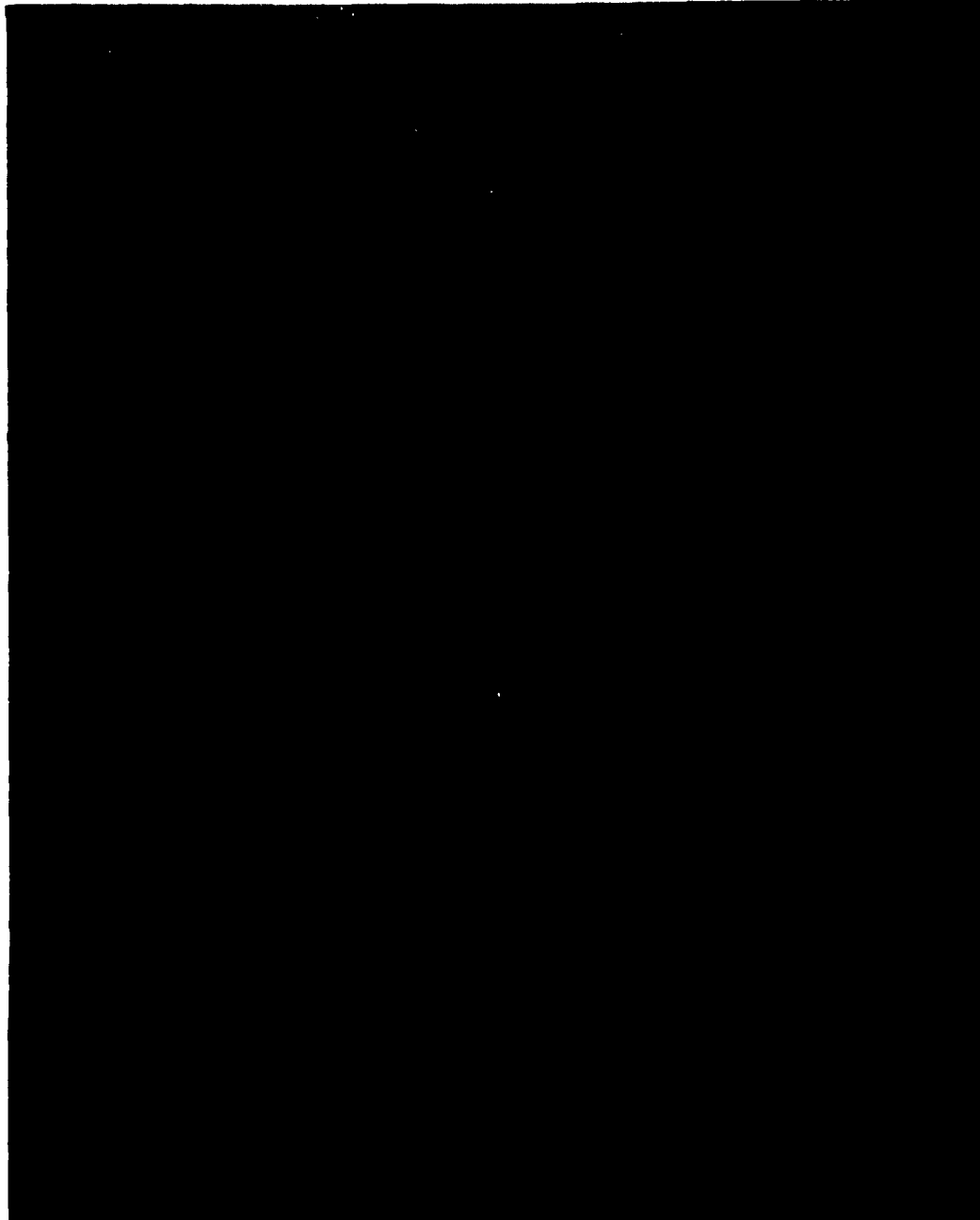


FIGURE 6
DYNAMIC CREEP MACHINE



reaction with any slight atmospheric impurities by a wrapping of molybdenum or tantalum foil.

During the past quarter, all components were fabricated and are currently being assembled. Ten specimens were machined in accordance with Figure 7.

Four S-N curves are to be generated with this apparatus--two with potassium-charged specimen cavities (1500° and 2000°F), and two with no potassium (also 1500° and 2000°F).

3. Cantilever Bending Fatigue of Cb + 1 w/o Zr,
Task 2.2.2.3

Fatigue tests are being run to evaluate the suitability of Cb + 1 w/o Zr as a bellows material for use in an accumulator for 800°F potassium liquid or 1600°F lithium liquid.

During the past quarter, several tests were lost because the automatic cutoff device was not working properly. The trouble was traced to lack of rigidity of the mounting for the sensing device, and this was remedied by suitable redesign.

Results of the seven valid tests run during the past quarter are shown in Table II and Figure 8. The endurance limit in reversed bending of Cb + 1 w/o Zr in liquid potassium at 800°F appears to be about 27,000 psi.



TABLE II

RESULTS OF CANTILEVER BENDING FATIGUE TESTS ON
Cb + 1 w/o Zr IN LIQUID POTASSIUM AT 800°F

Specimen Number	Deflection mils	Maximum Stress, psi ^①	Lifetime, kilocycles
3	45.0	49.5	16
4	35.0	38.5	120
9	32.5	35.7	143
5	30.0	33.0	643
6	27.5	30.2	1,108
7	25.0	27.5	> 4,328 ^②
8	25.0	27.5	> 10,000 ^③

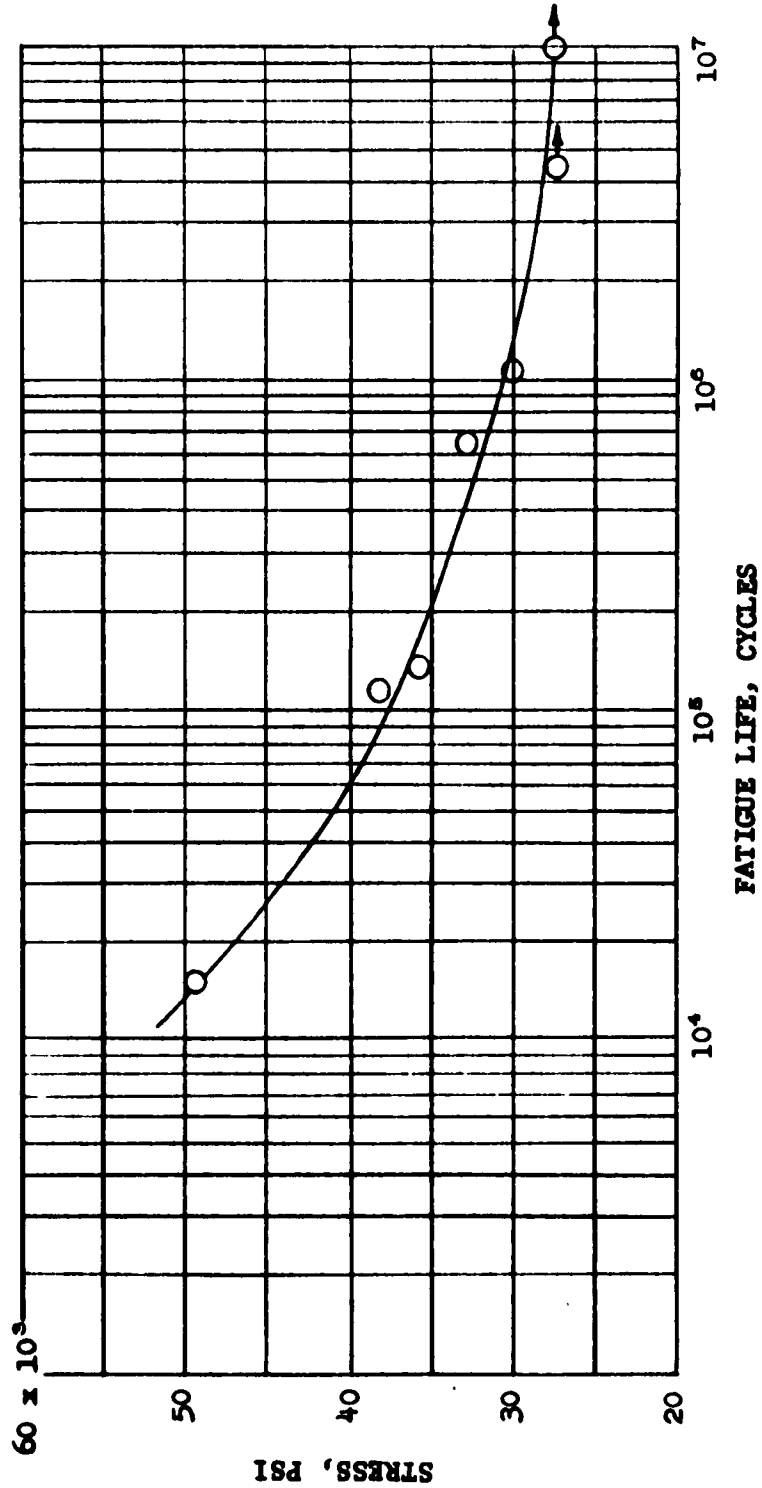
① Nominal maximum bending stress was calculated for a Young's modulus value of 15×10^6 psi.

② The specimen was removed from machine because there was some doubt about the action of the cutoff mechanism--the specimen did not fail.

③ The specimen did not fail.

Two more tests are scheduled, to fill in the gaps of Figure 8. Specimens 1, 5, and 7, together with an as-received Cb+1w/o Zr sample, are being analyzed for oxygen and nitrogen. Two as-received potassium samples were analyzed for oxygen by the mercury amalgamation method and showed 78 and 73 (± 10) ppm oxygen, respectively.

Tests in 1600°F lithium will be conducted in order to complete the Phase II work.



RESULTS OF CANTILEVER BENDING FATIGUE TESTS ON Cb + 1 w/o Zr IN LIQUID POTASSIUM AT 800°F		FIGURE 8
PREPARED		
WRITTEN		
APPROVED		

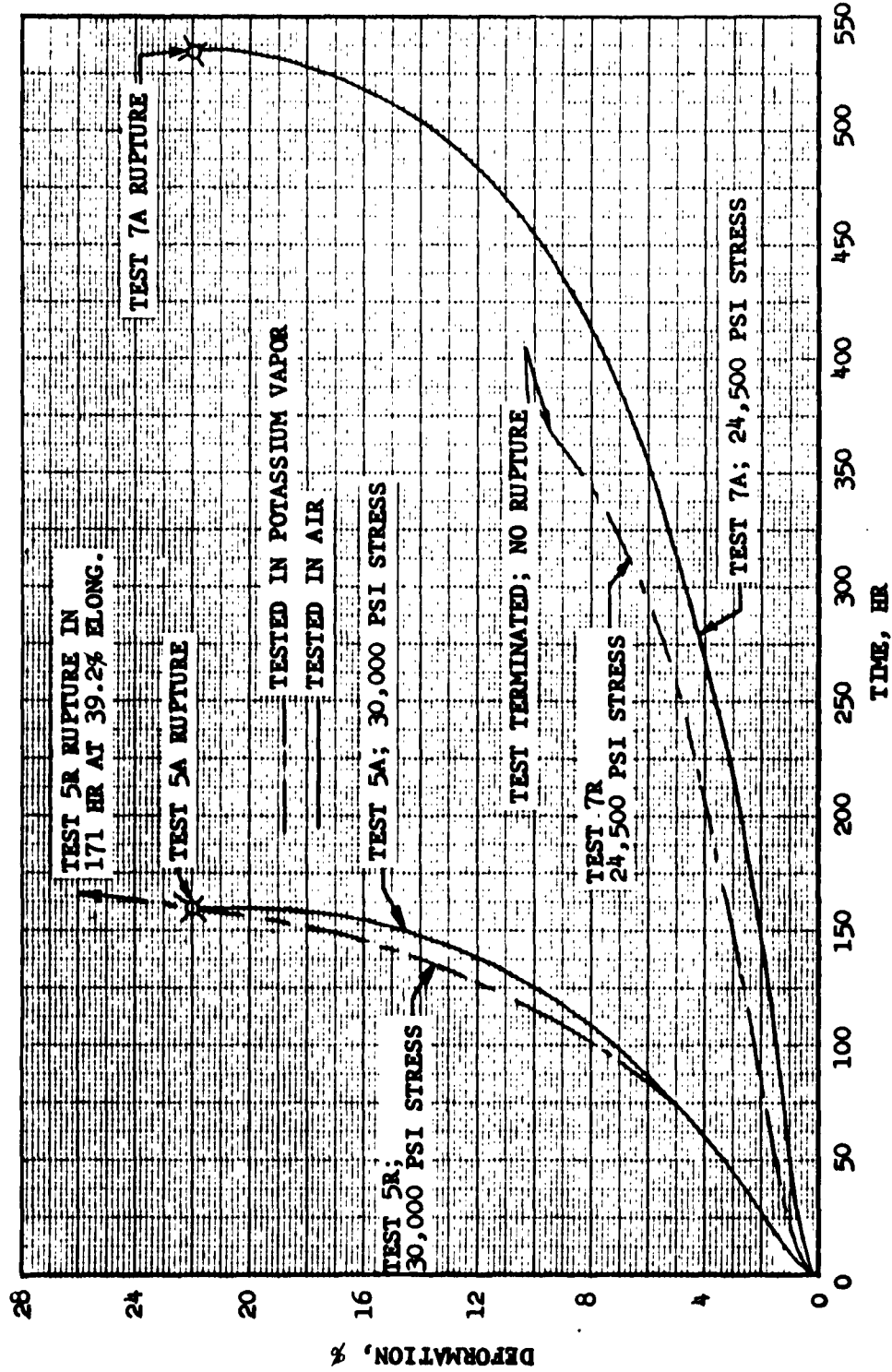


4. Creep-Rupture Properties of SAE 4340 Steel in
1000°F Potassium Vapor

During the previous contract period, creep-rupture tests were run on the candidate generator-rotor material, SAE 4340 steel, at 800° and 1000°F in both air and potassium vapor environments. The 800°F results indicated that the potassium vapor at this temperature is not detrimental to the creep properties. The tests in potassium vapor at 1000°F were invalid because of temperature gradients in the specimens during the tests. The objective of this task is to repeat two creep-rupture experiments in potassium vapor (with improved temperature control) for comparison with the corresponding tests in air.

The results indicate that potassium vapor has little or no influence on the creep characteristics of SAE 4340 steel at 1000°F. As can be seen in Figure 9, the 30,000-psi curves in air and potassium vapor (Tests 5A and 5R) are almost superimposed, and the spread between the two 24,500-psi curves is within the scatter band normally encountered in creep-rupture tests.

No explanation exists for the greater ductility of the specimen in Test 5R, as compared with that in Test 5A. Test 7R was terminated prior to rupture, because an operator error caused the specimen to over-heat, thus invalidating any further testing.



DEFORMATION-TIME CURVES FOR NORMALIZED SAE 4340 STEEL AT 1000°F		FIGURE 9
PREPARED		
WRITTEN		
APPROVED		



The results of Tests 5R and 7R are summarized in Table III, along with those from the corresponding air tests, for comparison.

TABLE III
CREEP-RUPTURE TESTS ON SAE 4340 STEEL AT 1000°F

Test No.	5A	5R	7A	7R
Stress, psi	30,000	30,000	24,500	24,500
Environment	Air	K vapor	Air	K vapor
Time to rupture, hrs.	161.9	171.0	536.7	--
Elongation at fracture, %	22	39.2	22	--
Reduction of area at fracture, %	53.6	61.8	59.6	--
Minimum creep rate, %/hr.	0.05	0.05	0.0104	0.015
BHN before test	316	316	316	316
BHN after test	255	277	260	--
Time, hrs., to reach				
0.5% elong.	1.9	1.9	9	2
1.0% elong.	9.8	9.8	50	10
2.0% elong.	28.3	28	128	70
5.0% elong.	75.8	75	288	245



5. Mass Transfer Tests with Two-Phase Flow,
Task 2.2.2.4

The fabrication of the loop components, including the condenser, flowmeter, pump, test section, and liquid-level tank, has been completed. The condenser, which is fabricated from 5/8-inch-outside-diameter Cb + 1 w/o Zr tubing, contains 515 circular fins, 1.55 inches in diameter and 0.015 inch thick. The fins are also fabricated from the columbium alloy. The fins were press-fitted to 42.8 inches of the condenser leg. The loop assembly will be initiated and completed during the next report period.

The liquid-level test was conducted at elevated temperatures in the vacuum dry box. The test chamber, as shown in Figure 10, contained four horizontal "I" tubes and one vertical "I" tube for liquid-level detection. The tank and the probes were fabricated from the columbium alloy. A temperature control system was provided for heating the potassium. Level control was accomplished by pressurizing a separate vessel of potassium by means of an argon cover gas which forced the potassium into the vessel containing the probes. The level was varied by the pressure differential and was observed through the plastic dome of the vacuum chamber. The test setup is shown in Figure 11. The test consisted of slowly raising the liquid level until the potassium contacted a horizontal probe. A millivolt output reading is taken for each probe level. A shift in the slope of the level position vs millivolt output was noted in the vertical

THE BARRETT CORPORATION
AirResearch Manufacturing Division
Phoenix, Arizona

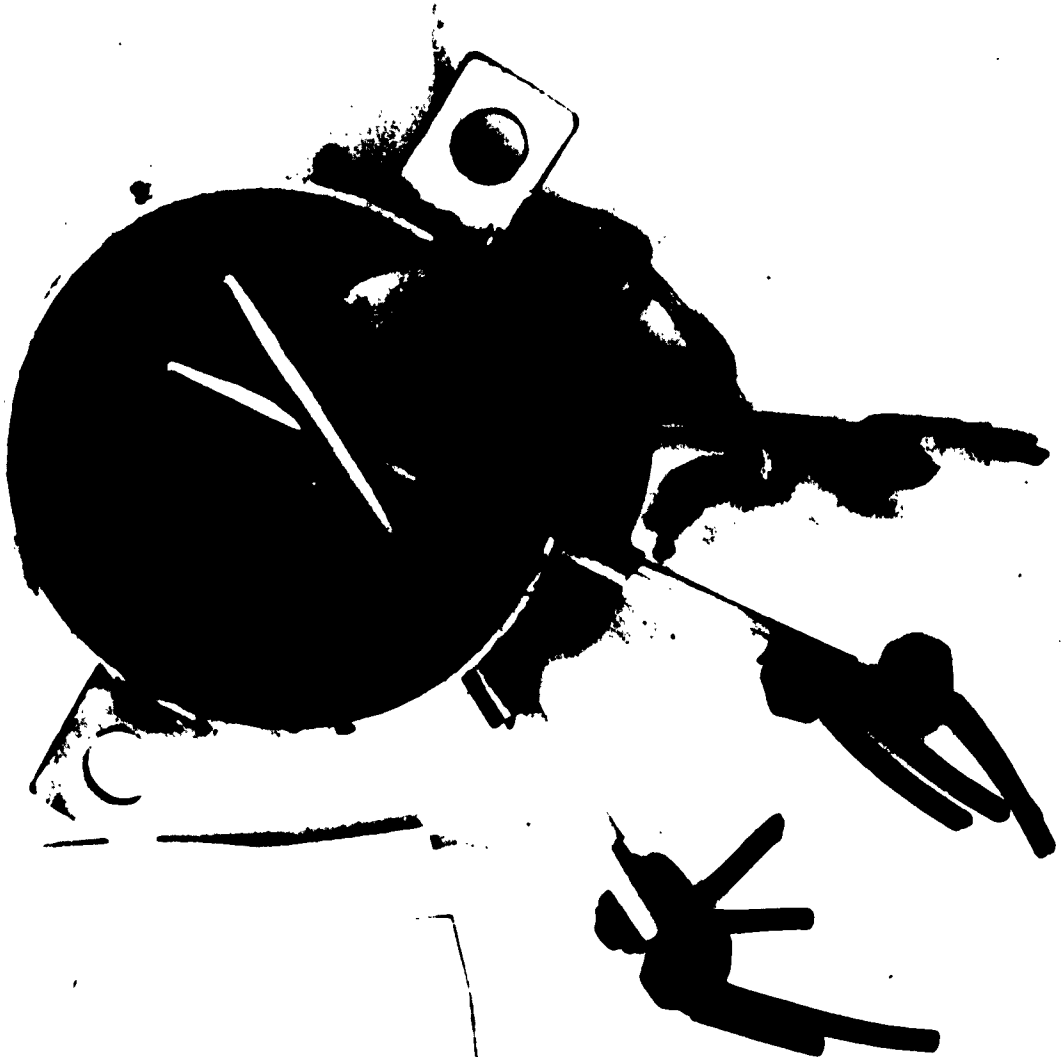


FIGURE 10
"I" TUBE TEST CHAMBER



probe; however, calibration of these probes can be accomplished by using the horizontal probes. The method of liquid level detection was proved satisfactory for the loop test.

The tantalum heater design required joining a tantalum bus bar, 3/32 inch thick, to the tantalum tube heater, 0.015-inch wall. The bus bar was TIG-welded to the tube with a 0.001-inch pure columbium foil placed between the tantalum bar and the tantalum tube. After TIG-welding the bus bar, the contact area of the bus bar to the tube was heated to braze the bar to the tube, using pure columbium as the braze material. This assured the maximum contact area for optimum electrical efficiency and, therefore eliminated any potential hot spots due to incomplete contact of the bus bar to the tube. All welding and brazing was performed in a vacuum dry box with a high-purity argon atmosphere.

A test was conducted on the heater to determine the electrical and mechanical integrity of the heater bus bar attachment. A test chamber, as shown in Figure 12, was constructed to provide the high-purity argon atmosphere for this test. Temperatures of the heater and the bus bar were measured with an optical pyrometer. The heater was electrically resistance-heated to 3100°F. During this test, the bus bar joint showed no hot spots. Figure 13 shows the test setup for the bus bar junction test.



FIGURE 11
"I" TUBE TEST SETUP

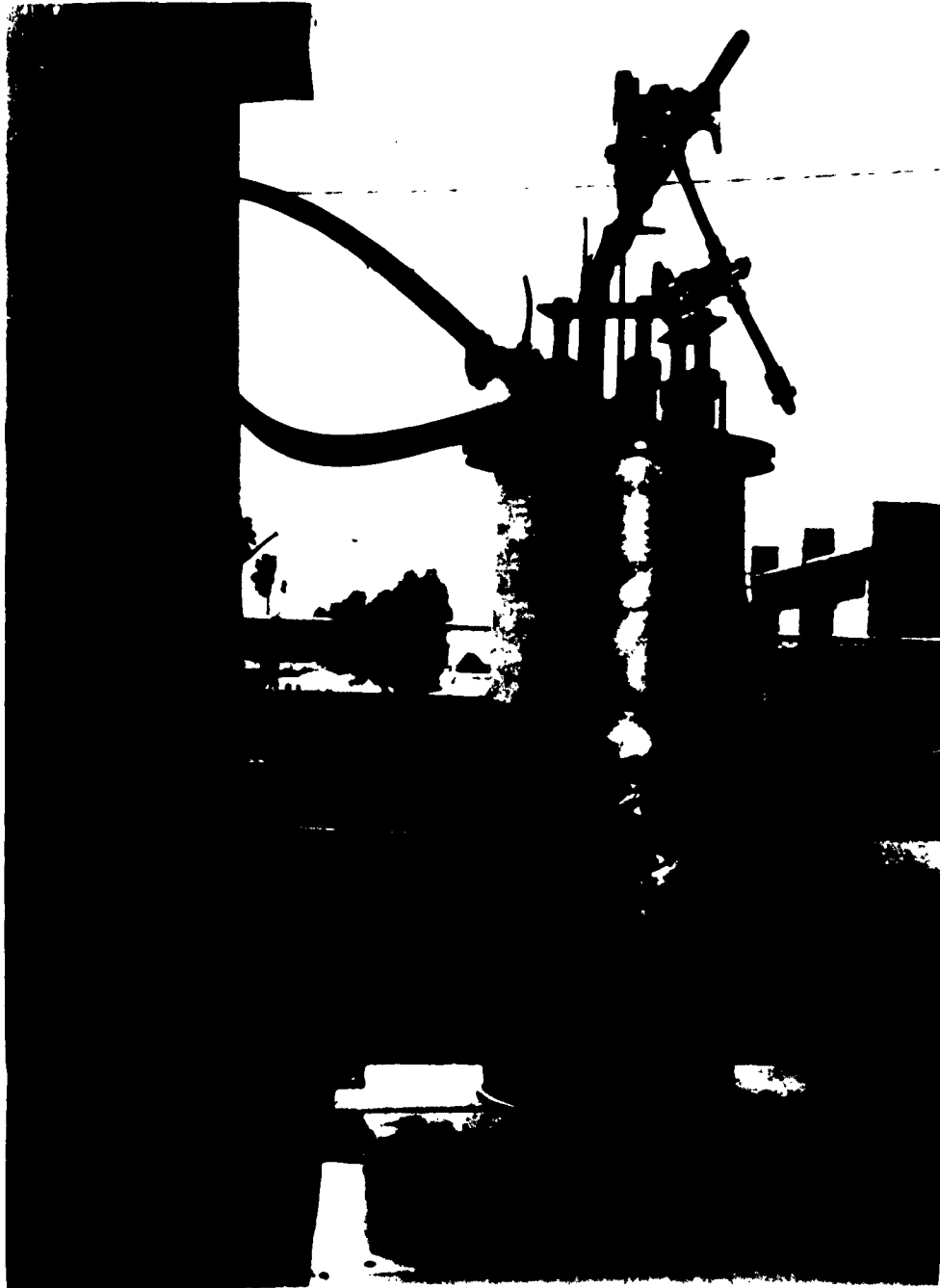


FIGURE 12
TANTALUM HEATER TEST SETUP

THE BARRETT CORPORATION
AirResearch Manufacturing Division
Phoenix, Arizona

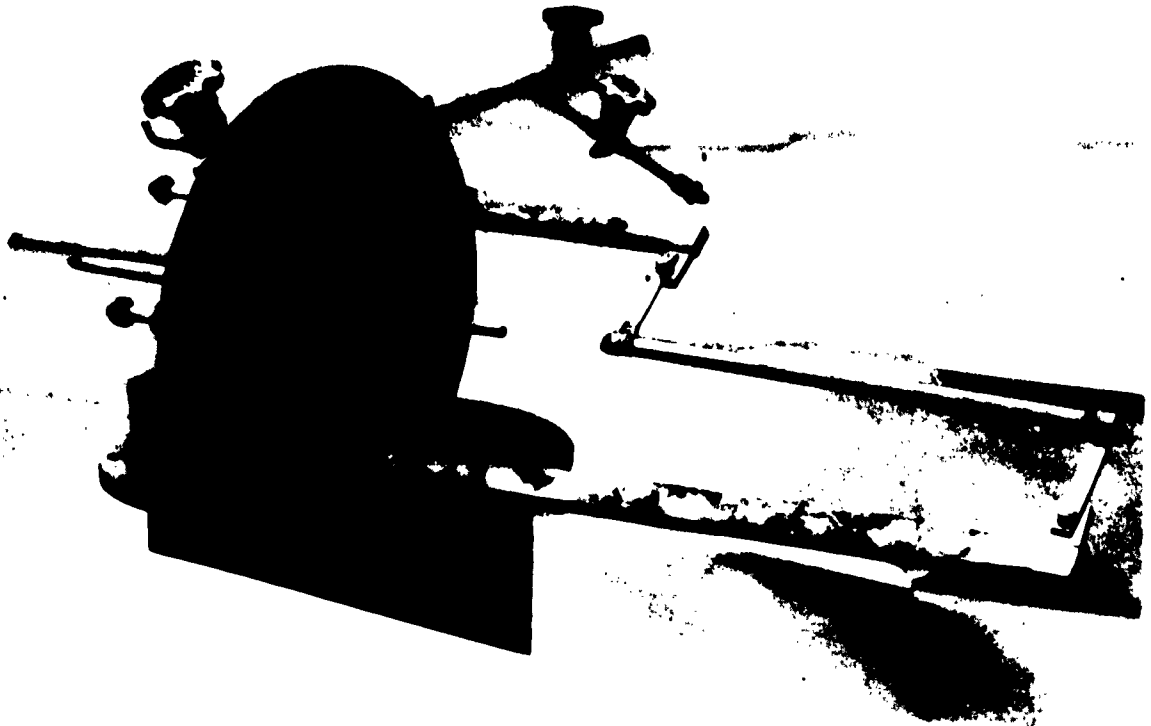


FIGURE 13
TANTALUM HEATER TEST
BUS BAR JUNCTION TEST



An additional test, in which a mock-up of the main loop heater and the adiabatic wall (annealing) heater was made, was conducted in the test chamber shown in Figure 12. The test included the loop thermal insulation (Foamsil) and the electrical insulation (boron nitride). Figures 14 and 15 show the heater test assembly prior to test. The adiabatic wall heater is shown on the left and the main loop heater on the right of the photograph. The heaters are complete with the tantalum radiation shields. Prior to test, the chamber was evacuated to 10 microns and back-filled with high-purity argon. This procedure was repeated two more times before the test heaters were operated. The adiabatic wall heater was operated for 2 hours at 2300°F while electrical and temperature measurements were made. Following this test, the main loop heaters were operated at 2000°F for 40 hours. Figure 16 shows the heater assembly after the test period. The tantalum heaters performed satisfactorily; however, contamination of the tantalum material was noted. The Foamsil prior to test was given a double vacuum bakeout at 2000°F; however, the boron nitride was only given an atmospheric elevated-temperature (1600°F) bakeout. Tests are to be conducted in a vacuum environmental chamber on boron nitride that is given the same bakeout as used in the heater test and on boron nitride that is baked out in a vacuum (10^{-6} torr) at a temperature of 2000°F.

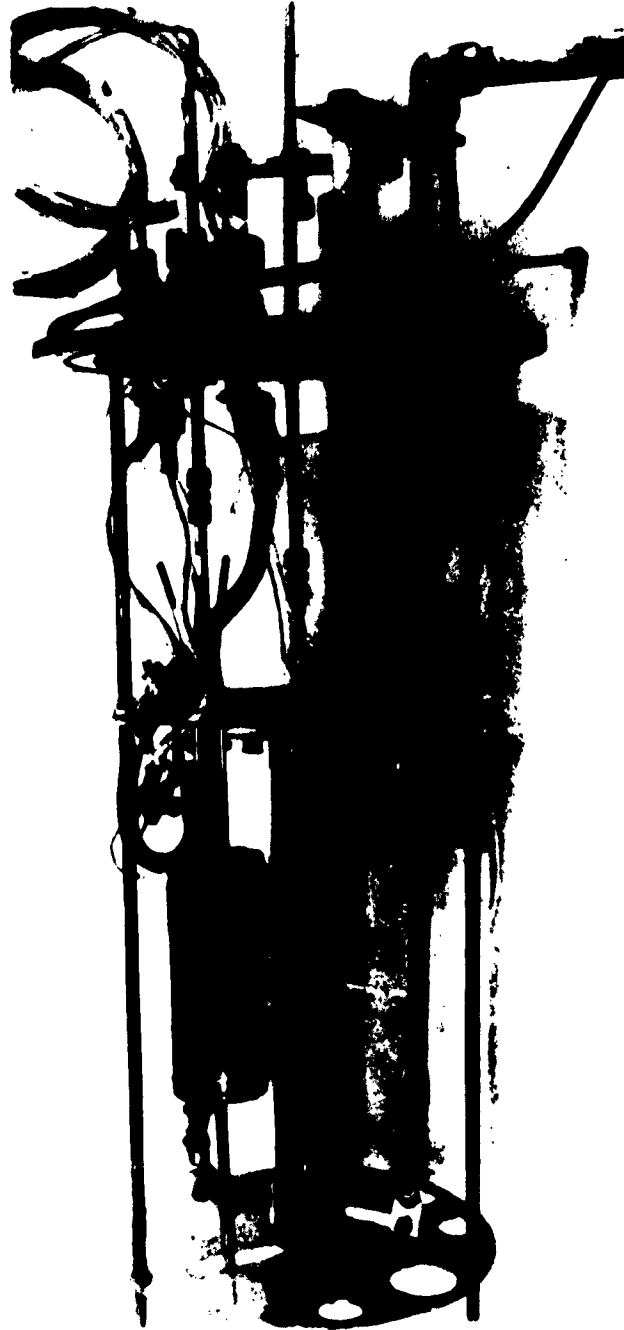


FIGURE 14

TANTALUM HEATER TEST ASSEMBLY



FIGURE 15
TANTALUM HEATER TEST ASSEMBLY



FIGURE 16
TANTALUM HEATER TEST ASSEMBLY, AFTER TEST

SY-5396-R3
Page 31.



The test chamber and associated gas-purification system have been assembled. Figures 17 and 18 show the titanium chip furnaces and the molecular sieves. All components are fabricated from Type 316 stainless steel. All valves in the system are bellows-seal valves, are fabricated from high-temperature materials. Figure 19 shows the main blower and the booster blower in a chamber that is connected to the test chamber and the purification system. The components have been pressure- and vacuum-leak-checked with the helium mass spectrometer. A system leak-check is presently being conducted on the system.

6. Liquid-Potassium Mass-Transfer Tests, Task 2.2.2.5

Mass-transfer characteristics of the Cb + 1 w/o Zr alloy, when used with liquid potassium will be ascertained by the construction and testing of a single-phase conversion loop. Incorporated in the Cb + 1w/o Zr alloy loop will be an electromagnetic pump and a flowmeter to maintain and measure potassium flow. The loop will be tested in a large stainless steel vacuum chamber, at a pressure of 10^{-8} torr.

Preliminary loop design has been initiated. Fluid flow will be 0.5 gpm at a velocity of 10 fps. The fluid temperature will vary over a 1400°F range. Heating by direct electrical resistance heating, (I^2R), of a portion of the Cb + 1 w/o Zr loop is presently contemplated.

THE BARRETT CORPORATION
AirResearch Manufacturing Division
Phoenix, Arizona



FIGURE 17
Cb + 1 w/o Zr TWO-PHASE LOOP,
ARGON PURIFICATION SYSTEM

SY-5396-R3
Page 33

THE BARNETT CORPORATION
AirResearch Manufacturing Division
Phoenix, Arizona



FIGURE 18
Cb + 1 w/o Zr TWO-PHASE LOOP,
ARGON PURIFICATION SYSTEM

SY-5396-R3
Page 34

THE GARRETT CORPORATION
AirResearch Manufacturing Division
Phoenix, Arizona



FIGURE 19
Cb + 1 w/o Zr TWO-PHASE LOOP,
ARGON BLOWER BOX

SY-5396-R3
Page 35



The vacuum chamber specifications have been prepared and submitted to prospective vendors for construction of the chamber. The chamber vendor will be responsible for vacuum testing the chamber to a pressure of 10^{-9} torr or less.

7. Capsule Tests

The metallography of the brazed "T" specimens tested in potassium is still pending. The weight measurements of the exposed samples are shown in Table IV.

8. Fabrication Studies, Task 2.2.2.7

The inert atmosphere welding chamber described in the Last Quarterly Progress Report has been received and is presently being installed in the Metals Joining Laboratory. The chamber will be capable of high-purity inert-gas atmosphere semiautomatic welding of refractory-metal components in sizes up to 36 inches long by 20 inches in diameter. Installation will be complete the third week of January, 1963.



TABLE IV
BRAZED "T" SPECIMENS WEIGHT MEASUREMENTS
500 HOUR TEST DURATION

Specimen area = 1.46 sq in. = 9.46 sq cm

Specimen	Braze Materials	Weight Loss (mg)	Weight Loss mg/cm ² /hr	Test Temp (°F)	Remarks
1A	Ni	8.0	0.0017	1500	
1B	Ni	2.2	0.0005	1500	
2A	Ni	0.4		2000	Failed
2B	Ni	-		2000	Failed
3A	Ti	0.7 ^①	0.0001	1500	
3B	Ti	0	--	1500	
4A	Ti	1.0	0.00020	2000	
4B	Ti	0.3	0.00006	2000	
5A	48 Ti - 48 Zr - 4 Be	6.3	0.0013	1500	
5B	48 Ti - 48 Zr - 4 Be	1.1	0.0002	1500	
6A	48 Ti - 48 Zr - 4 Be	18.5		2000	Failed
6B	48 Ti - 48 Zr - 4 Be	165.9(+)		2000	Failed
7A	60 Zr - 25 V - 15 Cb	1.0	0.0002	1500	
7B	60 Zr - 25 V - 15 Cb	0.7	0.0001	1500	
8A	60 Zr - 25 V - 15 Cb	40.5(+)		2000	Failed
8B	60 Zr - 25 V - 15 Cb	8.9(+)		2000	Failed
9A	58 Zr - 27 Ti - 15 Fe	4.8	0.0010	1500	
9B	58 Zr - 27 Ti - 15 Fe	2.9	0.0006	1500	
10A	58 Zr - 27 Ti - 15 Fe	125.8	0.0266	2000	
10B	58 Zr - 27 Ti - 15 Fe	84.7	0.0177	2000	
11A	63 Ti - 27 Fe - 10 Mo	1.8	0.0004	1500	
11B	63 Ti - 27 Fe - 10 Mo	0.6	0.0001	1500	
12A	48 Ti - 48 Zr - 4 Be	0.1	0.00002	1500	
12B	48 Ti - 48 Zr - 4 Be	0.4	0.00008	1500	

① Not detectable to 0.1 mg.



THE GARRETT CORPORATION
Air Research Manufacturing Division
Phoenix, Arizona

An automatic tube-to-header TIG welding gun was received from Revere Copper and Brass Company on December 15, 1962. A positioning mandrel is currently being fabricated from columbium + 1 w/o zirconium. Due to the close proximity of the tungsten electrode to the mandrel, it is felt that a refractory-metal mandrel is necessary to avoid contamination of the work and possible melting of the mandrel during welding of columbium + 1 w/o zirconium. The gun has been used to join stainless steel tubes and headers; excellent results were achieved.

Four columbium plates, 5/16 inch thick by 4 inches by 4 inches have been machined to simulate boiler header plates. Each plate contains sixty-eight 5/16-inch-diameter holes, spaced in a triangular array with a tube-to-tube center pitch of 0.470 inch.

Welding of columbium + 1 w/o zirconium tube-to-header joints will proceed during the second week in January with the automatic tube-to-header weld gun installed in a temporary inert atmosphere purge chamber.

A Wiedeke tube expander has been received for use in diffusion bonding studies.

Inverted Cb + 1 w/o Zr "T" specimens were brazed with four experimental braze alloys to determine flow temperature and wettability. A brazing gap was maintained by the insertion of 0.0015-inch-thick tungsten foil at both ends of each specimen, and columbium + 1 w/o zirconium wire was used to hold the assemblies



together. Brazing was done in an Abar high-temperature vacuum furnace equipped with tantalum heating elements. Furnace vacuum during brazing varied between 2×10^{-5} mm Hg and 1×10^{-4} mm Hg. Flow temperature was determined by visual observation of flow and measurement of temperature with a Leeds-Northrup optical pyrometer. After visual observation of flow, the specimen was held 5 minutes at temperature and then allowed to cool. All four alloys exhibited excellent wettability and flowability. Flow temperatures and preliminary metallographic observations are listed in Table V. The specimens are shown in Figure 20.

TABLE V

BRAZED Cb + 1 w/o Zr "T" SPECIMENS

	<u>Braze Alloy</u>	<u>Flow Temperature</u>	<u>Preliminary Metallographic Observations</u>
1.	59 Ti - 25 V - 8 Fe - 8 Co	2430 \pm 20 $^{\circ}$ F	Voids and porosity. Apparently overheated (brought to 2550 $^{\circ}$ F max.) Interdendritic second phase.
2.	59.5 Ti - 25.5 V 10 Fe - 8 Ni	2450 \pm 20 $^{\circ}$ F	Good fillet. Interdendritic phase but no porosity.
3.	59.5 Ti - 25.5 V 10 Co - 5 Ni	2490 \pm 20 $^{\circ}$ F	Good fillet. Interdendritic phase but no porosity.
4.	59.5 Ti - 25.5 V 10 Fe - 5 Zr	2390 \pm 20 $^{\circ}$ F	High fluidity and wettability; very small fillet. Voids and porosity apparently caused by overheating (brought to 2690 $^{\circ}$ F)

The flow temperatures of alloys 1, 2, and 4 are considered too low for 2000 $^{\circ}$ F service. A differential of at least 500 $^{\circ}$ F between service temperature and braze



FIGURE 20
BRAZED "T" SPECIMENS



flow temperature should exist. However, flow temperatures of these alloys can easily be raised by adjusting composition.

A vacuum retort is presently being constructed for use with an existing vacuum pump and furnace. Sections of brazed "T" specimens will be aged at 1800°F for 500 hours in a vacuum of 5×10^{-5} mm Hg or better to determine the extent of reaction between braze alloys and columbium + 1 w/o zirconium.



B. Testing Techniques

1. High-Temperature Heater Evaluation, Task 2.2.3.1

In order to establish a 5-megawatt heater design, a survey was conducted of current high-temperature heater and furnace technology. From this survey several reference designs were evolved. Configurations considered were (1) a radiant heat-transfer heater, (2) a conductive heat-transfer heater, and (3) a liquid-metal resistance-type heater using the liquid metal to be heated as the electrical resistor. Feasibility calculations were made on several heater configurations of each general type, and from these studies the following conclusions were reached:

- (a) The radiant heat-transfer heaters required extremely high temperature radiation surfaces for efficient operation. The physical configuration was complex and bulky due to the large radiation surfaces needed. In addition, complex insulation was required to prevent excessive heat losses. Operation and construction were shown to be very inefficient and costly. Temperature control is also foreseen to be a large problem.



- (b) The heaters using resistance heating in the walls and conduction to the liquid metal proved to be far simpler, more compact, easier to control, less costly, and more efficient than the radiant heaters. Material problems are also lessened due to the lower heater operating temperatures. The design is relatively simple and easy to install or replace on a loop. It has built-in redundancy due to the parallel heating elements, and appears to be more feasible than the radiant heat-transfer heaters.
- (c) The liquid-metal resistance heater is the simplest and most efficient of the reference designs. The main objections to this design are that the heater is not independent of the liquid-metal loop, there is no built-in redundancy or safety factor. Material problems due to temperature are minimized since the maximum temperature of the heater components does not exceed the maximum liquid-metal temperature and thus is lower than either of the preceding designs. From this analysis, the conduction and resistance heating designs were selected for further evaluation.



From the feasibility calculations conducted on the 5-megawatt heaters, operating temperatures, heat fluxes, materials, and the physical configuration were established. Using this information, twenty kilowatt heaters were designed (both conduction and resistance) for comparison and development. The heaters were designed to minimize costs and complexities. A test loop was then laid out using a natural-convection, closed lithium loop operated in a vacuum chamber.

A test program has been outlined for the two 20-kilowatt heaters. This program is designed to fully evaluate the heaters and permit final design of the 5-megawatt heater. This testing program has been deferred to a later phase of the program.



C. Bearing Development

1. Bearing Tests, Task 2.2.4.1.1

Potassium and Lubricant Compatibility

The three lubricants mentioned in the previous report were evaluated for compatibility with potassium. The best results were obtained with KK806C and Bayol 50. Fluid 2090-17C reacted with the potassium, causing a considerable increase in its viscosity. Fluid KK806C was selected for use in the bearing test rig because of its better viscosity characteristics for bearing lubrication.

A partial shipment of KK806C was received. The lubrication subsystem was then filled, and preliminary tests were successfully completed. Tests were run without the bearing test rig to check pump performance and circuitry.

Dynamic Face Seal

Proposals for the backup seal design shown in Figure 7 of the previous quarterly progress report were received and evaluated. All major design details were then resolved with the selected vendor, and seal assemblies were ordered. Two complete seal assemblies and one set of spare rotors are scheduled for delivery during the next report period. AM6323, chromium-plated, running against USG-2480 carbon, will be used



to seal the potassium vapor. The detail drawing for modification of the test shaft, spindle shaft, housing, and seal mounting plate will be completed in January.

Test Loop and Instrumentation

Preliminary checks were made to evaluate the marriage and performance of the drive motor and clutch, lubrication system, and argon cooling system.

The potassium loop was completed in December. However, during each leak checking, cracks were found in the EM pump adjacent to the Microbrazed tube/laminated cross section. It is not possible to repair the cracks by welding; therefore, a new pumping section and mica insulators have been ordered and will be installed in January.

All other loop subsystem modifications have been completed, and leak checking and line heater installation have been started.

Bearing Removal Procedure

During the bearing removal procedure simulation test, it was found that a special deburring tool was needed, with which the cutoff burr on the ID of the tube can be removed without metallic chips falling down into the tube. The desired tool has not yet been found, and alternate approaches to the problem are now being investigated.



The bolted flange "K" seal design planned for use between the bearing test rig and the potassium loop proved inadequate. Therefore, a welded sleeve joint will be utilized to connect the bearing test rig to the potassium loop.

Bearing Test Rig

Tests to establish induction drive motor starting and running torque characteristics were completed. A review of acceleration rates between various speeds and the time required to achieve full synchronous speed indicated a marginal condition of reserve power. Therefore, special starting-procedure tests were conducted, and the optimum field-excitation voltage and line currents required to obtain maximum power for starting and acceleration were established. Methods of increasing the power or torque capability of the motor are being investigated.



A leakage test of the face seal was conducted. The leakage rate of 0.004 cu ft per hr is considered acceptable. Runout tests on the spindle were also conducted. Runouts recorded with capacitance probes were: 0.0002 inch at 12,000 rpm; 0.0003 inch at 18,000 rpm; and 0.0004 inch at 24,000 rpm.

The bearing test rig is shown in Figures 20 and 21. Figure 21 shows the instrumentation leads and the potassium inlet line.

2. Bearing Analysis, Task 2.2.4.1.2

A complete analysis of journal bearing performance has been made possible by solving the basic Reynolds hydrodynamic equations, modified to include fluid inertia on an IBM 7090 digital computer. The computer program was set up to solve the modified equations for cases covering both the classical laminar assumptions and superlaminar operations (using liquid potassium as the lubricating fluid). For the former condition, combinations of three eccentricity ratios and two clearances at 24,000 rpm were considered. At the latter condition, combinations of three eccentricity ratios, two clearances, and three speeds were considered. In all cases, load, friction, flow, temperature rise, attitude angle, and the complete pressure distribution have been deduced; however, at the time of this report, all the results have not been plotted. Curves presenting the results of the calculations will be presented in a topical report.

THE BARRETT CORPORATION
AirResearch Manufacturing Division
Phoenix, Arizona

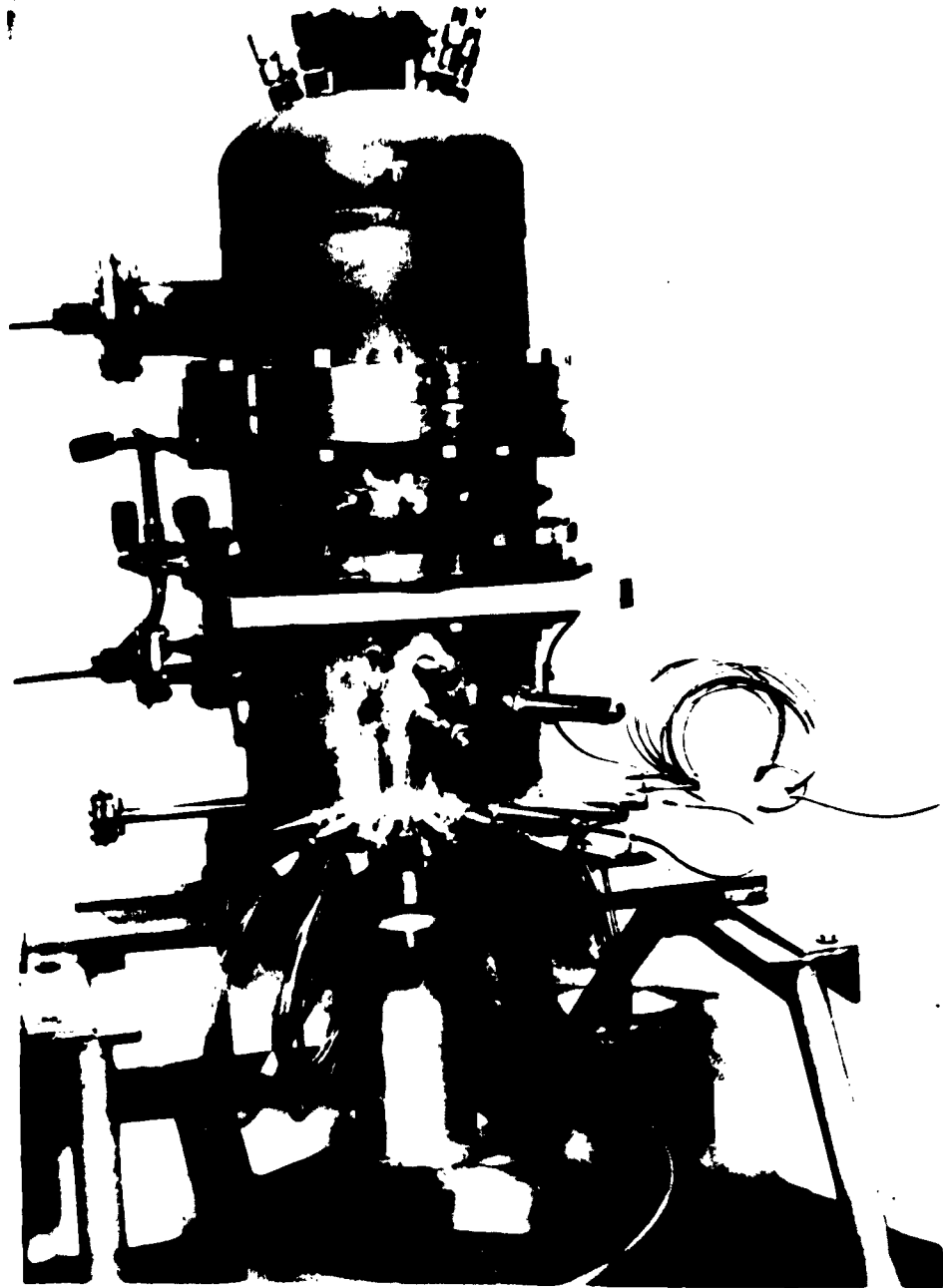


FIGURE 21
BEARING TEST RIG

SY-5396-R3
Page 49

THE GARRETT CORPORATION
AirResearch Manufacturing Division
Phoenix, Arizona



FIGURE 22
BEARING TEST RIG



D. Turbine Development

1. Turbine Test Rig Design

(a) Turbine Design

Blade Shapes and Velocity Distribution

In order to evolve the aerodynamic blade profile shape, the following procedure was used. The fluid was assumed to expand along an isentropic two-phase equilibrium path. The range of pressures considered was approximately 130 to 10 psi, which is the region of interest for the SPUR turbine. Specific isentropic expansions were examined from inlet pressures of 130, 90, 50, and 30 psia to an exit pressure of 10 psia. For each of these expansions, pressure versus volume of the mixture was determined and plotted. The resulting values of gamma were examined and an average value of 1.22 was selected to define the pressure-volume relationship of the working fluid. The value of gas constant, R , was chosen to satisfy the isentropic enthalpy drop of each individual turbine stage for the average value of gamma of 1.22. The fluid properties determined in this way were used in the normal perfect gas equation along with the equations of motion to calculate the local surface velocity distribution on the blades.



The actual blade profile design was performed for the conditions calculated to exist for the ninth turbine stage. This stage was chosen because its blade height and Mach numbers are greater than for the other turbine stages. Solutions were performed at seven constant radii for the rotor and five for the stator. Briefly the solutions consisted of specifying a blade channel shape and obtaining velocity gradients from an electrical analog. Local specific flows at the passage inlet and exit were determined from the vector diagram and compressible flow solutions performed on a high-speed digital computer. The passage shape was altered and the solution repeated until acceptable velocity distributions were obtained. The criterion used to measure whether or not a particular blade surface velocity distribution was acceptable is the total blade surface diffusion factor, which is the sum of the diffusion factors for the pressure and suction surface of the blade. The diffusion factor for the suction side of the blade is defined as:

$$D_S = \frac{V_{\max} - V_{\text{exit}}}{V_{\max}}$$

Where:

V_{\max} = maximum suction surface velocity

V_{exit} = velocity at blade exit in the plane of the trailing edge



For the pressure side of the blade:

$$D_P = \frac{V_{inlet} - V_{min}}{V_{inlet}}$$

Where:

V_{inlet} = inlet blade velocity (relative)

V_{min} = minimum velocity on blade pressure surface

The total blade diffusion is simply the sum of the suction and pressure surface diffusion.

$$D_T = D_S + D_P$$

For minimum blade profile loss D_S should approach zero and D_T should not exceed a value of about 0.4.

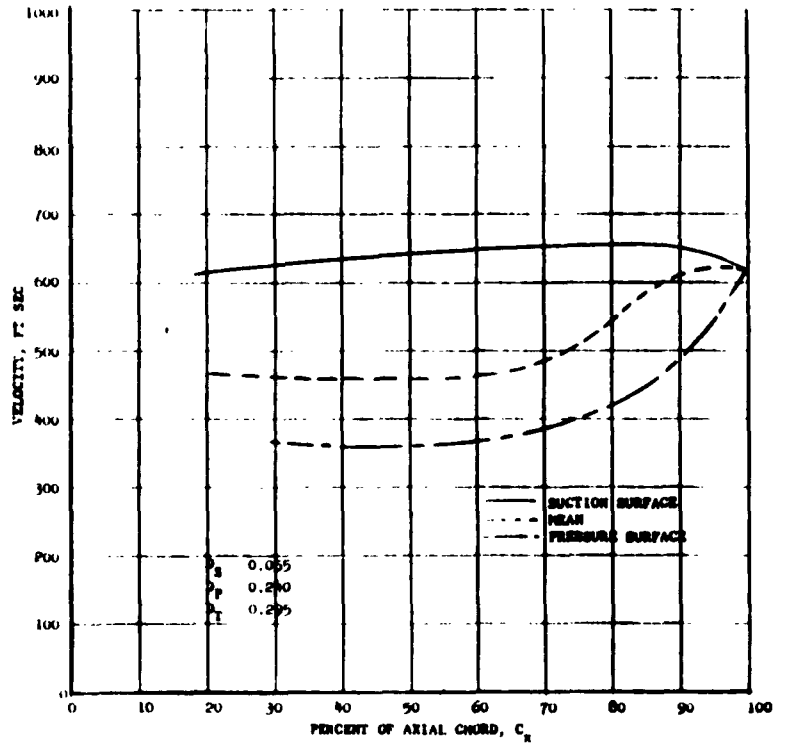
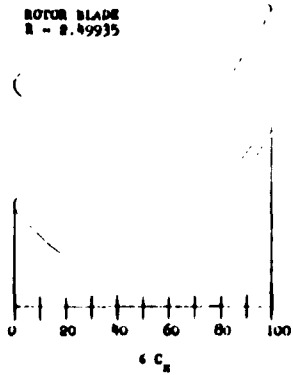
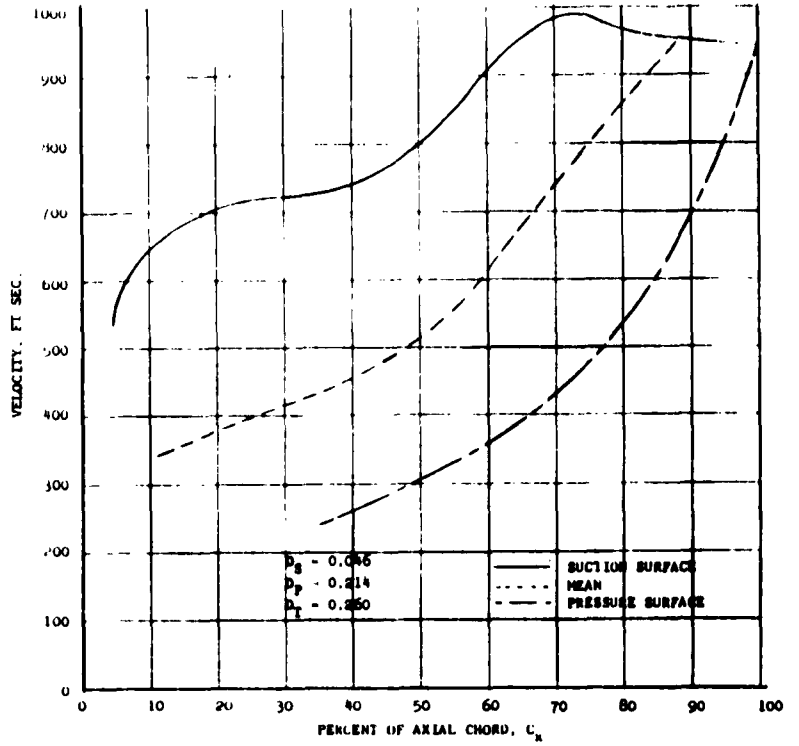
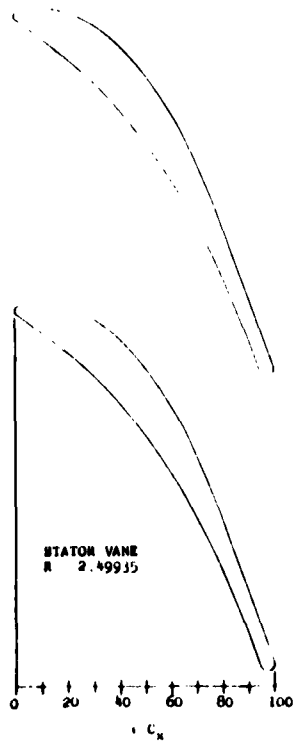
The final blade and passage shapes together with their velocity distributions and diffusion factors are given in Figures 23 through 27. Figure 28 shows the portions of the blades that are used in each of the turbine stages

Turbine Test Rig

The over-all design goal for the turbine test rig is twofold; first to provide a suitable vehicle to obtain aerodynamic turbine performance data, and second to provide a suitable vehicle to

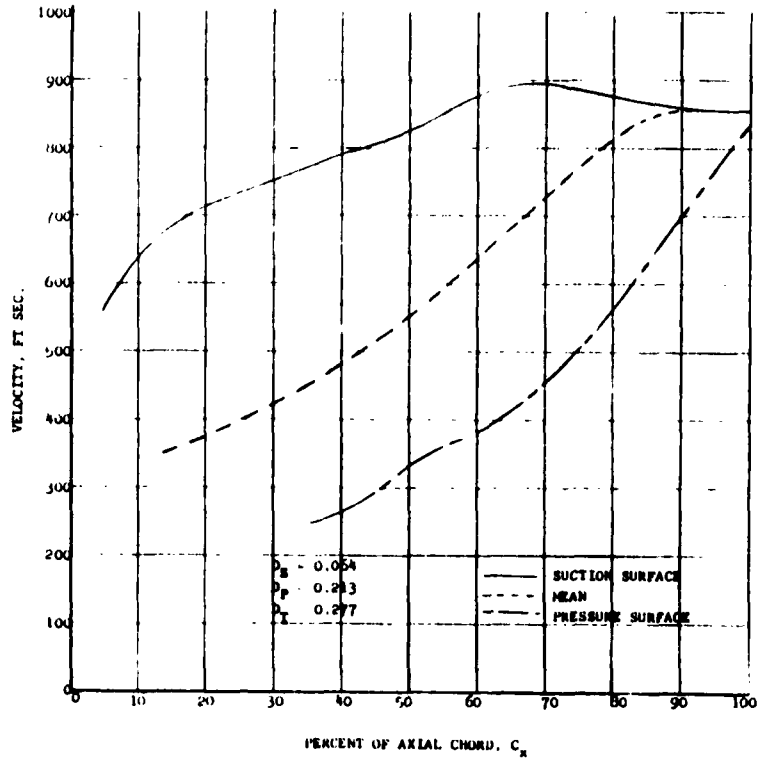
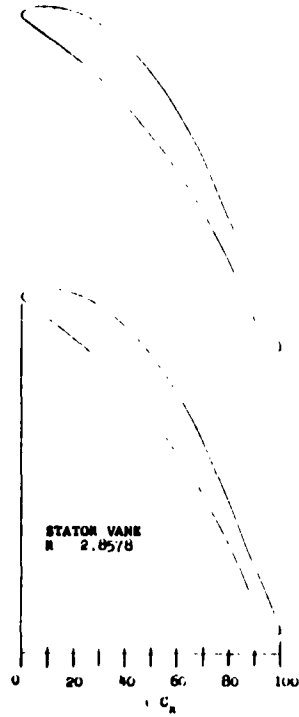
THE GARRETT CORPORATION
 AirResearch Manufacturing Division

Phoenix, Arizona



**BLADE SURFACE
 VELOCITY DISTRIBUTION**

**FIGURE 23
 SY-5396-R3
 Page 54**



ROTOR BLADE
R = 2.8578

BLADE SURFACE
VELOCITY DISTRIBUTION

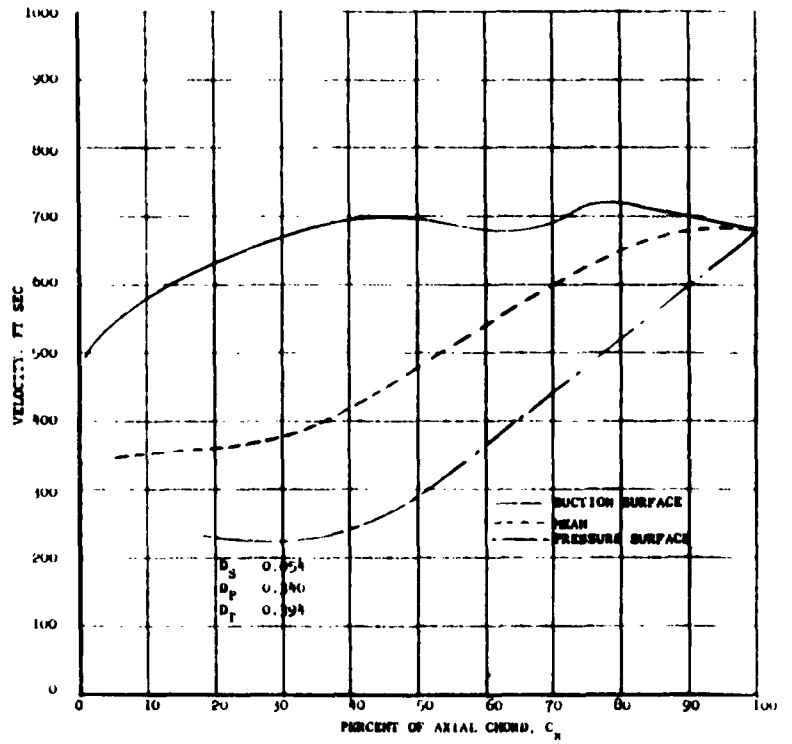
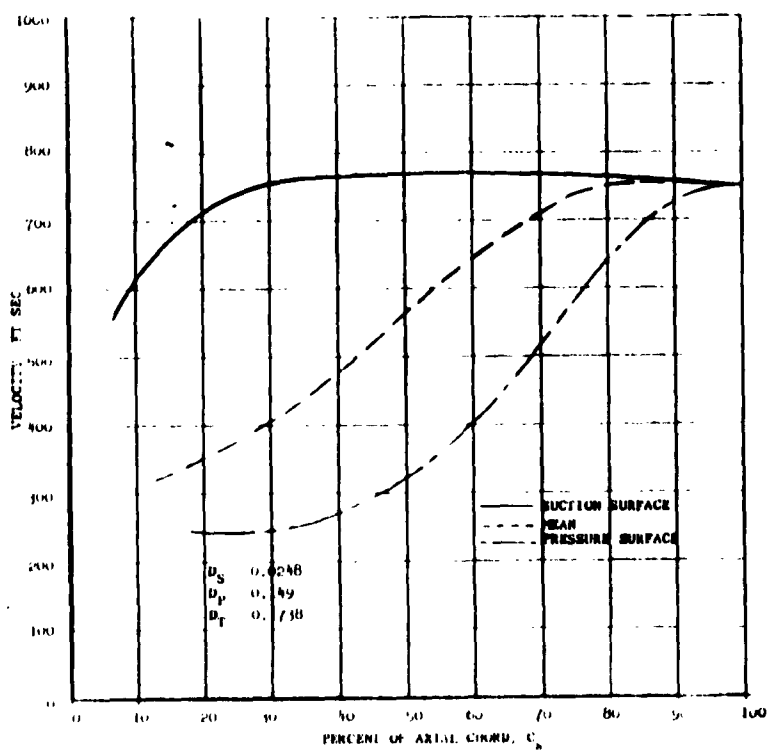
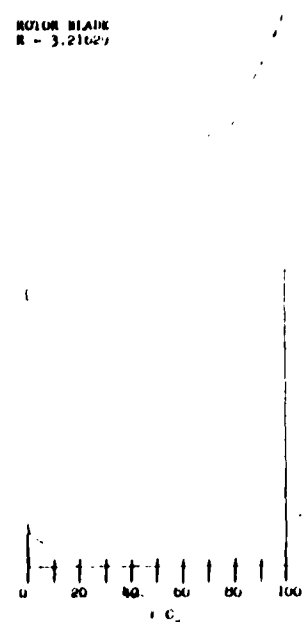
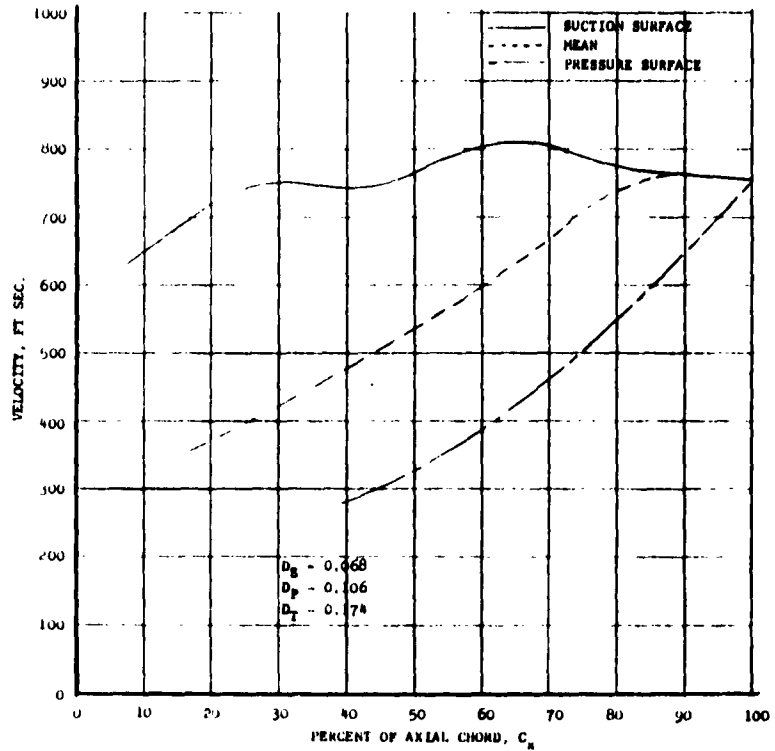
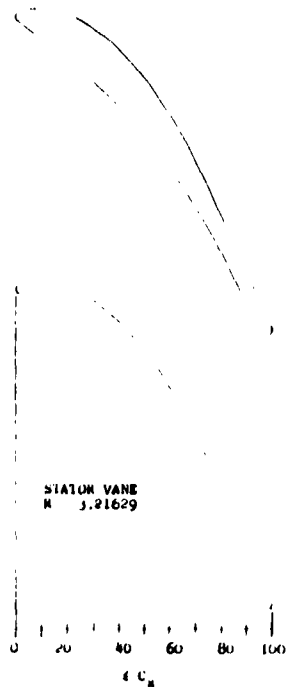


FIGURE 24
SY-5396-R3
Page 55

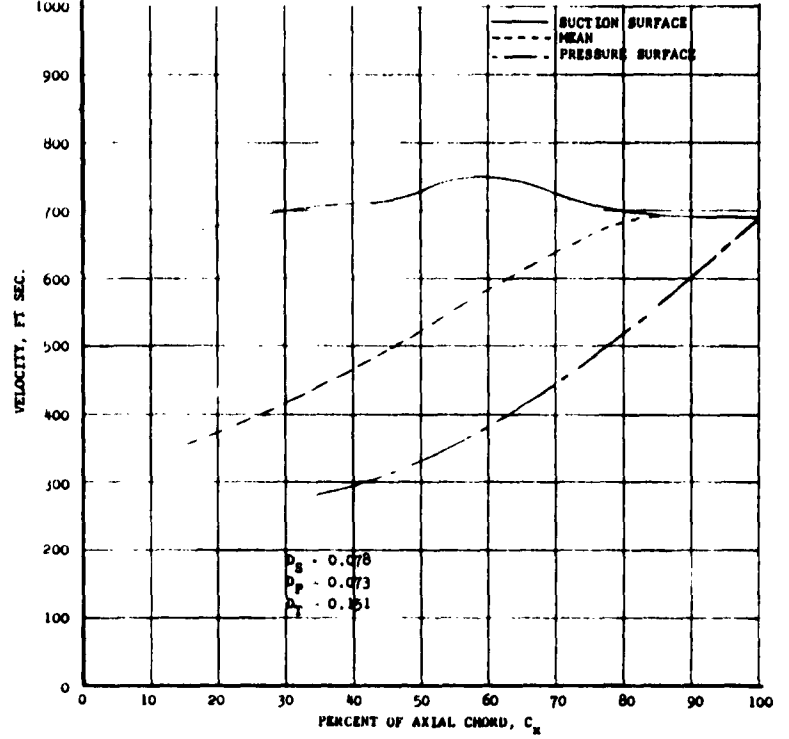
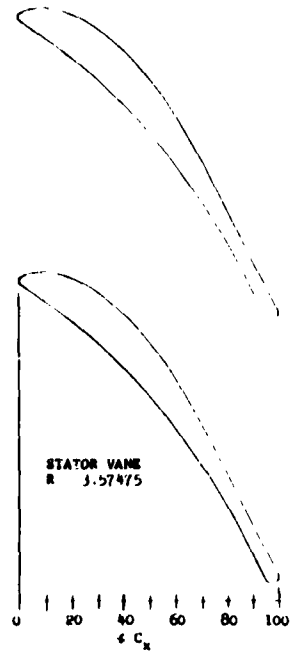


**BLADE SURFACE
 VELOCITY DISTRIBUTION**

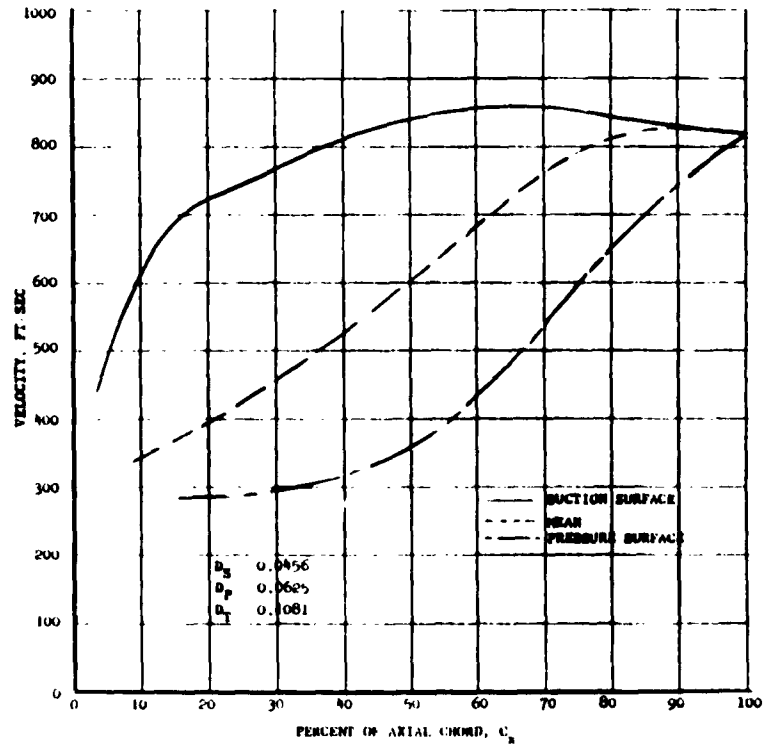
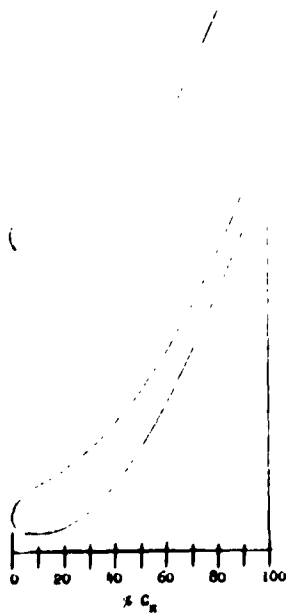
**FIGURE 25
 SY-5396-R3
 Page 56**



Phoenix, Arizona



ROTOR BLADE
R = 3.57475

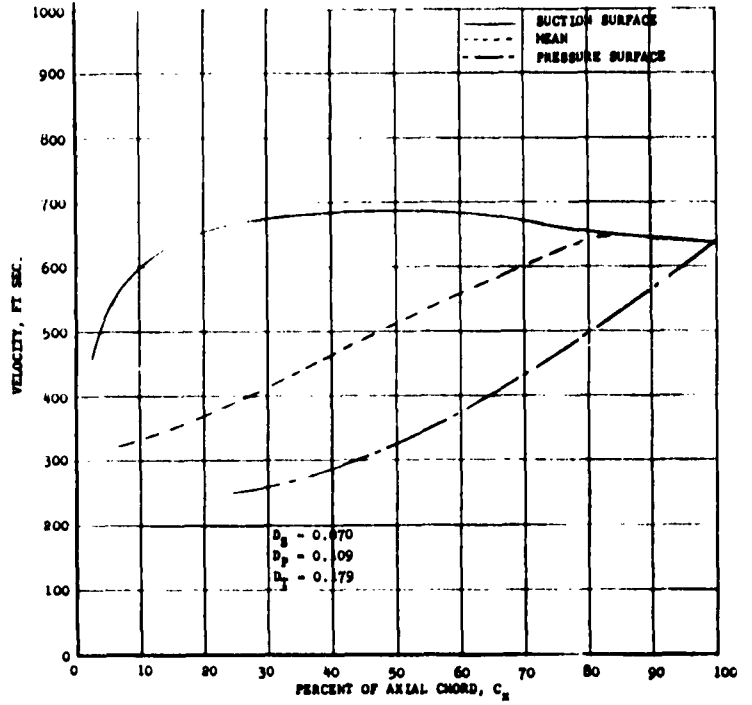


**BLADE SURFACE
VELOCITY DISTRIBUTION**

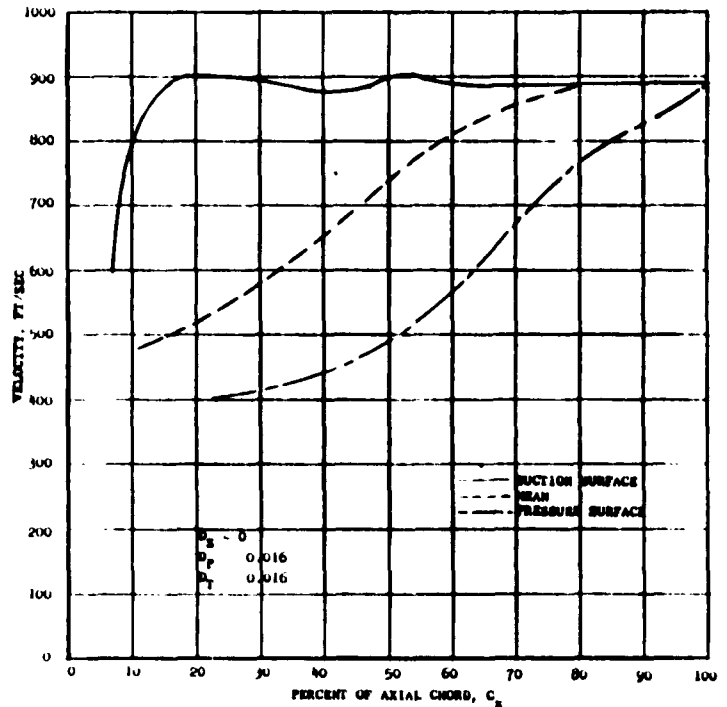
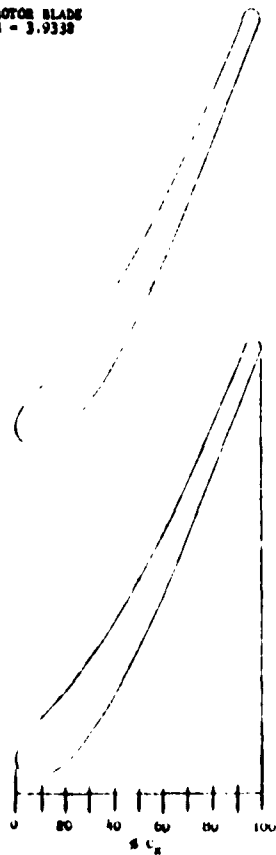
**FIGURE 26
SY-5396-R3
Page 57**



Phoenix, Arizona



ROTOR BLADE
 $R = 3.9338$



BLADE SURFACE
 VELOCITY DISTRIBUTION

FIGURE 27
 SY-5396-R3
 Page 58

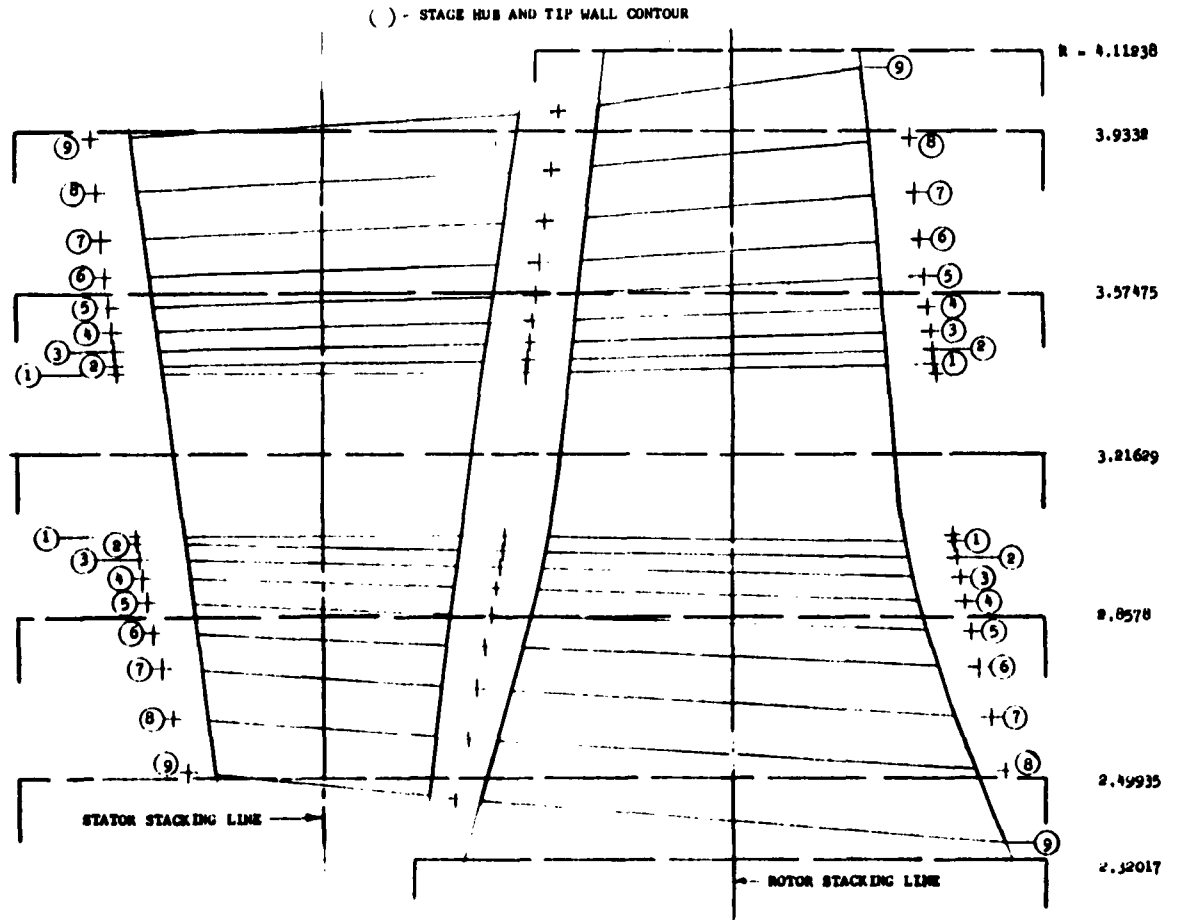


FIGURE 28
 TURBINE BLADE CROSS SECTIONS



evaluate blade erosion on candidate refractory materials within a reasonable period of time. In order to accomplish the first objective, satisfactory operation over a speed range from 19,000 to 29,000 rpm is required at inlet temperatures up to 1600°F. The design life of the unit was specified to be on the order of 100 to 1000 hours at 1600°F. This life expectancy was judged to be a satisfactory interval in which the aerodynamic turbine performance characteristics could be obtained.

To accomplish the second objective, refractory blading materials are required, with an extended life expectancy. Consequently the use of two types of materials was considered; ordinary high-temperature materials for the short term aerodynamic performance tests and refractory materials for the long term blade erosion tests.

Figure 29 shows the configuration of the test rig. The turbine rotor is cradled between two liquid potassium hydrodynamic floating journal bearings with the compressor brake overhung at one end. A potassium lubricated thrust bearing is also provided. The unit is capable of accepting one-, two-, or three-stage turbine configurations

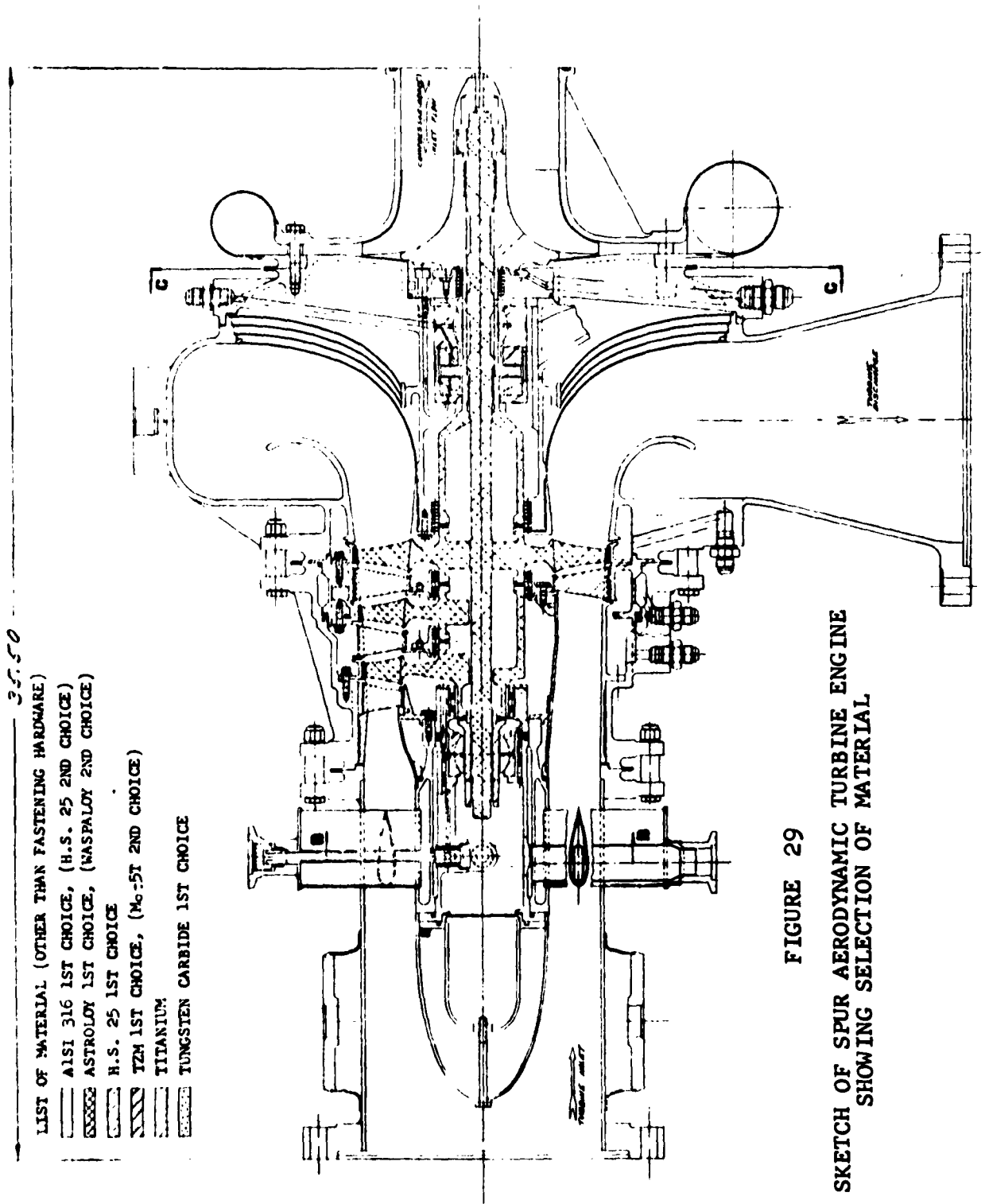


FIGURE 29

SKETCH OF SPUR AERODYNAMIC TURBINE ENGINE
SHOWING SELECTION OF MATERIAL



for testing. Provision has been made to collect and measure the amount of liquid removed at the exit of each stage. Detail analysis of the rig configuration is given in the following sections of this report.

Design and Stress Analysis

The structure of the rotor has been made as stiff as the mechanical design will allow. This has been done to provide as high a first critical speed as possible considering the system rigidly mounted. It is intended in this way to avoid any dynamic problems due to rotor flexibility as a consequence of having to encounter two critical speeds before attaining operating speed.

Close attention has been paid to the steady-state temperatures reached in the system as these are critical in regard to thermal expansions in the rotor, particularly in the region of the bearings.

Blade and Disc Design

Using Waspaloy as an initial, presently workable material, Figures 30, 31, and 32 show the geometric proportions of the final designs for the 7th, 8th, and 9th stage turbine discs for the test rig. The stress levels are shown



AirResearch Manufacturing Division
Phoenix, Arizona

300 KW SPUR TURBINE TEST RIG
SEVENTH STAGE TURBINE WHEEL
ROTATIONAL STRESSES AT 24,000 RPM
MATERIAL: WASPALOY

σ_t : TANGENTIAL STRESS, KSI
 σ_r : RADIAL STRESS, KSI

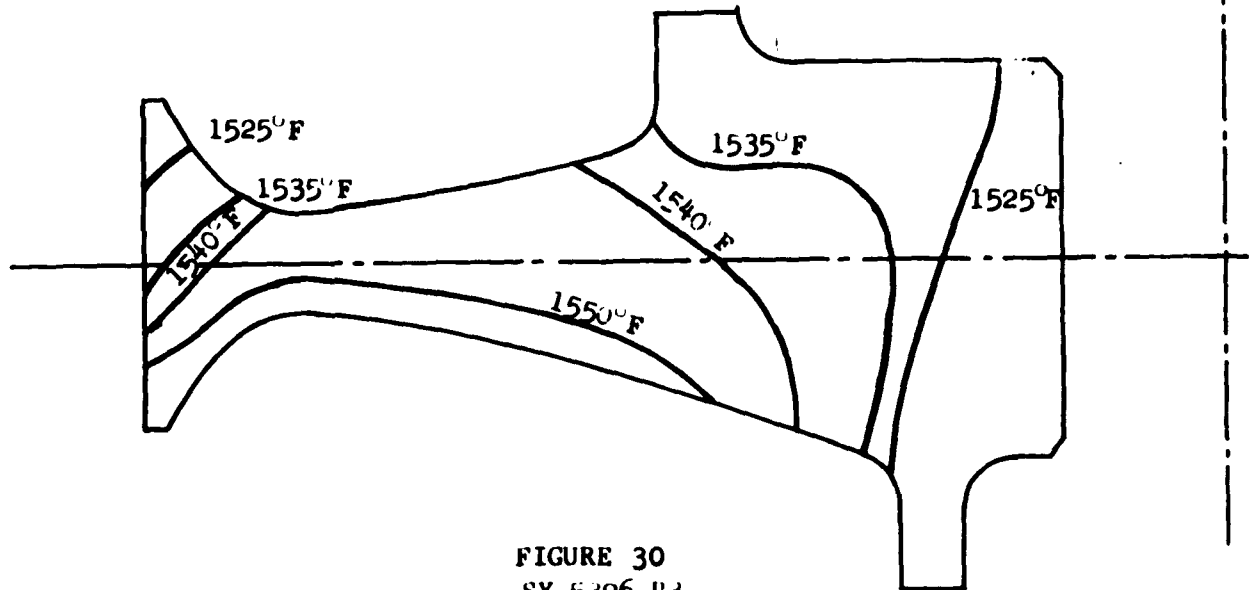
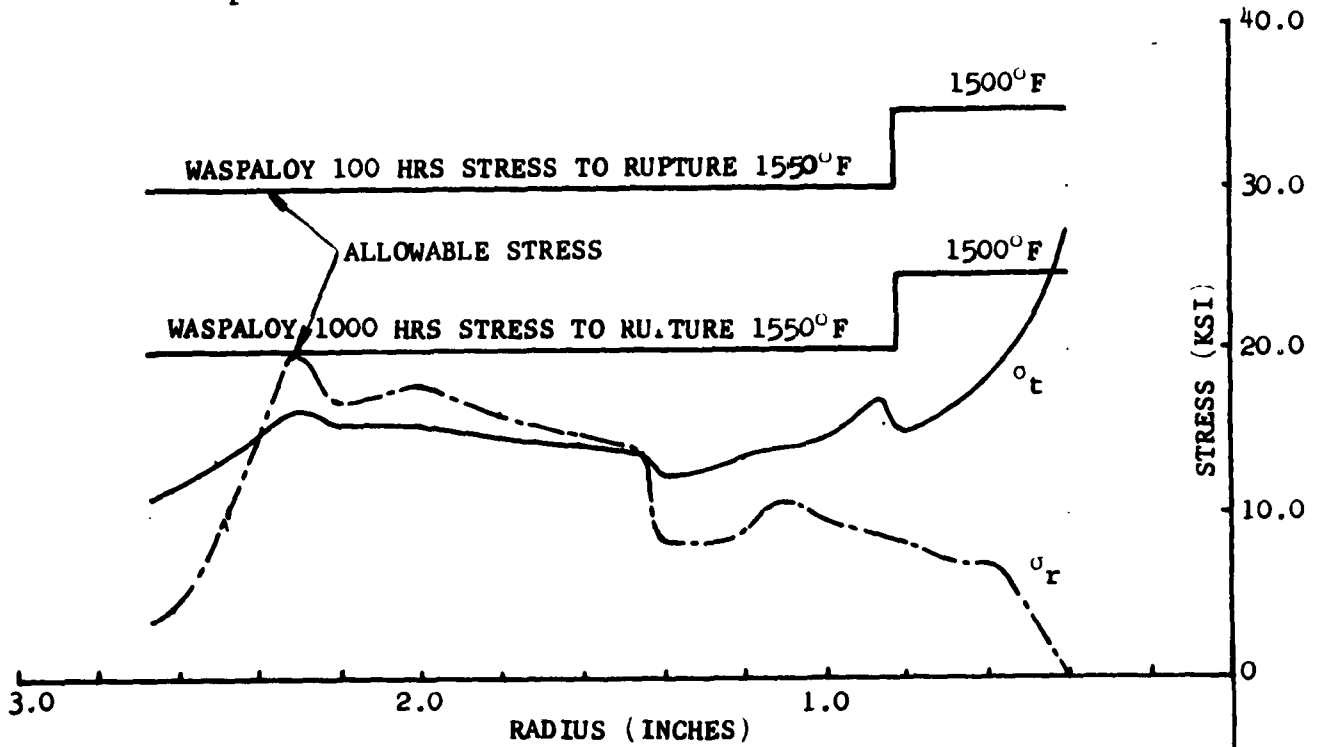


FIGURE 30
SY-5396-R3
Page 63



300 KW SPUR TURBINE TEST RIG
EIGHTH STAGE TURBINE WHEEL
ROTATIONAL STRESSES AT 24,000 RPM
MATERIAL: WASPALOY

σ_t - TANGENTIAL STRESS, KSI

σ_r - RADIAL STRESS, KSI

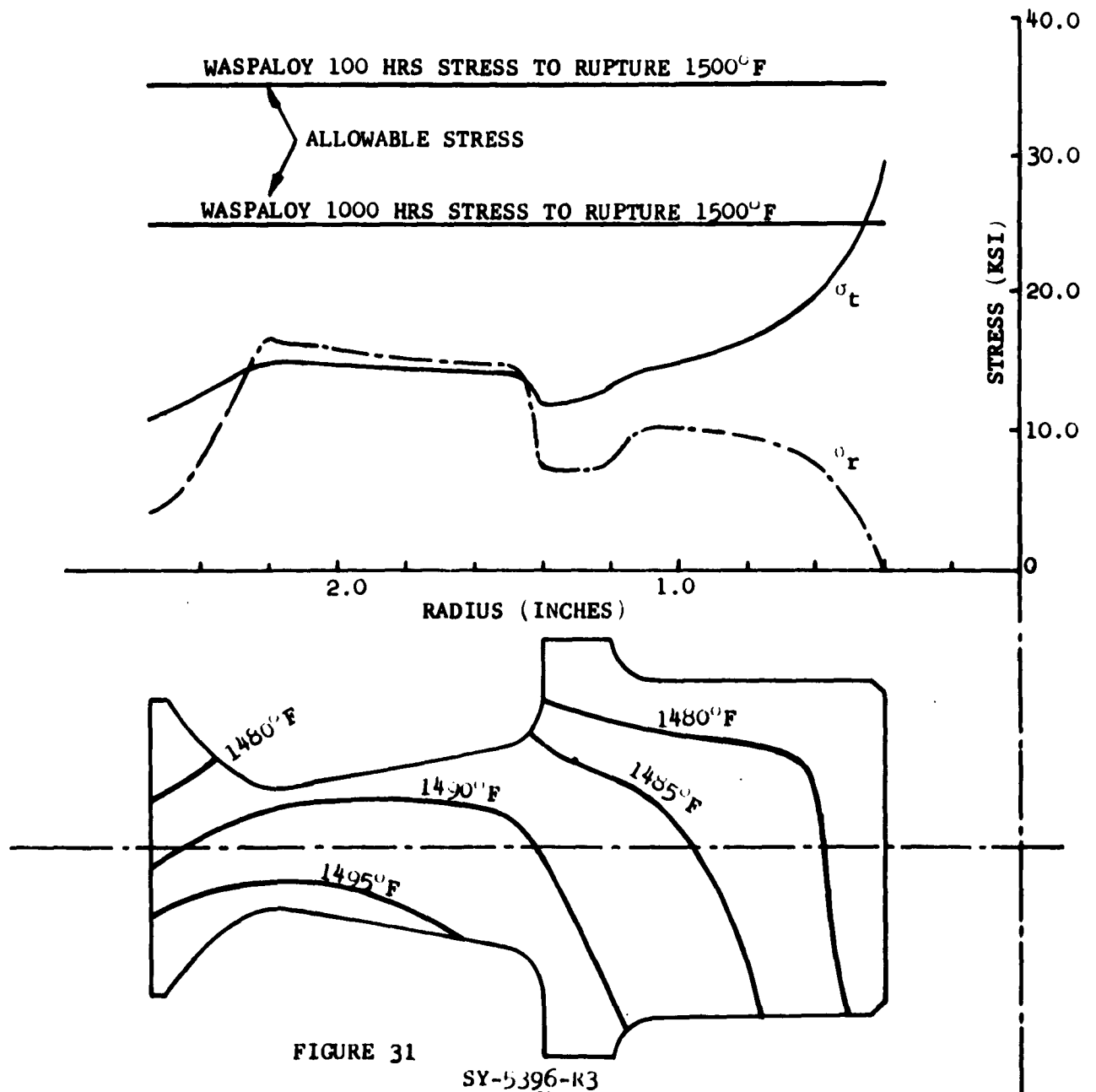


FIGURE 31



300 KW SPUR TURBINE TEST RIG
NINTH STAGE TURBINE WHEEL
ROTATIONAL STRESSES AT 24,000 RPM
MATERIAL: WASPALOY

σ_t TANGENTIAL STRESS, KSI

σ_r RADIAL STRESS, KSI

WASPALOY 100 HRS STRESS TO RUPTURE 1450°F

WASPALOY 1000 HRS STRESS TO RUPTURE 1450°F

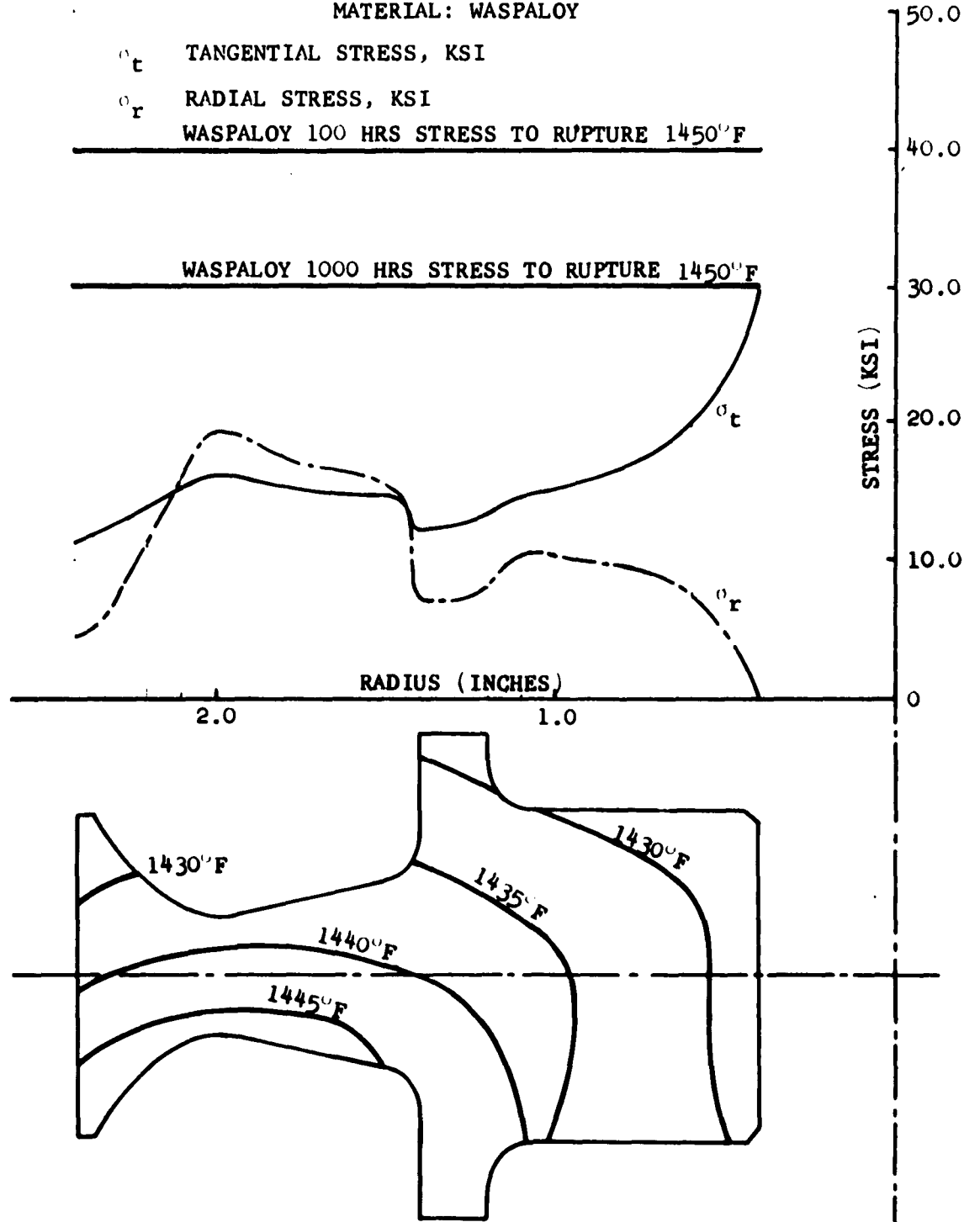


FIGURE 32
SY-5396-R3
Page 65



for an operating speed of 24,000 rpm. Shown plotted on the same curves are allowable stress levels for Waspaloy for 100 hours sustained operation. As can be seen, the operating levels will permit sustained running for considerably longer periods, although mass transfer may be the limiting factor with Waspaloy. The high stresses in the bore of the discs can be taken care of with yielding accomplished by overspeeding prior to use in the unit.

Plotted on the discs are temperature isothermals. These were obtained from steady-state thermal analysis of the rotor system.

The discs have also been stressed assuming TZM which has a density of 1.25 times that of Waspaloy but a strength capability 2.50 times that of Waspaloy. (100 hours stress to rupture at 1600°F.) Table VI presents the stresses of both the blade and discs with accompanying allowable rupture and creep stress for Waspaloy and TZM.

For any period of sustained operation, creep strength becomes the main criteria of comparative dependability, particularly in rotating assemblies. Thus, factors of safety on creep strength are shown. For TZM, factors are shown for 1000 hours sustained operation. These figures are based on information presently available and are discussed more comprehensively later in this report.



TABLE VI

300-KV SPUR TURBINE TEST RIG
DISC STRESSES AT 24,000 RPM
MATERIAL: WASPALLOY AND TZM (MOLYBDENUM BASE)

Stage and Temp of	Waspalloy			Molybdenum Base TZM		
	Average Tangential Stress (psi)	Maximum Stress (psi)	Allowable Stress 100 Hrs to 0.1% Creep Rupture (psi)	Average Tangential Stress (psi)	Maximum Stress (psi)	Allowable Stress (psi) Rupture 100 Hrs 0.1% Creep 1000 Hrs
7th 1550°F	16,000	19,200	30,000	20,000	24,700	78,000 72,000 74,000 64,000
8th 1500°F	15,700	16,650	35,000	19,500	20,500	80,000 76,000 74,000 72,000
9th 1450°F	15,500	18,000	40,000	19,300	24,300	84,000 79,000 74,000 74,000

Phoenix, Arizona

BLADE STRESSES AT 24,000 RPM
MATERIAL: WASPALLOY AND TZM (MOLYBDENUM BASE)

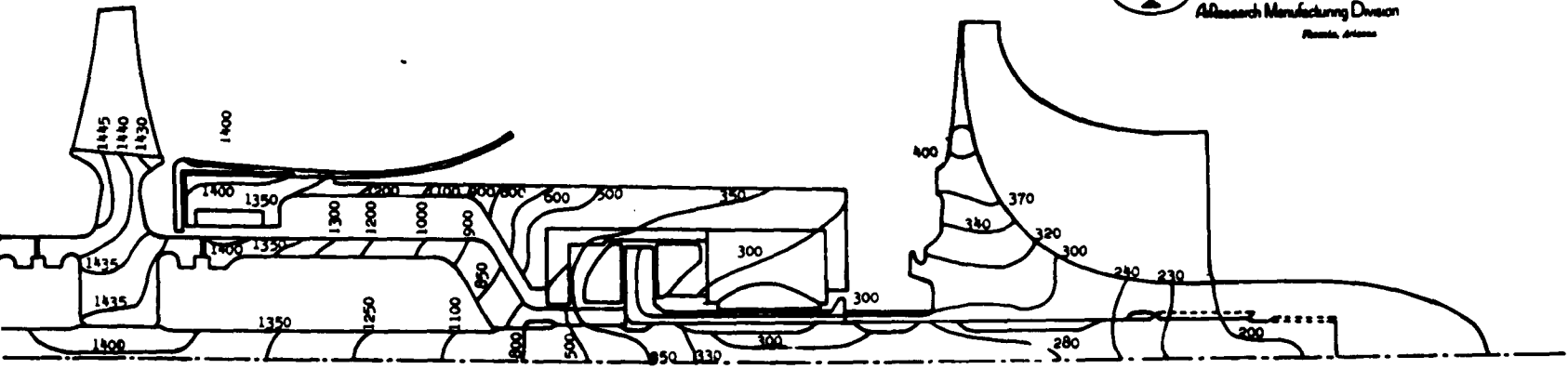
Stage	Waspalloy			Molybdenum Base (TZM)		
	Calculated Maximum Temp of	Maximum Stress Radial (psi)	Allowable Stress 100 Hrs to 0.1% Creep Rupture	Maximum Stress (Radial) psi	Allowable Stress Rupture 100 Hrs 0.1% Creep 1000 Hrs	0.1% Creep 1000 Hrs
7	1600	13,520	24,500	17,000	75,000 68,000 72,000 64,000	72,000
8	1500	14,400	35,000	18,000	80,000 75,000 74,000 72,000	72,000
9	1450	14,620	40,000	18,300	84,000 78,000 74,000 74,000	74,000



Temperature Analysis

Because of the nature of the working fluid and the projected sustained operation capabilities of the unit, it was felt that an accurate knowledge of the temperature distribution throughout the system was essential. For example, with the design as it is, an accurate distribution of temperature in the central tie-bolt and the turbine rotors is necessary to determine the differential growth at operating temperatures. This enables an accurate calculation of the tightening torque necessary at room temperature assembly to result in a reasonable bolt load at operating temperatures which can be maintained without detriment.

The results of the analysis (performed on the IBM 7090) are shown by isothermal plots on Figure 33. An inlet temperature of 1600°F was used. Two-phase heat transfer was considered, and the bearings were treated as heat sinks, maintained at a constant temperature of 300°F. Two separate studies were carried out to obtain this data. The forward bearing housing comprised one part of the total system while the rotor comprised the other. The heat being supplied to the bearing from each of these sources was evaluated. Separate studies were carried out with different rotor materials, i.e., Waspaloy and TZM. The resulting temperatures were closer together



1/ SPUR TURBINE TEST RIG
 STATE TEMPERATURE ANALYSIS
 TURBINE INLET TEMPERATURE
 FLUID TEMPERATURE 300°F
 ISOTHERMS REPRESENT °F

FIGURE 33

2



than originally anticipated. The compressor (brake) was included in order to determine just what flow of heat was being transferred to this end of the system from the turbine. Performance measurements necessitate the accurate determination of temperature rise in the compressor fluid. It is therefore necessary to minimize the heat transferred to the compressor from the turbine. The heat transferred from the turbine exhaust diffuser annulus to the compressor is minimized by means of a heat shield. The heat supplied to the compressor through the heat shield was calculated to be 1 hp with the present design.

The following data was deduced as a result of the temperature studies conducted:

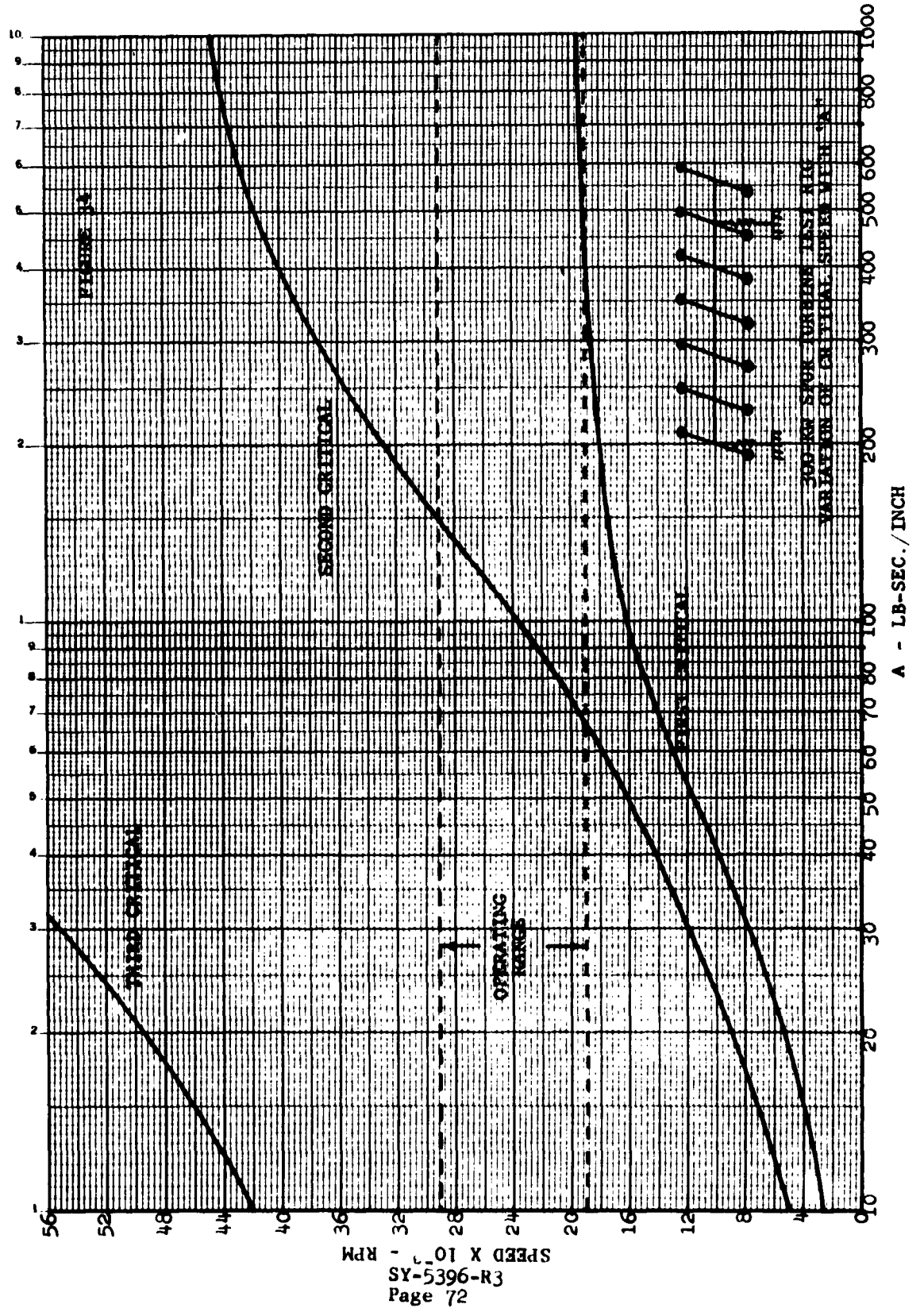
<u>Heat Source</u>	<u>Btu per hour</u>
Total heat flow to front end bearing	6571.0
Total heat flow to rear bearing (combined radial end thrust)	3401.0
Estimated frictional hp developed in both bearings (2 hp)	5094
Total input to all bearings	<u>15,066</u>



	<u>Btu per hour</u>
Fluid capability of heat removal assuming a flow rate of 3 gallons per minute	204 per °F
Limiting the temperature rise in the fluid to 100°F, fluid heat removal capability with a flow rate of 24 cu ft per hour	20,400

Critical Speeds

A design change from an overhung to a straddle mounted system was accomplished, mainly to increase the stiffness of the over-all system. Subsidiary benefits result from such a change, in the method of bolting the over-all assembly together and sealing. As far as the design would permit, the rotor stiffness has been kept to the maximum permissible. In this manner, all the flexibility is restricted to the bearings and larger rotor deflections are avoided. Figure 34 shows the results of a critical speed analysis conducted on the rotor as a plot of critical speed against the function "A". An interpretation of "A" follows:



A - LB-SEC./INCH



In the calculation, the bearing stiffness has been considered as a linear function of speed in the relation

$$K_i = K_i^* + A_i \omega$$

For a Sommerfeld Number ≤ 50 $K_i = \frac{W}{C}$

For Sommerfeld Numbers ≥ 50

$$K_i = 0.041 \left(\frac{L}{2R} \right) \left(\frac{W}{C} \right) S_i$$

$$S_i = \left(\frac{R}{C} \right)^2 \mu \frac{N}{P} \quad \text{and} \quad P = \frac{W}{2LR}$$

Where

K^* is the rotor stiffness in lbs per inch

W is the static bearing load in lbs

L is the axial bearing length in inches

D is the bearing diameter in inches

R is the bearing radius in inches

C is the bearing radial clearance in inches

μ is the lubricant viscosity in Reyns

N is the journal speed in rpm

S is the Sommerfeld Number $\frac{\text{Second} - \text{Rev.}}{\text{Min.}}$

P is the static load per unit projected area (psi)

i is subscript defining value at a particular speed



For a "nonfloating" type of bearing

$$K_i = 0.041 \left(\frac{L}{2R} \right) \left(\frac{W}{C} \right) \left(\frac{R}{C} \right)^2 \mu \frac{N}{W} LD$$

Using $C = 0.0014$ (actual test rig value) and maintaining an L/D ratio of 1.00, $L = 1.20$ in.

$$N = \frac{30\omega}{\pi} \quad \frac{R}{C} = 417$$

$$K_i = 39.6\omega$$

Thus for a "nonfloating" type of bearing $A = 39.6$. Reasoning from the design that the stiffness of a full floating type of bearing will be a maximum of half that of the nonfloating type - since the latter with two films in series can be considered analogous to stiffnesses of springs in series - the value of "A" should be in the regime of 15.0. Looking at the curves one can see in this region the two criticals encountered are at approximately 5000 and 10,000 rpm with the third critical completely out of the operating range. Since the operating range is between 19,000 and 29,000 rpm, the half-speed whirl frequency, which comes in at twice the critical speed values and persists until about three times this value, may be present. However, tests run on a similar rig using a floating type bearing but with oil as a lubricant indicated no deleterious effects from oil whip.



The assumption has been made that the fluid film varies linearly with speed, and this stiffness has been combined with the rotor stiffness to calculate the critical speed of the system. This approximation has been found to give reasonable correlation.

Bearing Design

The finalized turbine test rig design incorporates a radial bearing of the full floating hydrodynamic type. The thrust bearing is also of the hydrodynamic variety. The bearing is installed in spherical seats to accommodate possible misalignment and/or shaft eccentricities. In view of the problems associated with turbulent operation (losses and possible physical damage to the surfaces), it is believed that one feasible method of eliminating completely or drastically reducing the turbulence is to use a free floating ring design. This consists in allowing the bearing ring to rotate at approximately half speed by adjusting the O.D. and I.D. running clearances. It can be shown that for the same clearance a reduced Reynold's number results due to a reduction in relative velocity. It is evident that for a given shaft radius, kinematic viscosity and bearing clearance, the reduced surface velocity would raise the threshold for turbulent operation.



Selection of Materials

Tentative material selections are:

Rotor and tie bolt (Astrolloy alternate, with molybdenum base alloy in a subsequent turbine)	Waspaloy
Turbine housing (HS 25 alternate)	AISI 316
Stators	HS 25
Bearings	TZM and Tungsten Carbide

Turbine Test Facility

During the last quarter substantial progress was made on the supporting loop and subsystems for the turbine test rig. Design work remaining to be done is mainly concerned with controls and instrumentation. Work is in progress in all other areas: piping loop perspectives are being generated and will be used in the piping flexibility analysis; vacuum and argon subsystem studies and layouts have been made and details are in progress; controls and instrumentation investigations continue and schematics are being generated.



Visits were made to MSA Research in Callery, Pennsylvania, and to General Electric Re-entry Systems Division in Evendale, Ohio. Information of a general nature with respect to liquid metal loop design criteria, argon and potassium purification, and instrumentation was obtained at MSA. The trip to General Electric was made specifically to investigate the feasibility of the argon-efflux method of measuring liquid and vapor potassium pressures, and generally to see and obtain information concerning the proposed turbine test loop and facility. A side trip was made to Ohmart Corp., Cincinnati, for information pertaining to nuclear radiation type level gauges suitable for liquid metal.

Many vendor contacts have been made on all items to be purchased and the information obtained is being continuously evaluated. On components where information from qualified vendors is judged inadequate, vendor contact is continuing. Obtaining adequate information and suitable proposals from qualified vendors has been a major problem.



Significant progress in the instrumentation area has been effected. Use of the argon efflux type pressure measuring devices is planned where pressure measurements of high accuracy are required. Wiancko twisted bourdon tube transducers will be used in some less-critical areas. Nuclear-type liquid level gauges offer significant advantages and their use is planned. Some of these advantages include the ability to keep working parts cool, the ability to be reused, the elimination of parts in contact with liquid metal, and a higher order of accuracy. Three vendors have been contacted and requested to submit proposals on suitable units. Venturis for measurement of potassium vapor and argon flow have been designed. The use of Geminol thermocouples (surface type) and adiabatic walls is planned for measurement of critical temperatures, but resistance-type devices are still being studied.

Work remaining includes: piping flexibility analysis, for which a computer program is available; completion of various structures and supports for piping, walkways, etc.; continuation of detail and checking work on various components; and continuation of control system, instrumentation, and graphic panel work.



2. Turbine Material Erosion Tests, Task 2.2.4.2.2

Fabrication of the components for the loop was essentially completed during the previous quarter. Assembly of the loop was accomplished as shown in Figures 35 and 36 (Photographs taken prior to start-up of the loop) The loop was filled and testing was commenced in December.

After approximately 20 hours of operation the main heater failed. By increasing power to the auxiliary line heaters it was possible to continue operating at reduced temperature (1000°F). After 26.6 hours of operation the brushes on the drive motor failed, terminating the test. The loop was subsequently drained and the test section removed and opened. Figure 37 shows the test section immediately after opening. After decontaminating the unit, the specimens were removed and examined. No visible erosion was apparent on any of the specimens. Weighing the specimens also indicated that no discernible erosion occurred. A complete analysis of test results has not yet been made; however, preliminary observations indicate that for the materials tested the erosion problem in potassium at elevated temperature is less severe than in water under conditions of similar impact velocity, stream diameter, and nozzle-to-specimen clearance. A complete analysis of test results will be presented in the final report.

THE BARRY CORPORATION
AirResearch Manufacturing Division
Phoenix, Arizona

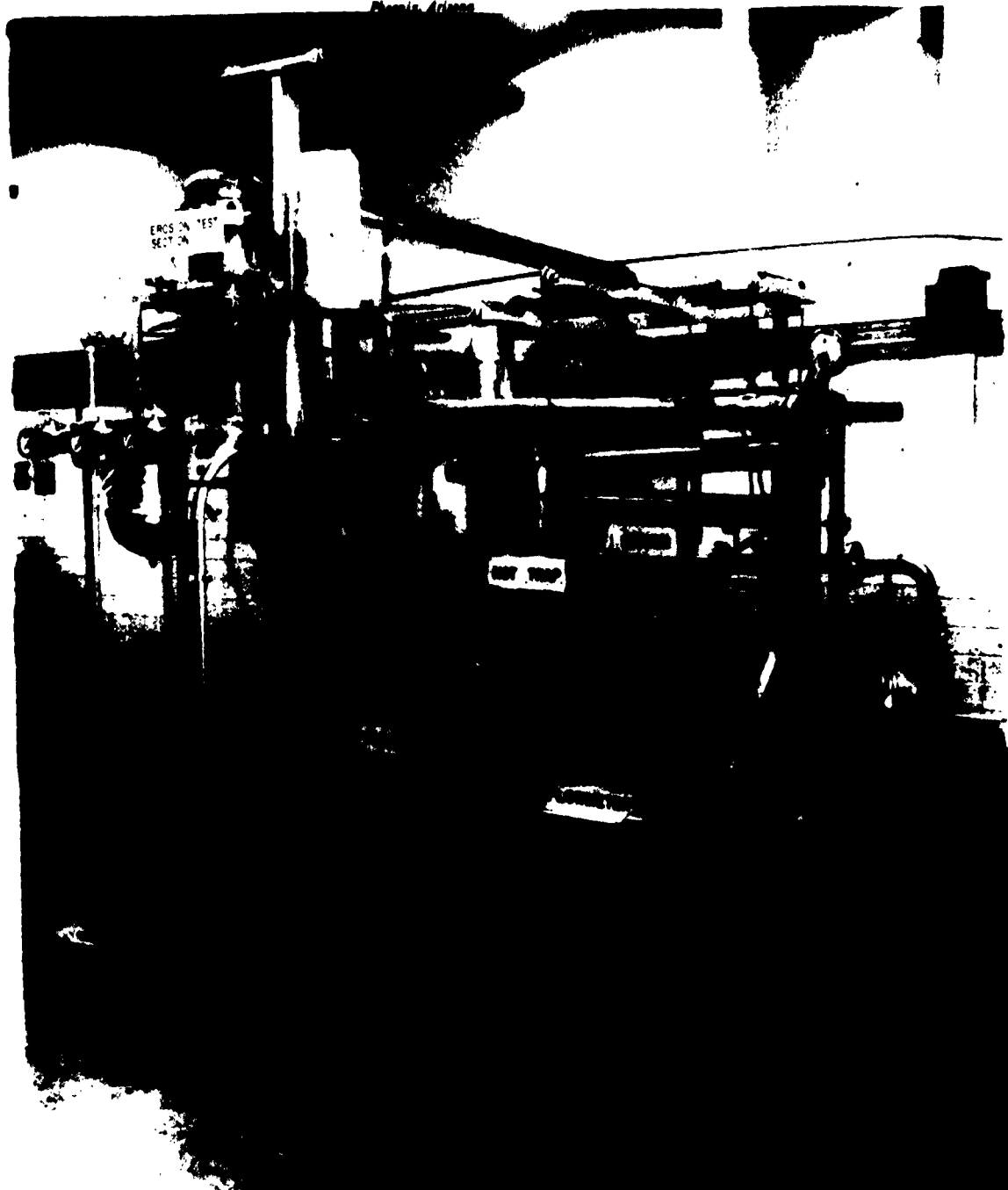


FIGURE 35
EROSION TEST RIG

SY-5396-R3
Page 80

THE GARRETT CORPORATION
AirResearch Manufacturing Division
Phoenix, Arizona

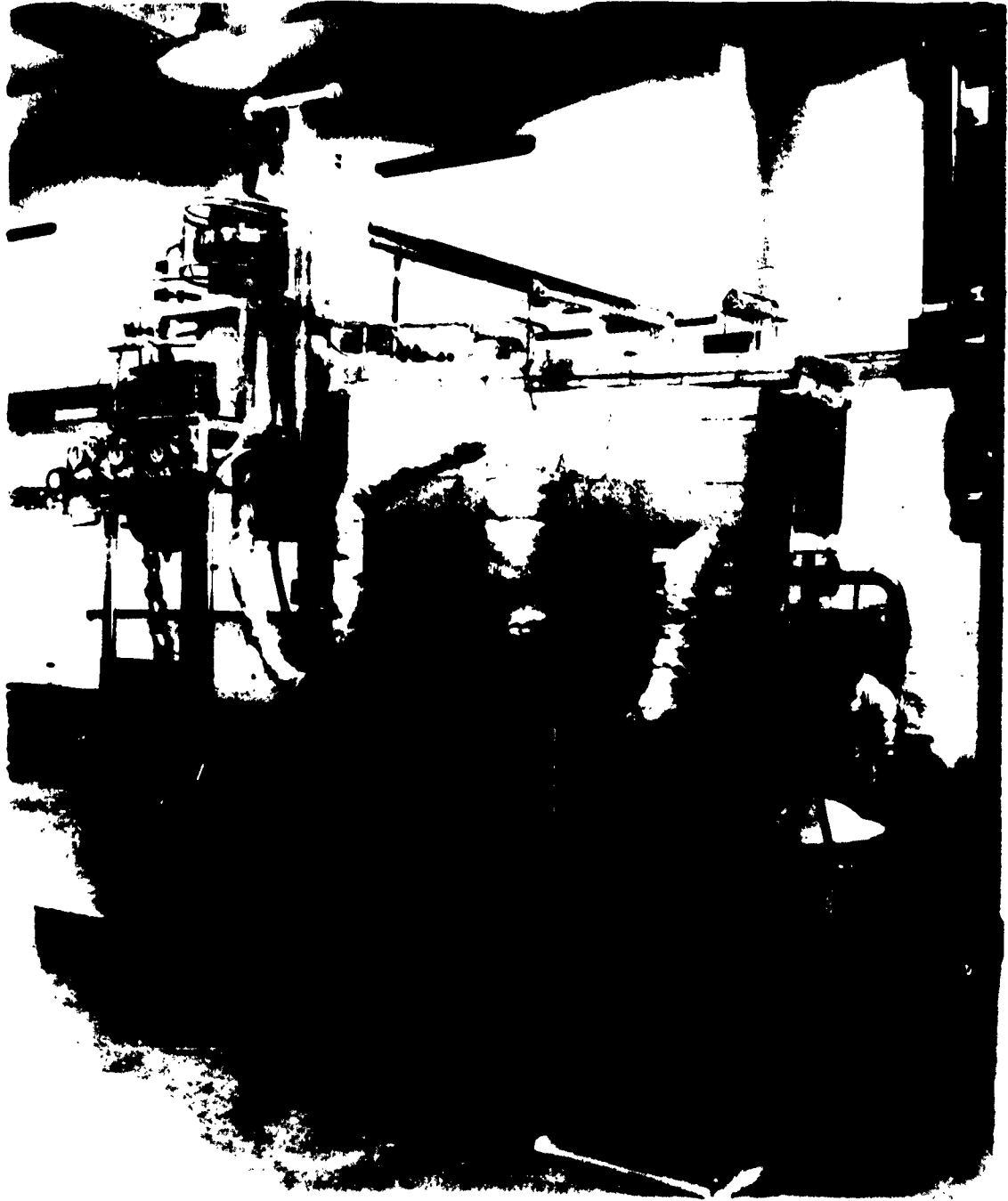


FIGURE 36
EROSION TEST RIG

SY-5396-R3
Page 81

THE SASETTI CORPORATION
AirResearch Manufacturing Division
Phoenix, Arizona



FIGURE 37
EROSION TEST SECTION



E. Generator Development

1. Generator Design, Task 2.2.4.3.1

The generator design has been completed through completion of the layout drawing. The following table presents the basic generator operating and performance data.

TABLE VII

Power rating (kilowatts)	
at 1.0 power factor	467
at 0.75 power factor lagging	350
Rated terminal volts	120/208
Rated line current (amps)	1298
Winding connection	Wye
Rated frequency (cps)	3200
Minimum rated power factor (lagging)	0.75
Liquid metal coolant	Potassium
Approximate coolant temperature (°F)	600
Efficiency (1.0 P.F. - rated current)	91.5%
Efficiency (0.75 P.F. lag - rated current)	89.5%
Weight	406.
Over-all length (inches)	16.6
Over-all diameter (inches)	18.5

Construction Summary

The stator is hermetically sealed to permit operation with a vacuum in the cavity. This sealing will exclude any surrounding fluid and prevent damage to stator components by the potassium vapor existing in the rotor



cavity. The seal between the stator and the rotor is a high purity alumina cylinder supported by columbium end pieces. The external frame seal is a thin columbium shell which encloses the columbium end to Hiperco 27 frame mechanical joints and the field coil cover joints.

Table VIII contains a summary of the materials to be used in the SPUR generator. This table has been consolidated to group all parts utilizing the same materials. Those parts which are exposed to potassium liquid or vapor are so indicated.

TABLE VIII
SUMMARY OF CONSTRUCTION MATERIALS

<u>Component(s)</u>	<u>Material</u>
Rotor ^{1,2}	H-11 Steel
Coolant tubes ²	Columbium alloy, B-33
Seal end supports ¹ , Frame mounting brackets ¹	Columbium alloy B-33
Ceramic seal ¹	Alumina (99.5% pure)
Frame parts, punchings	Hiperco 27 alloy
External frame seal	Columbium alloy, B-33
Current carrying members	Copper, Nickel-plated
Slot liners, terminal insulators	Alumina (99% pure)
Wire insulation	Glass-served-silicone impregnated
Field coil insulation	Mica sheet
Punching insulation (interlaminar)	Aluminum-ortho-phosphate
Stack end insulation	Mica sheet

¹Exposed to potassium vapor

²Exposed to liquid potassium



Armature Winding

The armature winding is a three-phase wye-connected fractional slot winding with eight parallel paths and five series turns per phase. The effective phase belt grouping is sixty degrees.

Armature Slot

There are eight conductors per slot with the top and bottom coil sides composed of four parallel conductors. The conductors are nickel plated rectangular copper wires insulated with filament type glass yarn impregnated with a silicone varnish. Wire insulation thickness is approximately 0.0055 inch per side. The silicone varnish is used to facilitate winding of the armature and will burn off at operating temperatures. Slot liners will be "U" shaped channels made from 99% pure alumina to assure adequate heat transfer and mechanical strength.

Armature Stack

The stator stack is a laminated assembly of Hiperco 27 punchings with interlaminar insulation. The punching thickness is 0.004 inch with an 0.00018 inch thick aluminum-ortho-phosphate coating on each side. The stacks are held together at the outer diameter by axial welds, the punchings first being aligned to insure minimum deviation of the slot contours. Final machining of the outer diameter is then completed, and the stack is shrunk into the frame.



Field Winding

The field coil is located in the stator between the armature stacks. It consists of two coils connected in series. One coil of 120 turns is located in the region between the a-c windings and the cooling tubes. The other coil of 208 turns is located outside the cooling tubes. The conductors are nickel plated rectangular copper wire with the same insulation as specified for the armature winding. Laminated mica sheet is used for insulating the coil from the frame, cooling tubes, and armature conductors.

A-C Stator Winding Connections

In most a-c generators, parallel connections are made by placing paralleling leads around and behind the coil extensions. However, with 60 degree phase belts, this space must be reserved for the connections between coil groups. Paralleling or bus rings were therefore placed at the anti-drive end of the generator as concentric rings. There are four rings; the three inner rings are line connectors and the outer ring is the neutral connector.

Ring busses were chosen because of the greater ease of supporting them over other types. The bus location simplifies the connections to the external generator terminals.



Generator Terminals

Standard high-temperature insulated terminals are used for the d-c field leads. The leads are brought through alumina insulators in the frame and are joined to the terminals. The terminals are brazed to the frame external seal. Threaded studs are provided for the external connections.

Ceramic Stator Seal Assembly

The SPUR generator will operate with potassium vapor in the rotor cavity. A seal is required to isolate stator parts which are incompatible with this vapor. The seal for this purpose consists of a 99.5% pure alumina cylinder with columbium end supports.

Rotor

The SPUR generator rotor is constructed from a single forging of H-11 steel, AISI 4340. All poles are integral with the core to provide the greatest assurance of mechanical integrity.

Cooling is provided by passing liquid potassium through an axial hole in the core of the rotor. At each pole group the fluid is diverted to pass into the poles through parallel radial passages, and then back to the central passage. Flow is from the antidrive end.



The pole sides are contoured to remove excess material below the pole tips and to reduce core stresses. The pole faces are slotted to reduce eddy-current losses.

Weight Breakdown

Rotor		125.33
Stator seal	5.64	
Frame seal	7.68	
Frame	83.34	
Frame end (drive)	18.28	
Frame end (antidrive)	19.68	
Stacks, slot liners, wedges	72.02	
Coolant tubes and plenums	12.47	
Armature wire (insulated)	17.58	
Field wire (insulated)	31.22	
Field coil insulation and fins	3.69	
A-c output connections and terminals	9.19	
Stator Total	<u>280.79</u>	<u>280.79</u>
Generator Total		<u>406.12</u> pounds



Electrical Performance

(a) Saturation Characteristics

Generator no-load and load saturation characteristics are shown in Figure 38. Load curves are given at minimum speed (i.e., the worst condition) for both rated power factor and unity power factor loads. The curve intercepts with the horizontal rated voltage line giving the magnitude of field mmf required for the respective operating conditions.

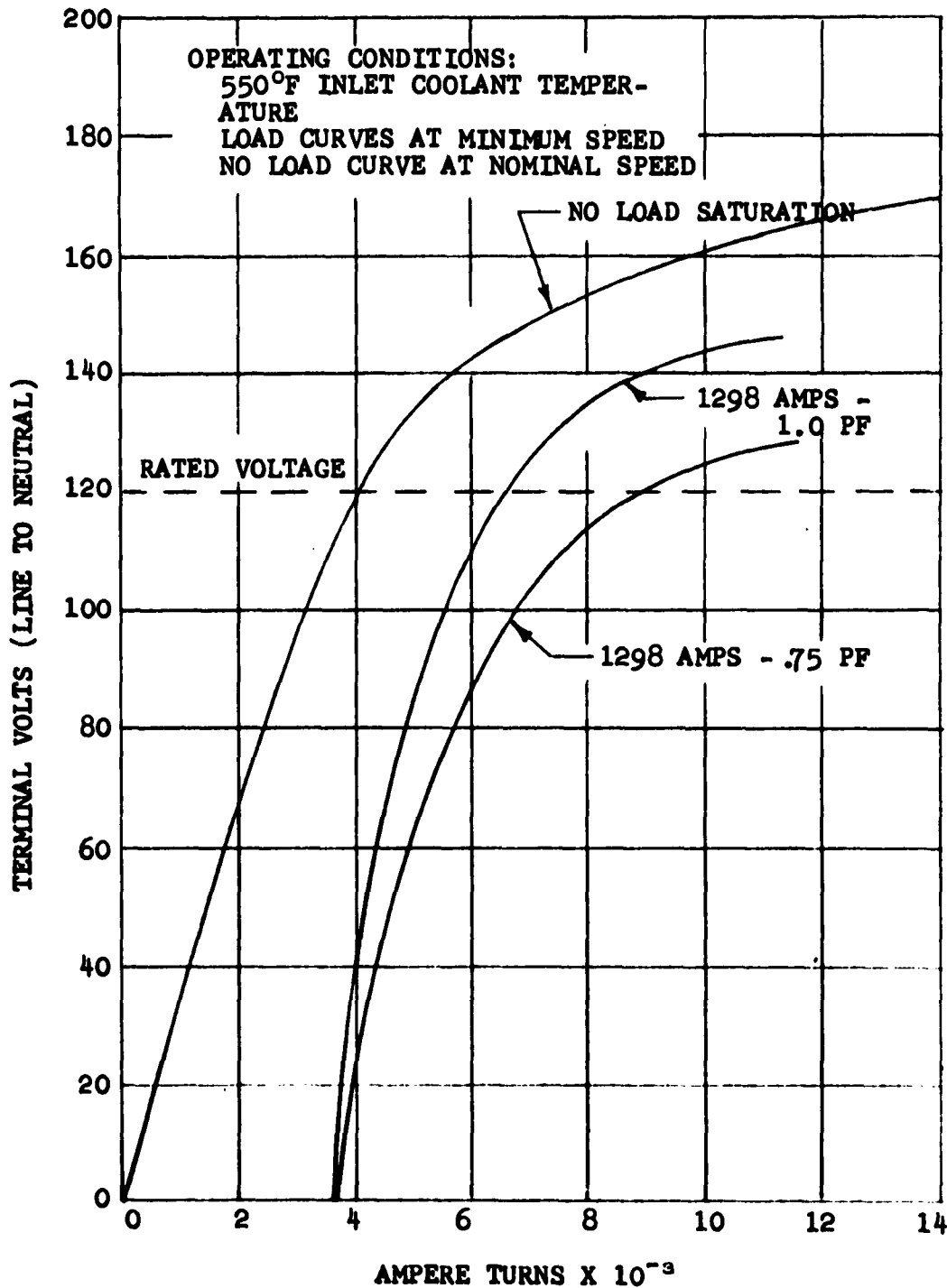
(b) Current Densities

Current density in units of amperes per square inch are set forth below for the armature and field coil windings under rated load conditions.

Winding	
Armature	Field
9100	4450

(c) Magnetic Circuit Flux Densities

<u>Area</u>	<u>Kilolines per inch²</u>
Frame	115
Armature core	70
Armature teeth	120
Air gap	56
Rotor core	86



NO LOAD AND LOAD SATURATION CURVE

FIGURE 38

(d) Generator Impedances

All values are given in ohms.

R_a	A-c armature winding resistance at 25°C	0.000582
X_L	A-c armature leakage reactance	0.0281
R_f	Field winding resistance at 25°C	1.65
X_d	Direct axis synchronous reactance	0.0875
X_q	Quadrature axis synchronous reactance	0.051
X'_d	Direct axis transient reactance	0.0378
X''_d	Direct axis subtransient reactance	0.0378
X_2	Negative sequence reactance	0.0445
X_0	Zero sequence reactance	0.00326
R_2	Negative sequence resistance	0.000582
R_0	Zero sequence resistance	0.000582

(e) Generator Power Losses

A breakdown of power losses for the final design is presented below. Losses are given in kilowatts and as a percentage of the total loss.



<u>Loss</u>	<u>Kilowatts</u>	<u>Percent</u>
Field copper	4.20	10.26
Armature copper	8.16	19.92
Armature teeth	6.62	16.16
Armature core	13.04	31.82
Rotor pole face	7.21	17.62
Rotor windage	<u>1.72</u>	<u>4.22</u>
	40.95	100.00

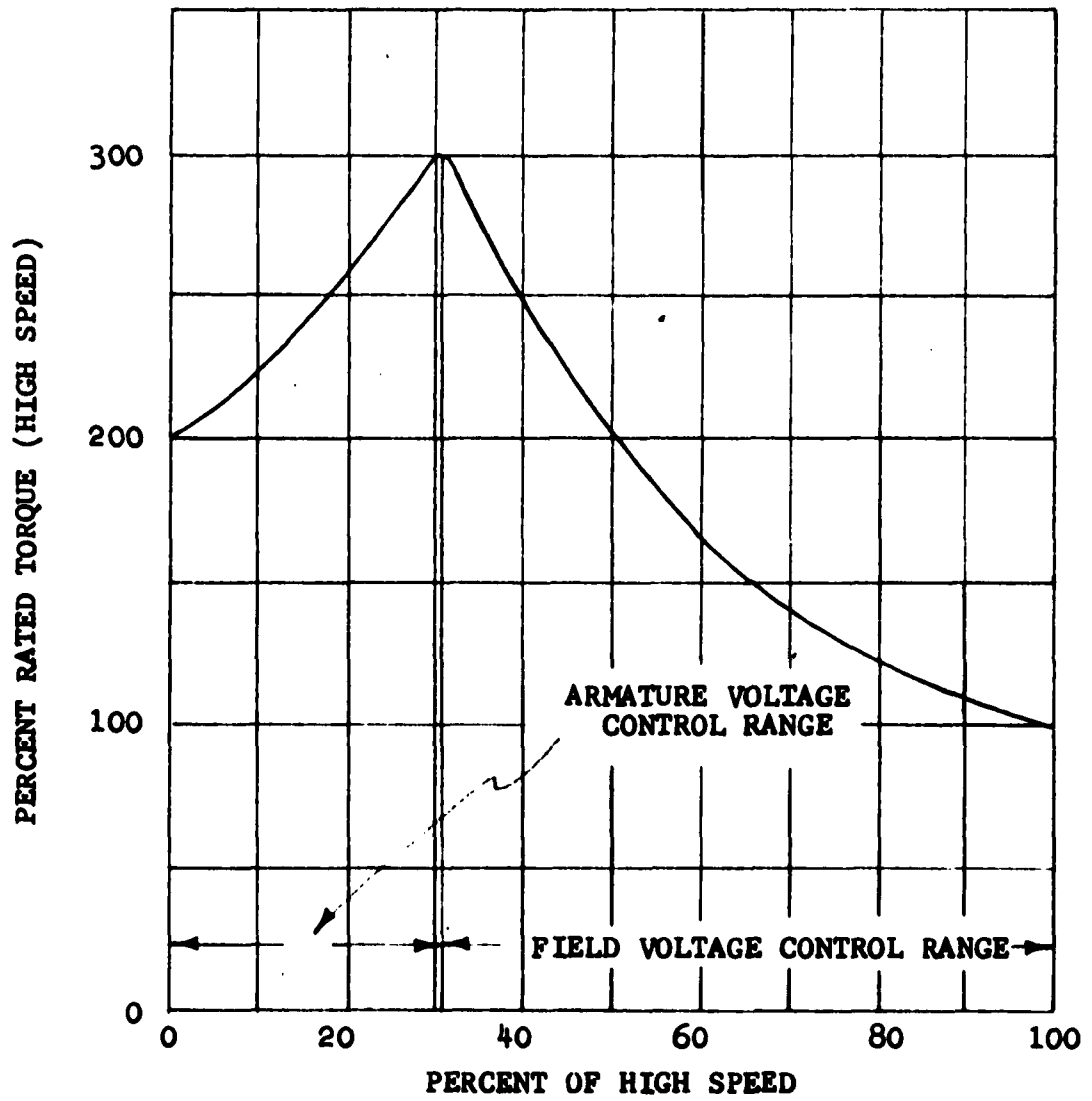
2. Generator Test Rig Design, Task 2.2.4.3.2

The objective of this task is to design a test rig for conducting electrical and mechanical tests on the SPUR a-c generator. This task includes design analyses, layout drawings and specifications for the test rig components.

Drive Stand

Detailed operating and control procedures for the 700 horsepower Rectiflow drive have been completed. Estimated part speed torque characteristics are shown on Figure 39.

The design and selection of the drive system components (drive stand, a-c starter, control cabinet, and operator's panel) was completed.



CONTINUOUS TORQUE RECTIFLOW DRIVE

FIGURE 39

SY-5396-R3

Page 93



Generator Coolant System

Generator coolant systems were investigated using potassium and using a nonmetallic fluid. Numerous nonmetallic fluids were considered. Monsanto Chemical Company's OS-124, a polyphenyl ether, was determined to be the most satisfactory for high-temperature operation, with minimum sludging problems.

Cooling system designs were completed for both the potassium and the OS-124 coolants. Figures 40 and 41 show the loop and instrumentation schematics for the potassium cooling system. The flow schematic for the nonmetallic fluid cooling system is shown in Figure 42.

Accessory Equipment

A complete list of equipment and instrumentation required for test of the SPUR generator was compiled. Equipment meeting these requirements was selected or, where no existing equipment was available, was designed. Specialized equipment included a load bank and a torque measurement device.

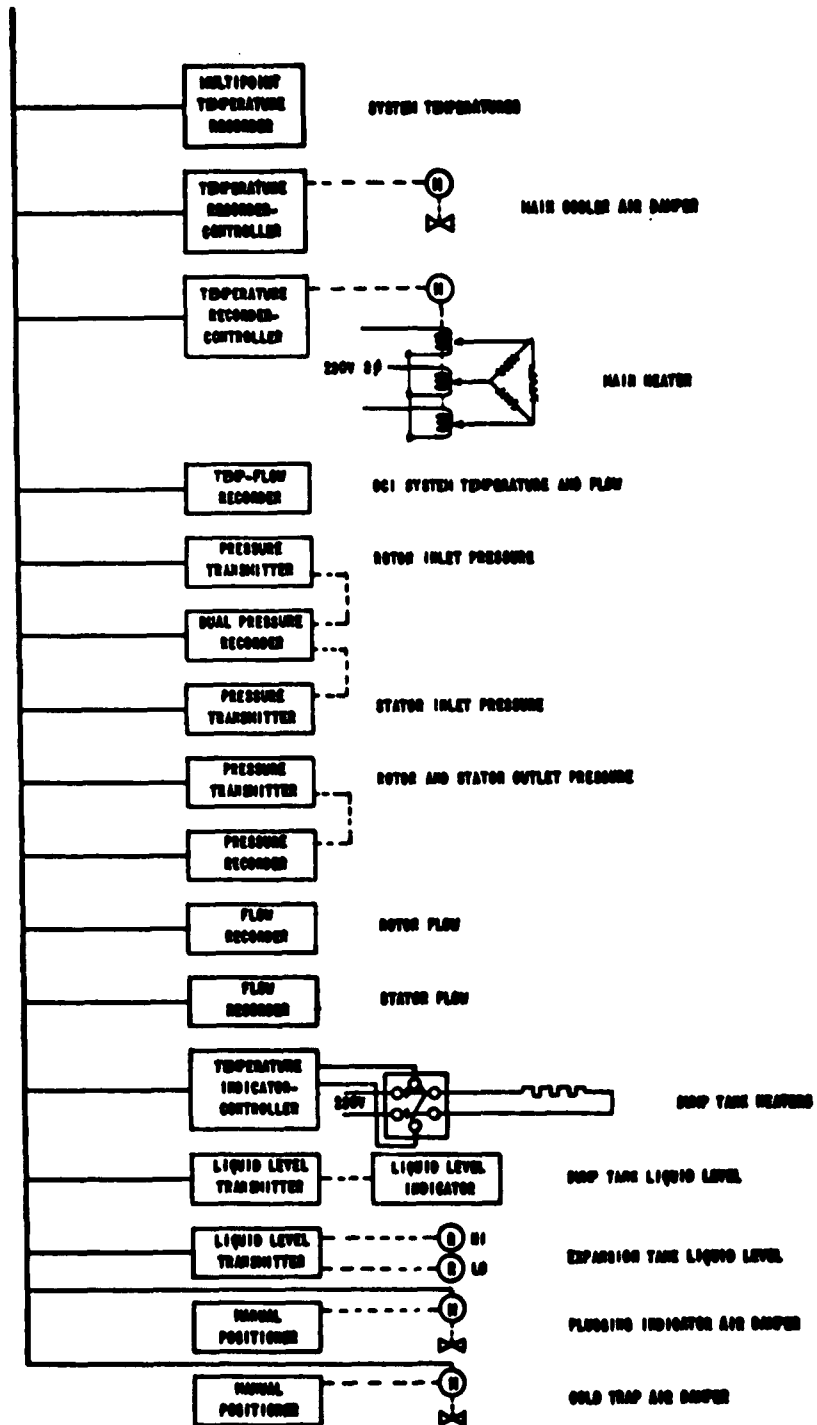


FIGURE 40
 GENERATOR LIQUID METAL TEST LOOP INSTRUMENTATION

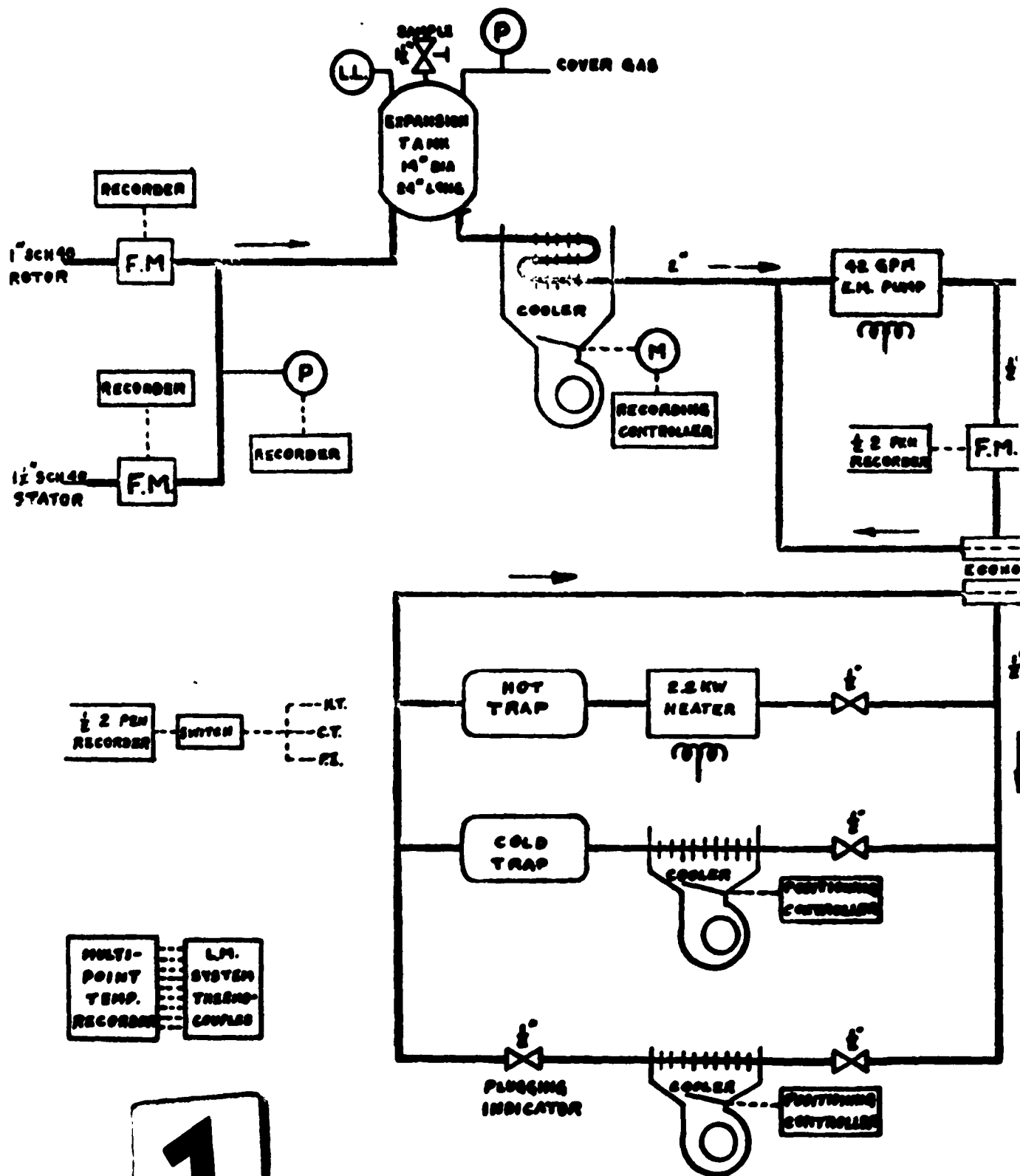


FIGURE 41
GENERATOR LIQUID METAL TEST LOOP

1

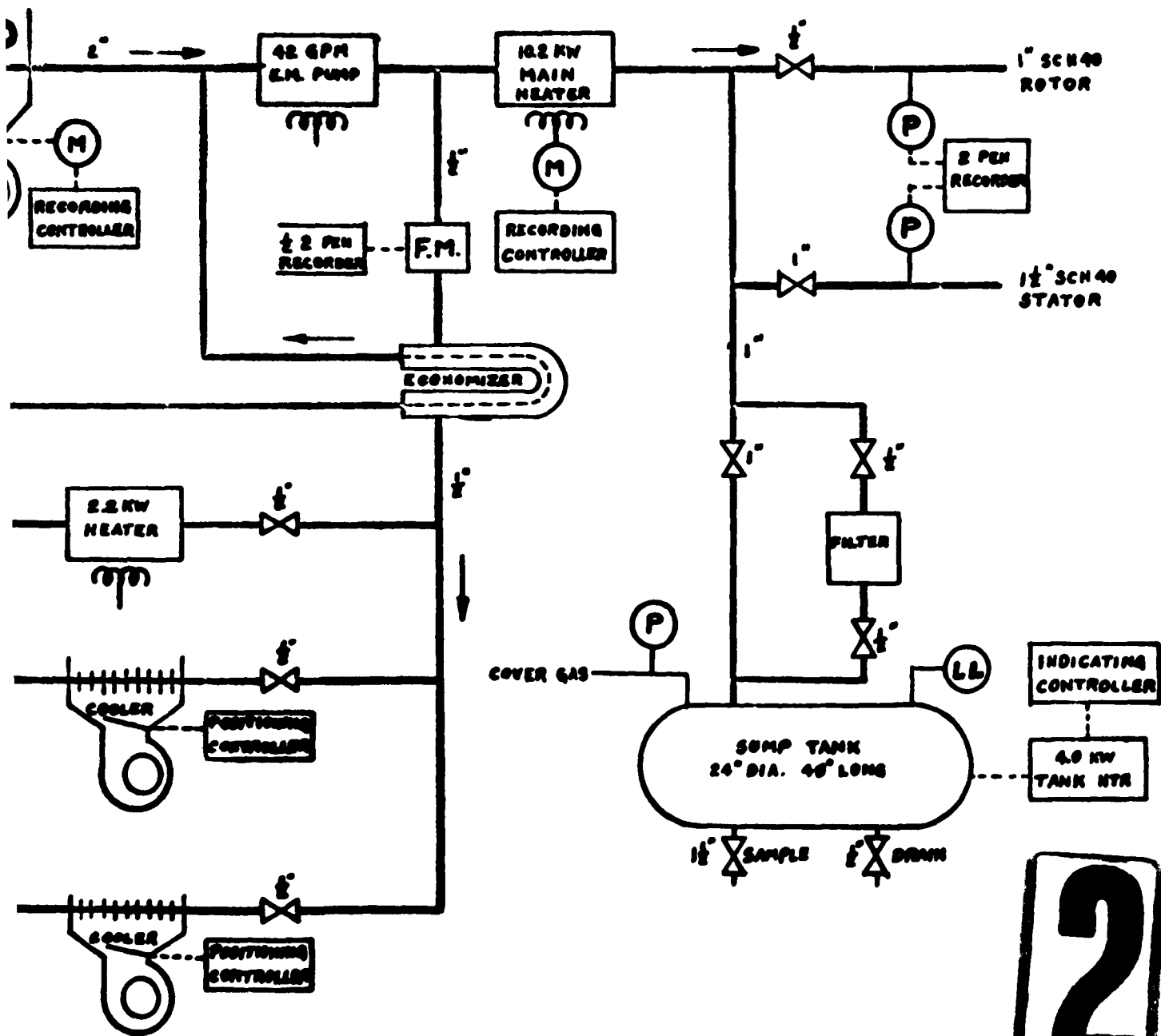


FIGURE 41

GENERATOR LIQUID METAL TEST LOOP FLOW SCHEMATIC

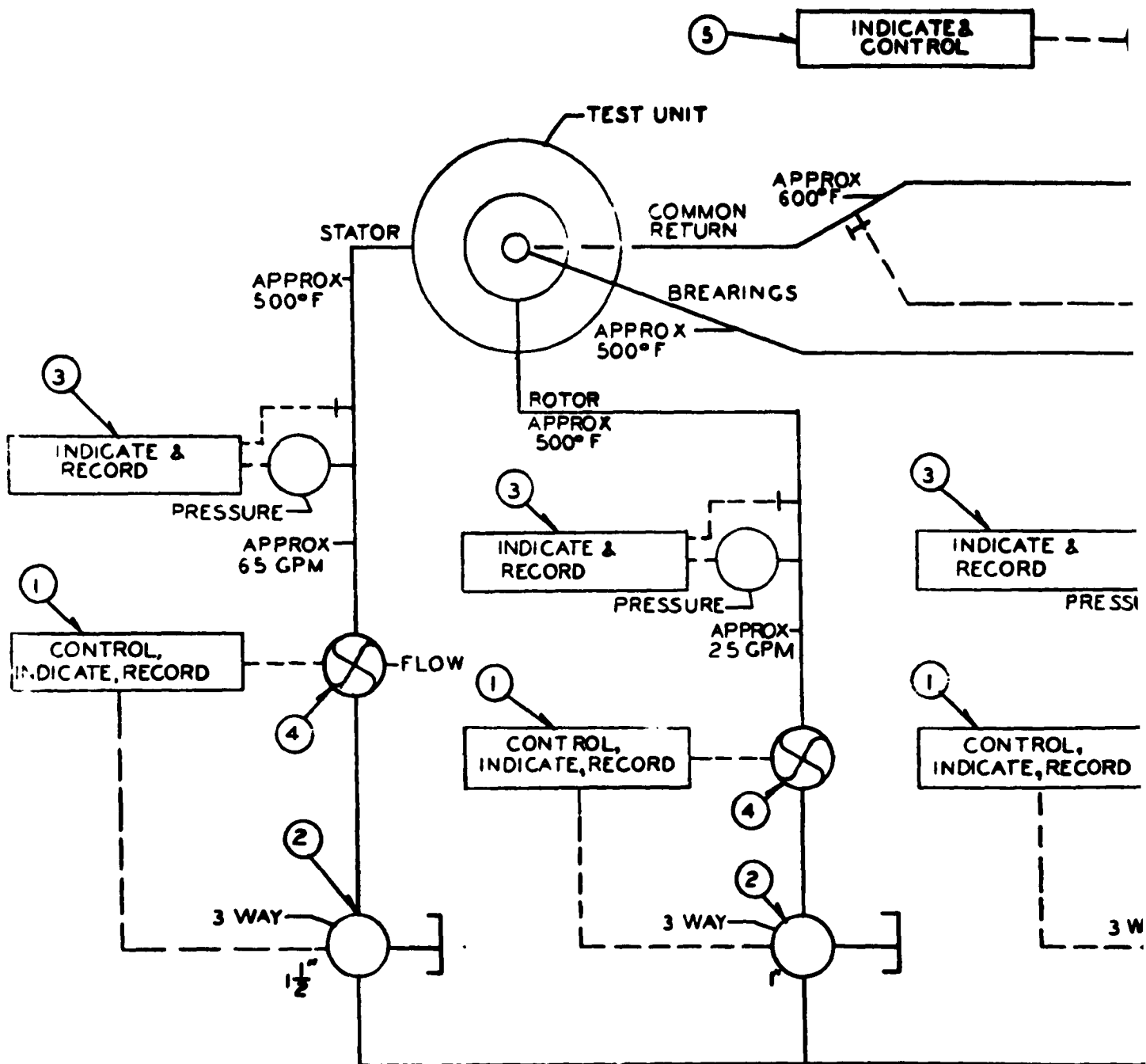


FIGURE 44
GENERATOR NONMETALLIC COOLANT TI

1

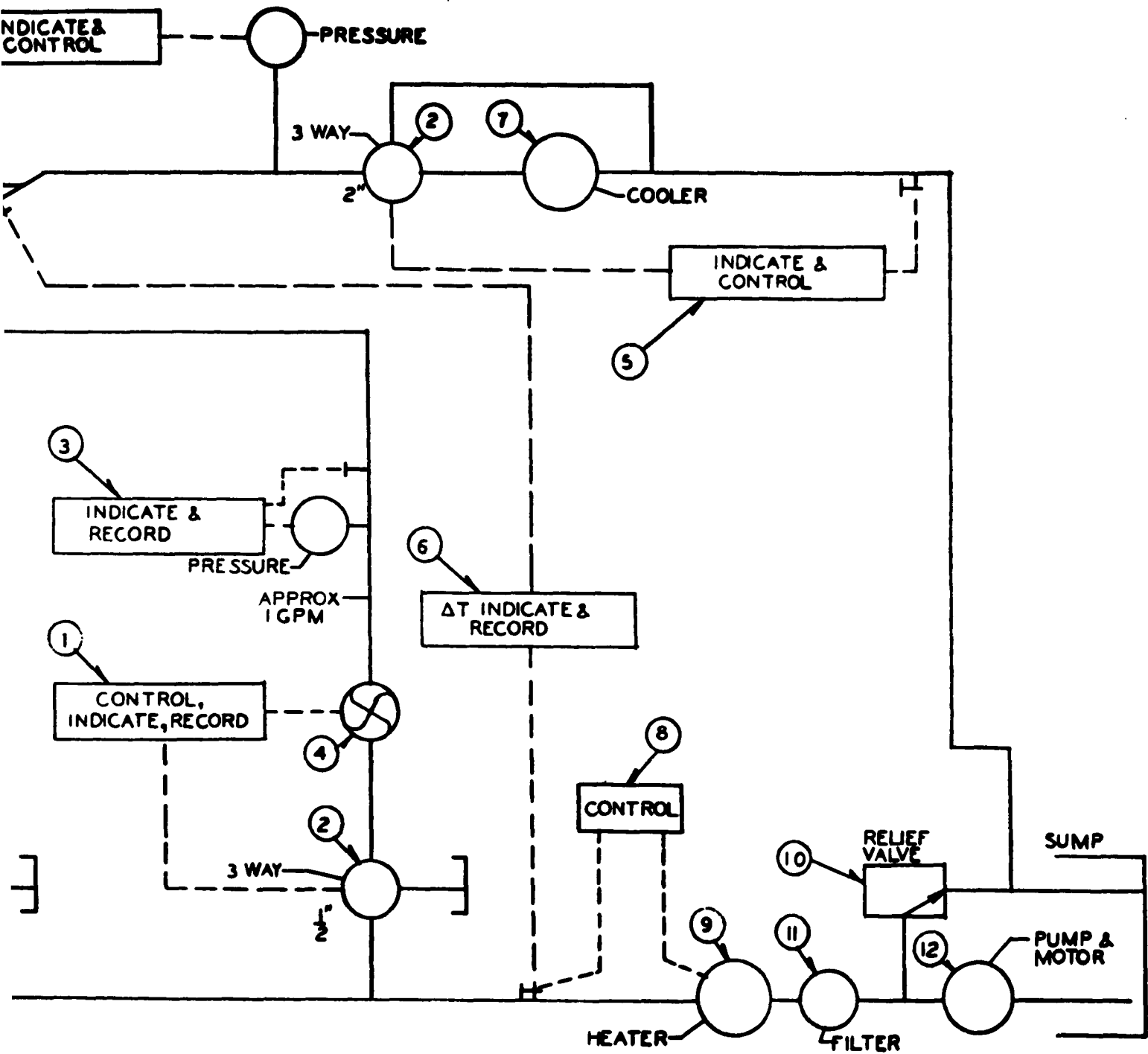


FIGURE 42

NONMETALLIC COOLANT TEST LOOP FLOW SCHEMATIC

2



Test Generator

In conjunction with the design of the generator test rig, the design of bearings and brackets necessary for test of the SPUR generator has been completed. (The bearings and brackets for use in SPUR will be supplied as a part of the turbogenerator, and hence are not being designed as a portion of the generator design, Task 2.2.4.3.1.) It is presently planned that the initial generator tests will be accomplished using oil lubricated ball bearings.



3. Stator Ceramic Seal, Task 2.2.4.3.3

Joints Between Metal and Ceramic Components

(a) Materials

Brazing alloys selected for trial in this portion of the program for brazing to columbium were chosen on the basis of their probable resistance to attack by hot potassium vapor. The eutectic-type alloy of 72 percent titanium and 28 percent nickel was one chosen for trial in brazing to columbium because it exhibited resistance to potassium attack when brazed to Kovar alloy in the preceding work phase. The AMS-4778 nickel-base alloy containing 4.5 percent silicon and 3 percent boron was used from two suppliers and is known as Microbraz 130 by Wall-Colmonoy and Coast Metal's alloy No. 52. The nickel-copper alloy produced by diffusion of a thin layer of molten copper into a surface coating of nickel was also employed.

It is recognized that nickel and its alloys may seriously attack columbium to form brittle intermetallic compounds.¹ An iron barrier layer was employed on the columbium to minimize this effect. Behavior in service and examination by the electron microprobe are expected to show whether this technique is effective.

¹Diffusion of Niobium with Chromium, Iron, Nickel, Molybdenum, and Stainless Steel: L. S. Birks, and R. E. Seebold, N.R.L. Report 5461, March 31, 1960.



(b) Test Specimens

Four types of test specimens were prepared as described below.

Tensile Specimen

The CLM-15 ceramic tensile specimen used in the preceding phase was also employed in this development work to evaluate various ceramic compositions and brazing methods. It is now planned that all specimens will include columbium alloy washers in the brazed joint.

Corrosion Specimen

Figure 43 shows the construction of cup samples to contain boiling potassium for evaluation of corrosive attack on 2-inch diameter alumina tubes with brazed-on columbium bottoms. The open top end of each test assembly is welded to a seal-support flange for potassium exposure.

Helium Permeation Specimen

Figure 44 shows one of the 2-inch diameter alumina tube assemblies produced for evaluation of the helium gas permeation rate through each of the test ceramics at elevated temperature. The

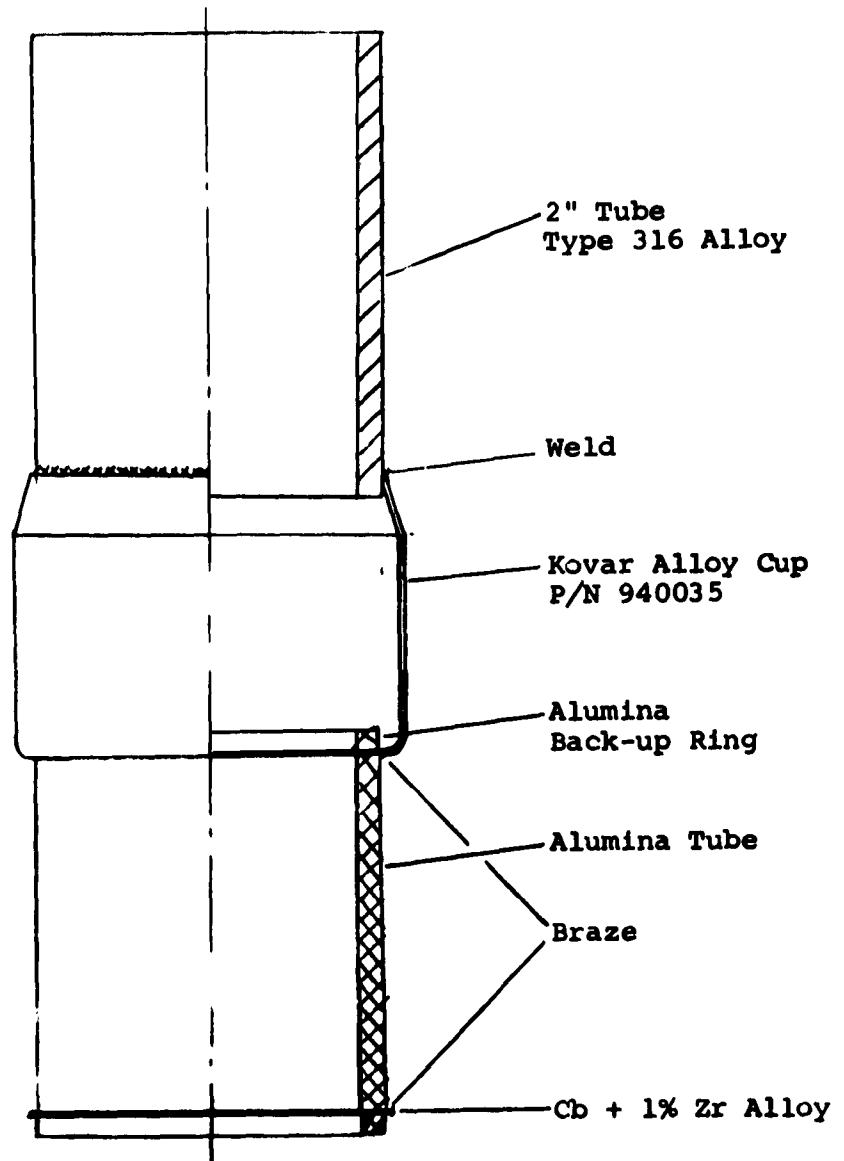


FIGURE 43

CONSTRUCTION OF CERAMIC CUP SAMPLES
(SHOWN WITHOUT SEAL-SUPPORT FLANGE)



Kovar alloy enclosure around the 4-inch midsection of the tube is cemented on in order to provide a helium atmosphere around the section to be tested while the whole assembly is surrounded by a fill of granular vermiculite as thermal insulation. The tubular electric heater, embedded in a silica tube, is inserted through the top section to provide a means of achieving the test temperature while a mass spectrometer type of leak detector is connected to the side tree.

Full Size Ceramic Seal

One of the full-size tubes produced in the preceding work phase was tested mechanically as described in the last Quarterly Progress Report.

(c) Tests

Tensile Tests

Tensile testing of brazed CLM-15 ceramic specimens have been started using a 0.006-inch-per-minute speed of head travel. Specimens are held during testing on a special split fixture having a rubber ring at each end between the specimen rim and the loading ring. The maximum load attained on each specimen before failure is automatically recorded.



FIGURE 45
CERAMIC TENSILE SPECIMENS
WITH TEST CAPSULE

SY-5396-R3
Page 104



Photomicrographs

Photomicrographs of sections through the developmental brazed ceramic-metal joints have been made.

(d) Conclusions and Current Task Status

Ceramic Tensile Specimens

Nickel in brazing alloys tends to form brittle intermetallic compounds with columbium, which cause joint leakage or failure. This indicates the desirability of investigating nickel-free brazing alloys.

Consideration of the substantial differential in thermal expansion between alumina and columbium at high brazing temperatures shows that locked up stress in the brazed joint would be reduced by the use of pure columbium, which has a lower creep strength than its alloys.

Bond strength of the brazed joint to alumina bodies of low silica content is improved by presence of a columbium component.

Further conclusions will be made upon completion of the work still going on. Exposure of specimens to potassium vapor for 1000 hours is still proceeding at 1100°F.

Cup Specimens

Work on the production of test specimens is incomplete.

Helium Permeation

Tube assemblies are currently undergoing test at elevated temperatures.



Tensile specimens for potassium exposure are shown in Figure 45, prior to loading into stainless steel test capsules. Groups of eight brazed CLM-15 ceramic tensile specimens, after loading, will be heated for 1000 hours at a temperature of 1100°F as a screening test of the several combinations of ceramic grades and brazing techniques. At the conclusion of the potassium exposure, the cover will be machined from each test capsule to remove the specimens. The exposed specimens will be tested by tensile loading and examination of the joint cross section.

Gas Permeation

Measurement of helium gas permeation through the tubular ceramic specimens was done at temperatures of 700°F, 900°F, and 1100°F. During each test, the specimen assembly had helium surrounding its 4-inch mid-section by introduction and free exhaust of that gas through concentric tubes at the top of the Kovar alloy enclosure sealed around the zone. Comparison of meter readings on a mass-spectrometer leak detector, alternately from the evaluated specimen cavity and a calibrated standard leak of 5.9×10^{-9} cubic centimeters per second, served to gauge the helium permeation rate for each test.



4. Electrical Insulation, Task 2.2.4.3.4

Statorettes for Enclosed Design

Four combinations of insulating materials were applied to the six statorettes. The statorettes were divided into two types, encapsulated and alumina sphere-filled.

Two forms of magnet wire insulation were used. The first was double glass-serving and the second was a ceramic enamel coating. The magnet wire was nickel plated copper. All six statorettes were lap-wound, using both the served and enameled wires in combination. A section of each statorette amounting to approximately one-third of the circumference was wound with the enameled conductor. The remaining two-thirds of the slots were wound with the served conductor. (See Figure 46.)

Efforts to obtain continuous lengths of ceramic-enamel rectangular magnet wire were not successful. The corners of the rectangular wire have not coated satisfactorily with these enamels. Ceramic enamel quality and thickness varies excessively in continuously coated rectangular conductors. It was necessary to form the magnet wire into coils, then spray and fire the coils individually. The coated pieces were then wound as normal, high temperature coils.



FIGURE 46

PARTIALLY WOUND ENCLOSED INSULATION STATORETTE
COILS AT LEFT: CERAMIC ENAMELED CONDUCTORS
COILS AT TOP AND BOTTOM: GLASS SERVED CONDUCTORS



The slot insulation was the same flexible micapaper-glass cloth laminate used in the earlier program.

The slot wedges were of the same design as the previous program and were composed of alumina.

In all statorettes, the lead wire was AWG18, stranded nickel plated copper covered with a high temperature glass and asbestos fiber braid.

All statorettes contained silicon steel stator cores, insulated between laminations with a tightly-adherent iron oxide coating. The ends of the cores were insulated with punchings made from rigid phlogopite mica laminate.

The filling material used on three stators was the Westinghouse developed refractory compound R125-4-3. The compound was applied in two stages. In the first application, the end turns of the coils were coated to approximately one quarter inch thickness and then completely fired. (See Figure 47.) The steel tube simulating the ceramic tube, was then inserted in place and the remaining compound applied and fired.

The filling material for the second group of three statorettes was solid alumina spheres measuring between 3/16-inch and 1/16-inch in diameter. The inner steel tube was positioned in the bore and one end of the stator was compactly filled. The end supporting ring was then

THE GARRETT CORPORATION
AirResearch Manufacturing Division
Phoenix, Arizona

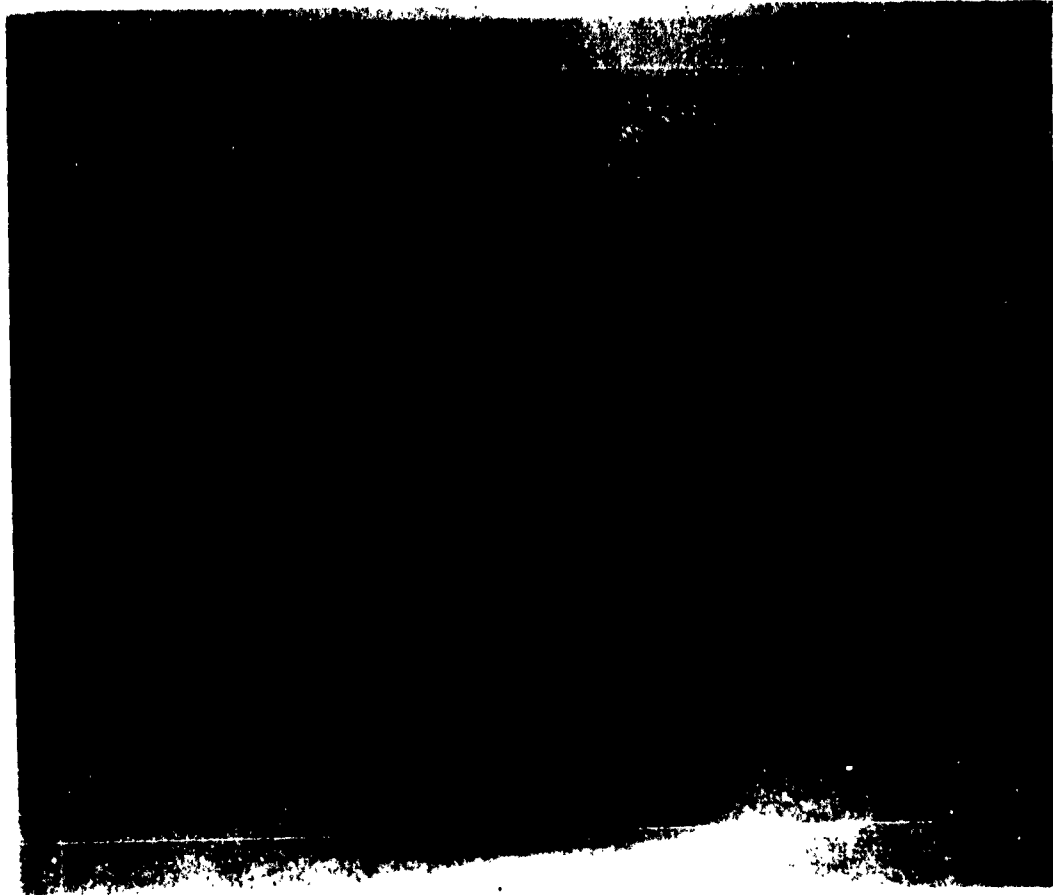


FIGURE 47
PARTIALLY ENCAPSULATED STATORETTE
ENCLOSED INSULATION SYSTEM

SY-5396-R3
Page 110



put in place and spot welded. The statorette was inverted and the opposite end was filled with alumina spheres, covered with the end ring and welded.

Testing

The six statorettes with their simulated frame enclosures have begun tests involving various combinations of thermal shock, high temperature aging, and vibration and mechanical shock, to evaluate the combinations of materials used in construction. As a preliminary check, the electrical leakage, in microamperes from phase to phase and from phase to ground was measured at a potential of 500 volts (lower potentials were used where leakage was excessive at 500 volts).

Heat aging of two stators is being conducted at 800°F in air for 1000 hours. One stator has refractory compound encapsulation and the other has alumina spheres as end fill material. Electrical leakage measurements are made every 200 hours.

Two stators, one of each end fill material, are being subjected to thermal cycling consisting of three cycles as follows: (1) room temperature to 800°F in one hour; (2) from 800°F furnace directly to room temperature exposure without forced air cooling.



The vibration tests are being conducted in accordance with MIL-E-5272C, paragraph 4.7.14.1, with the exception that vibration is ± 15 g's instead of 20 g's and the unit is vibrated in the axis perpendicular to the axis of rotation only (vertical axis).

The shock tests are conducted in accordance with MIL-L-5272C, paragraph 4.15.5.1 (Procedure V). Three impact shocks of 15 g's, 11 milliseconds duration each are applied in the vertical axis.

Conclusions

The testing of the six statorettes is not yet complete, however, the following preliminary conclusions are presented.

The preparation of the plated conductor was satisfactory with the exception of excessive copper hardness. It is recommended that hardness limits be placed on future material specifications.

The double glass-serving performed satisfactorily during manufacturing and forming.

The ceramic-enamel coated conductor can not be prepared in continuous lengths. The conductors must be formed into coils and then spray-coated and fired.



The glass-mica laminate has performed well under the test conditions. High leakage values occurred at 1000°F which indicate that this temperature is at or somewhat over the maximum operating temperature as a basic ground insulation.

The alumina slot wedges present no major manufacturing or application problem, and no problems have been encountered in preparation of the refractory compound or the alumina spheres end fill material.

No significant differences from normal winding techniques are required for the preparation of these statorettes, although the use of ceramic slot wedges requires more careful handling than ordinary laminated wedge materials.

The refractory encapsulant must be carefully applied and fired to achieve proper performance. Multiple applications of the material are recommended for significant stress reduction in completed unit.

No conclusions regarding temperature effects or vibration and shock effects may be drawn until the test program is completed.



5. Generator Rigid Insulation

The two statorettes to be produced under this program have been assembled and the thermal and mechanical tests have been initiated. Figure 48 shows a partially wound statorette and Figure 49 shows a fully wound statorette after the end connections had been welded. Insulating and winding components are shown in Figure 50.

Before initiating the tests, as a preliminary electrical check, the leakage currents between phase windings and to ground were measured. High values of leakage current during this check indicated some internal faults. Examination disclosed that some of the ceramic slot liners had been broken by excessive deflection of coil end connections during the final shop welding operation.

The thermal and mechanical tests being conducted on these stators are the same as the tests being conducted on the six statorettes discussed under Task 2.2.4.3.4. The tests are still in process, and determination of the physical properties of the ceramic test specimens is incomplete. However, it has been noted that a solid fill between slot liners and core iron will be required to avoid breakage of ceramic liners during manipulation of coil ends for welding. Also, accurate preforming of individual coils is necessary to minimize breakage of slot liners during assembly of windings.



FIGURE 48
PARTIALLY WOUND STATORETTE
RIGID INSULATION SYSTEM

THE BARRETT CORPORATION
AirResearch Manufacturing Division
Phoenix, Arizona



FIGURE 49
FULLY WOUND STATORETTE
RIGID INSULATION SYSTEM

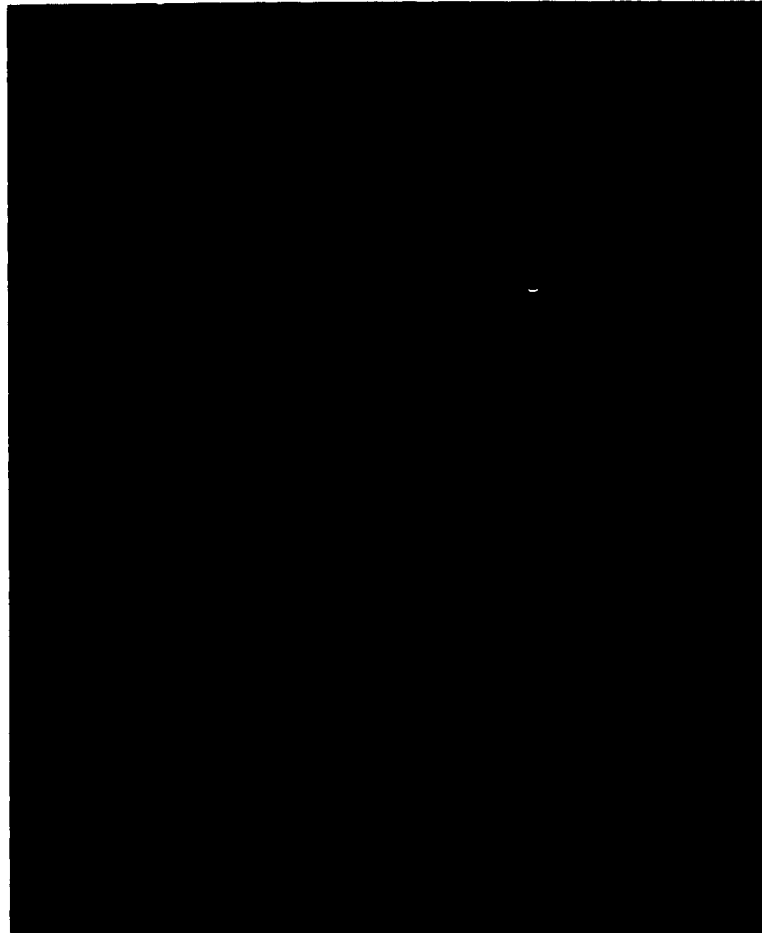


FIGURE 50
RIGID CERAMIC INSULATION
COMPONENTS AND COIL
TOP ROW: END EXTENSION PIECES
MIDDLE ROW: SLOT CELL, PHASE SEPARATOR, SLOT WEDGE
BOTTOM: FORMED COIL



6. Joining Hiperco 27 Alloy to Columbium

In the proposed application of joining columbium to Hiperco 27, the operating temperature is 900°F. The maximum brazing temperature, however, may be limited to 1670°F, the first transformation temperature of the Hiperco 27. For this reason, gold and silver alloys with melting points under 1670°F are of most interest. Alloys with higher melting points are also being considered.

A number of brazing alloys were selected and wetting tests were made on columbium + 1 w/o zirconium, columbium + 4 w/o vanadium (Westinghouse columbium alloy B-33), and on Hiperco 27. Wetting tests were performed by placing 0.1 gram of brazing alloy on a 1/2-inch square of the columbium alloy (0.025-inch thick) and induction heating in a vacuum (5×10^{-4} torr) to about 120°F above the melting point of the alloy, and holding at temperature for one minute. Wetting tests of the silver alloys were made in helium because of the high vapor pressure of molten silver. The plates were sectioned through the area of the brazing alloy, the contact angle was estimated, and the amount of erosion was determined. The results of these tests are listed in Table X. All wetting tests, except those noted, were conducted in a vacuum.

Wetting tests indicated that the gold-nickel, gold-nickel-silver-copper, silver-manganese, and AMS 4775 alloys appeared most promising. The AMS 4775 alloy, gold-nickel, and silver manganese caused some erosion of the base metal. However, erosion is expected to be less in the actual joint when the ratio of filler metal to area covered is reduced.

TABLE IX
BRAZING ALLOY WETTING TESTS

Brazing Alloy Composition	Brazing Alloy Melting Temp. (c)	Wetting Test Temp. (C)	Contact Angle*	Comments
82% Au, 18% Ni	950	1050	15°	Excellent wetting and flow, but alloy dissolved 40% of base metal thickness.
60% Au, 20% Cu, 20% Ag	860	930	80 - 90°	Alloy balled and wetted, but did not flow. No erosion.
60% Au, 20% Cu, 20% Ag	860	1050	60°	Alloy balled, wetted and flowed a little. No erosion.
58% Au, 20% Cu, 20% Ag, 2% Ni	870	910	40°	Wetted, but did not flow well. No erosion.
55% Au, 20% Cu, 20% Ag, 5% Ni	870	910	30 - 40°	Wetted and flowed some. No erosion.
80% Au, 20% Cu	950	970	90°	Wetted, but did not flow. This specimen not yet sectioned. Test to be rerun.
Gold (Au)	1060	1110	15°	Wetted and flowed well, but dissolved or eroded 50% of base metal thickness.
Silver (in Helium)	960	1050	80°	Alloy formed droplet and wet, but did not spread.
Silver - 15% Manganese (In Helium)	960 - 970	1090	30°	Good wetting and flowing, some reaction at interface, but no erosion.
72% Silver, 28% Copper, (In Helium)	780	800		No wetting.
65% Ag, 5% Mn, 28% Copper, 2% Ni (In Helium)	750 - 850	900	60°	Wet but did not spread well, reaction at interface, but no erosion.
Copper	1083	1120	60°	Wetted, but did not flow. Some reaction at interface, but no erosion.
<u>Cb + 4 w/o Vanadium Base Metal</u>				
82% Au, 18% Ni	950	1010	15°	Wetted and flowed well, but brazing alloy dissolved 20-30% of base metal thickness.
AMS 4775 Cr - 13.5% C - 0.8% B - 3.5% Si - 4.5% Fe - 4.5% Ni - Bal.	977 - 1040	1100	15°	Excellent wetting and spreading, but alloy dissolved 20% of base metal thickness. This alloy reacted the same on the Cb + 1 w/o Zr alloy.
55% Au, 20% Cu 20% Ag, 5% Ni	870	900	50°	Wetted and flowed some. Appears adequate for brazing.
<u>Hiperco 27 Base Metal</u>				
82% Au, 18% Ni	950	1010	15°	Alloy wet and spread very well, but dissolved about 0.005 inch of base metal.
55% Au, 20% Cu 20% Ag, 5% Ni	870	910	30°	Excellent wetting and flow.
AMS 4775	977 - 1040	1110	15°	Excellent wetting and flow, but some solution of the base metal.

*Approximate contact angle of brazing alloy on base metal.



Wetting tests were also made to determine whether fluxes are needed for brazing columbium with silver alloys. Trials were made using copper-cadmium-zinc alloy with commercially available low temperature flux and with the silver-copper eutectic using a boron modified flux. These trials were conducted in a helium atmosphere. Wetting was achieved in both cases. Figures 51 through 54 show typical wetting test specimens.

On the basis of the wetting tests, several alloys were selected to make joints for subsequent tensile tests at room temperature and at 900°F. Alloys are as follows:

- (1) 82 percent gold, 18 percent nickel; approximate melting temperature 1470°F.
- (2) 55 percent gold, 20 percent silver, 20 percent copper, 5 percent nickel; approximate melting temperature 1600°F.
- (3) AMS 4775, 13.5 percent chromium, 4.5 percent iron, 3.5 percent boron, 4.5 percent silicon, 0.8 percent carbon, remainder nickel; approximate melting temperature 1920°F.

The lap joints were made with one member of columbium + 4 w/o vanadium (0.035-inch x 0.25-inch x 2.0-inch) and one of Hiperco 27 (0.030-inch x 0.25-inch x 2.0 inch). Induction heating was used in all cases and the brazing was done in vacuum (10^{-4} torr) to prevent interstitial embrittlement of columbium induced by contamination with oxygen or nitrogen.



FIGURE 51

TYPICAL WETTING TESTS

1. 60% Au, 20% Ag, 20% Cu on Cb + 1 w/o Zr; 1710°F
2. 60% Au, 20% Ag, 20% Cu on Cb + 1 w/o Zr; 1920°F
3. 58% Au, 20% Ag, 20% Cu, 2% Ni on Cb + 1 w/o Zr; 1670°F
4. 100% Au on Cb + 1 w/o Zr; 2030°F
5. 100% Cu on Cb + 1 w/o Zr; 2070°F

ALL TESTS WERE CONDUCTED IN VACUUM.



FIGURE 52

TYPICAL WETTING TESTS

7. 100% Ag on Cb + 1 w/o Zr; 1920°F
8. 85% Ag, 15% Mn on Cb + 1 w/o Zr; 2000°F
9. 60% Au, 20% Ag, 20% Cu on HIPERCO 27 in helium; 1920°F
10. 65% Ag, 28% Cu, 5% Mn, 2% Ni on Cb + 1 w/o Zr in helium; 1650°F
11. 58% Au, 20% Ag, 20% Cu, 2% Ni on Cb + 4 w/o V; 1670°F

TESTS WERE CONDUCTED IN VACUUM UNLESS OTHERWISE NOTED.

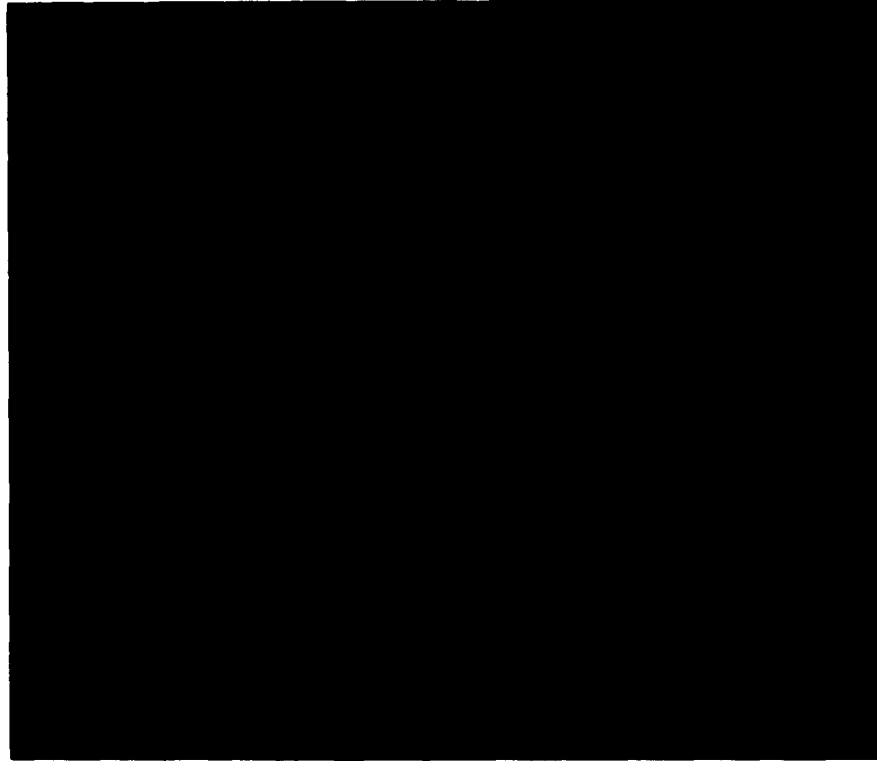


FIGURE 53

TYPICAL WETTING TESTS

- 13. 82% Au, 18% Ni on Cb + 1 w/o Zr; 1920°F
- 14. 55% Au, 20% Ag, 20% Cu, 5% Ni on Cb + 1 w/o Zr; 1670°F
- 16. AMS 4775 on Cb + 1 w/o Zr; 2010°F
- 17. 55% Au, 20% Ag, 20% Cu, 5% Ni on HIPERCO 27; 1670°F

ALL TESTS WERE CONDUCTED ON VACUUM.



FIGURE 54

TYPICAL WETTING TESTS

19. 60% Au, 20% Ag, 20% Cu on Cb + 4 w/o V; 1920°F
20. 82% Au, 18% Ni on Cb + 4 w/o V; 1850°F
21. 55% Au, 20% Ag, 20% Cu, 5% Ni on Cb + 4 w/o V; 1650°F
22. AMS 4775 on Cb + 4 w/o V; 2010°F
23. 82% Au, 18% Ni on HIPERCO 27; 1850°F

ALL TESTS WERE CONDUCTED IN VACUUM



The gold-nickel alloy was brazed at temperatures of 1820°F; the AMS 4774 at 2100°F. All joints were held at room temperature for one to two minutes and cooled in a vacuum. It was not possible to attain proper wetting with the gold-silver-copper-nickel alloy, and further trials with this alloy were discontinued.

Joints were tested in the as-fabricated condition. Two specimens made with each alloy were tested at room temperature and three were tested at 900°F. The results are listed in Table XI.

Only two of the specimens failed in the joint. The breaking stress is computed on both the shear area and the cross-section of the Hiperco 27. The joints made with gold-nickel alloy provided superior to those made with AMS 4775 in shear strength and in ductility. The AMS 4775 alloy appeared to dissolve considerable Hiperco 27. These joints failed in the Hiperco 27 at the edge of the fillets. Some of the fractures appear faceted and there was no necking down at the fractures. Reducing the amount of alloy and time at temperature should minimize this effect. The extent of diffusion of the two brazing alloys into the base metal has not yet been determined by metallographic examination.

TABLE - X
STRENGTH OF BRAZED COLUMBIUM TO HIPERCO 27 JOINTS

<u>Test Temp. (°F)</u>	<u>Shear Area (In.)</u>	<u>Load (lbs)</u>	<u>Ultimate Strength Joints (psi)</u>	<u>Base Metal (psi)</u>	<u>% of 1.0 Inch Elongation</u>	<u>Remarks Location of Fracture</u>
<u>Gold Nickel Brazing Alloy</u>						
75	.277 x .120	700	17,550	62,000	3.0	Failed in the brazed joint, poor wetting.
75	.277 x .120	652	---	67,300	3.0	Failed in Hiperco at the edge of the overlap
900	.268 x .200	546	---	58,200	15.0	Failed in Hiperco, 1/2 inch from joint.
900	.269 x .120	622	---	66,100	5.3	Failed in Hiperco, 1/2 inch from joint, the Hiperco necked down-ductile fracture.
900	.273 x .200	639	---	66,900	12.3	Failed in Hiperco 5/16 inch from joint. Hiperco necked down at fracture.
<u>AMS 4775</u>						
75	.296 x .15	712	---	59,900	7.0	Failed in the Hiperco at the edge of the joint, some solution in the brazing alloy.
75	.285 x .17	744	15,350	---	6.8	Failed in the brazed joint.
900	.252 x .19	150	300	20,000	1.9	Failed in the Hiperco 1/8 inch from joint. Hiperco fracture had faceted appearance, some solution in base metal.
900	.319 x .19	684	---	61,300	5.8	Failed in the Hiperco at the edge of the joint, cracks observed in brazing alloy.
900	.298 x .17	594	---	56,950	7.6	Failed in Hiperco at the edge of the joint, some solution of Hiperco in brazing alloy.



Welding

Electron beam welding presented a welding method which would hold brittle intermetallic formation to a minimum. An electron beam welding feasibility program was established and lap joints were fabricated between columbium + 1 w/o zirconium (0.050-inch x 1-inch x 2-inch) and Hiperco 27 (0.100-inch x 1-inch x 2-inch).

Cracks were clearly visible across electron beam welds made between the columbium alloy and Hiperco 27 using several different welding parameters. These initial trials substantiate the existence of brittle phases in the weld area.

Conclusions

Brazing tests, conducted to the present time, indicate the gold-nickel alloy to be the most promising filler metal for joining Hiperco 27 to a columbium alloy. Satisfactory joints can be made by brazing but cycling, creep, impact, and fatigue tests are necessary to properly evaluate the joining practice. Other brazing alloys may be useful if higher brazing temperatures can be employed. The higher temperatures



are expected to degrade the magnetic properties of Hiperco 27, however, this effect may be minimized by several modifications on over-all joint design. The use of fluxes could also increase the number of brazing alloys suitable for joining Hiperco 27 to columbium.

The indication of a brittle phase forming in electron beam weldments between Hiperco 27 and columbium alloy casts considerable doubt on this approach to making a joint directly between these materials.

7. 50 KW Liquid Metal Model Generator Development

The detailed generator layout and detailed manufacturing drawings have been complete. Separate detailed designs of test pieces, where verification or additional development is required, are in process and will be completed by January 30, 1963.

Purchase orders have been issued for all of the new materials for the stator, the generator frame, the rotor, the end bells, the stator and field wire, and other lesser components. Fabrication will be initiated as components become available.

The mechanical layout of the generator is shown in Figure 55. Within design limits, the SPUR generator was scaled as nearly as practicable.



The stator windings will be protected from potassium vapor by the alumina seal passing through the air gap. The rotor and stator are cooled from separate potassium coolant flow circuits. Rotor coolant is supplied through the drive bearing, then into passages under each pole with radial passages leading to the pole tips, and then discharged from the generator at the rear bearing. The stator coolant is supplied through axial tubes located on the outside of the stack. Inlet and outlet manifolds are provided at the anti-drive end of the generator.

The generator stator is hermetically enclosed in order that it may be evacuated or filled with an inlet gas, as desired. Thermocouples will be located at various points in the field and stator windings and in the stator iron. Thermocouple leads will be brought out through hermetic connectors.

The generator is designed to be cantilever-mounted. Figure 56 shows the mounting configuration and the external plumbing requirements.

The materials being used in the model generator have been chosen to duplicate those used in the SPUR generator, except where material procurement or joining problems might delay the program unnecessarily. (The procurement of columbium cooling tubes and large diameter forgings is an example, and stainless steel



has been substituted for columbium.) Materials that duplicate those of the SPUR generator include: Hiperco 27 frame and stator punchings, SAE 4340 alloy steel rotor, and nickel clad copper conductors with glass served insulation. Slot liners, wedges, fin insulation, and field coil dielectric insulation are alumina to aid in heat transfer. End bells, cooling tubes, and other components are being fabricated from Type 315 stainless steel.

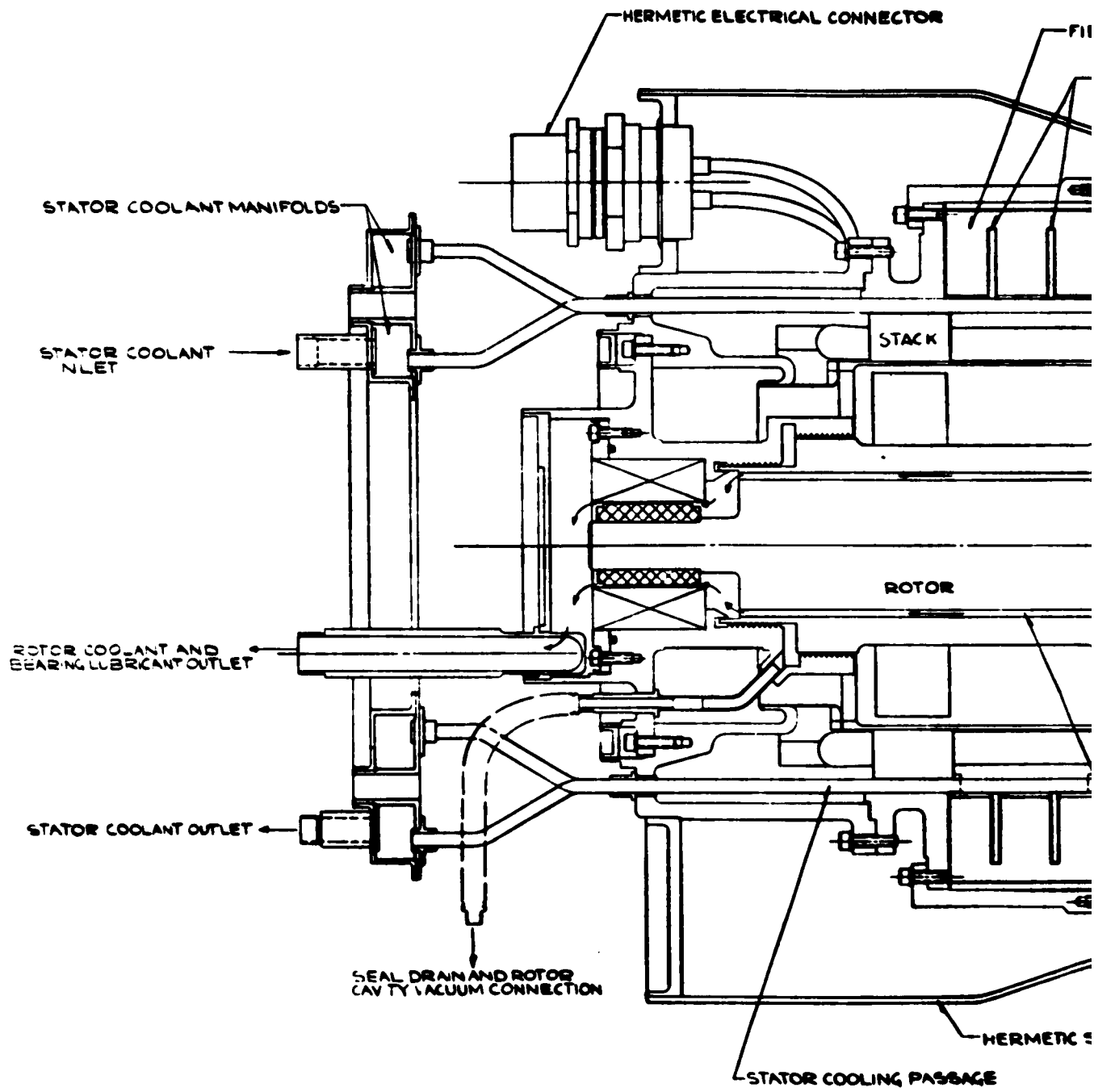


FIGURE 55
 CROSS-SECTION OF LIQUID FOIL
 MODEL GENERATOR

1

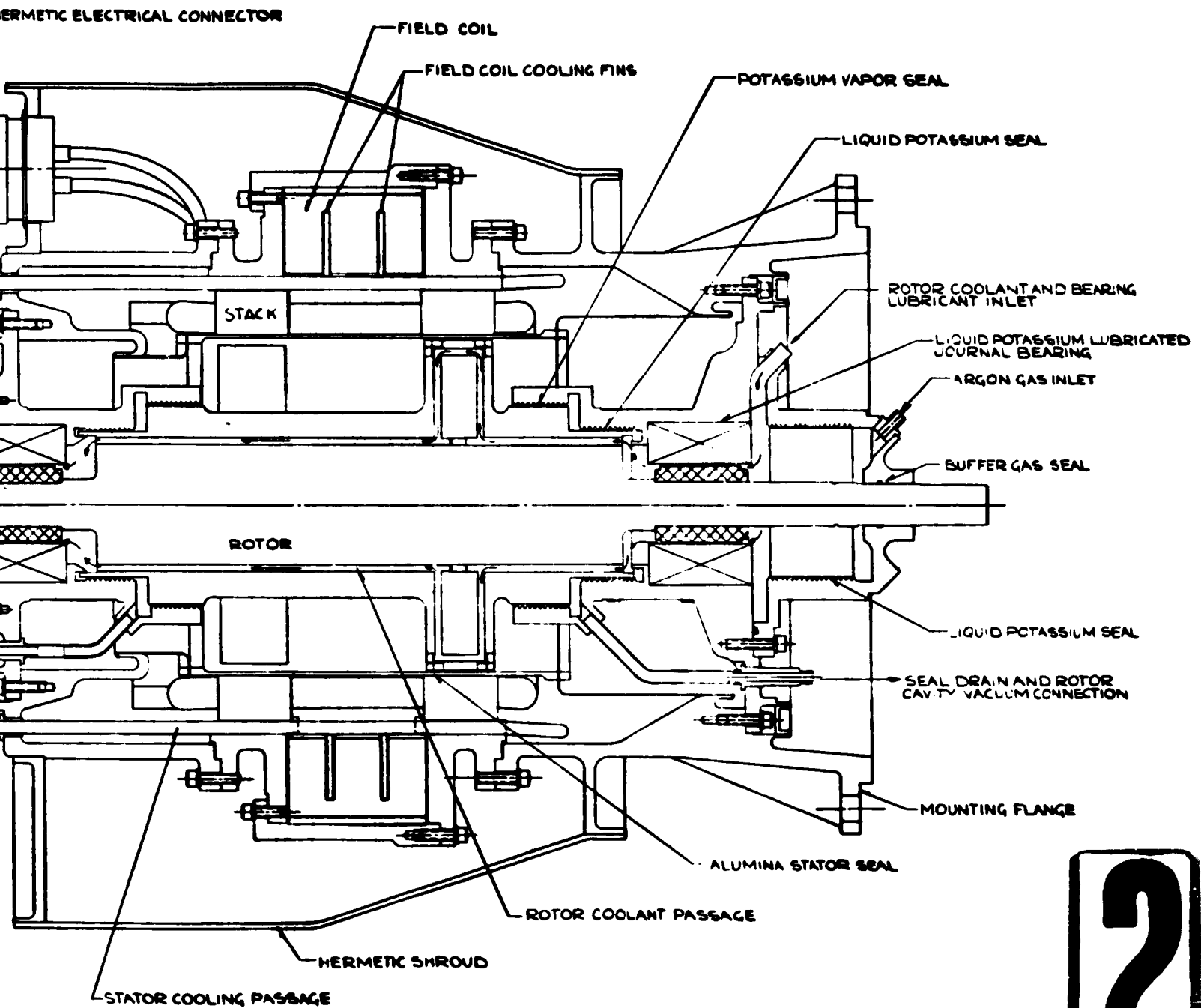
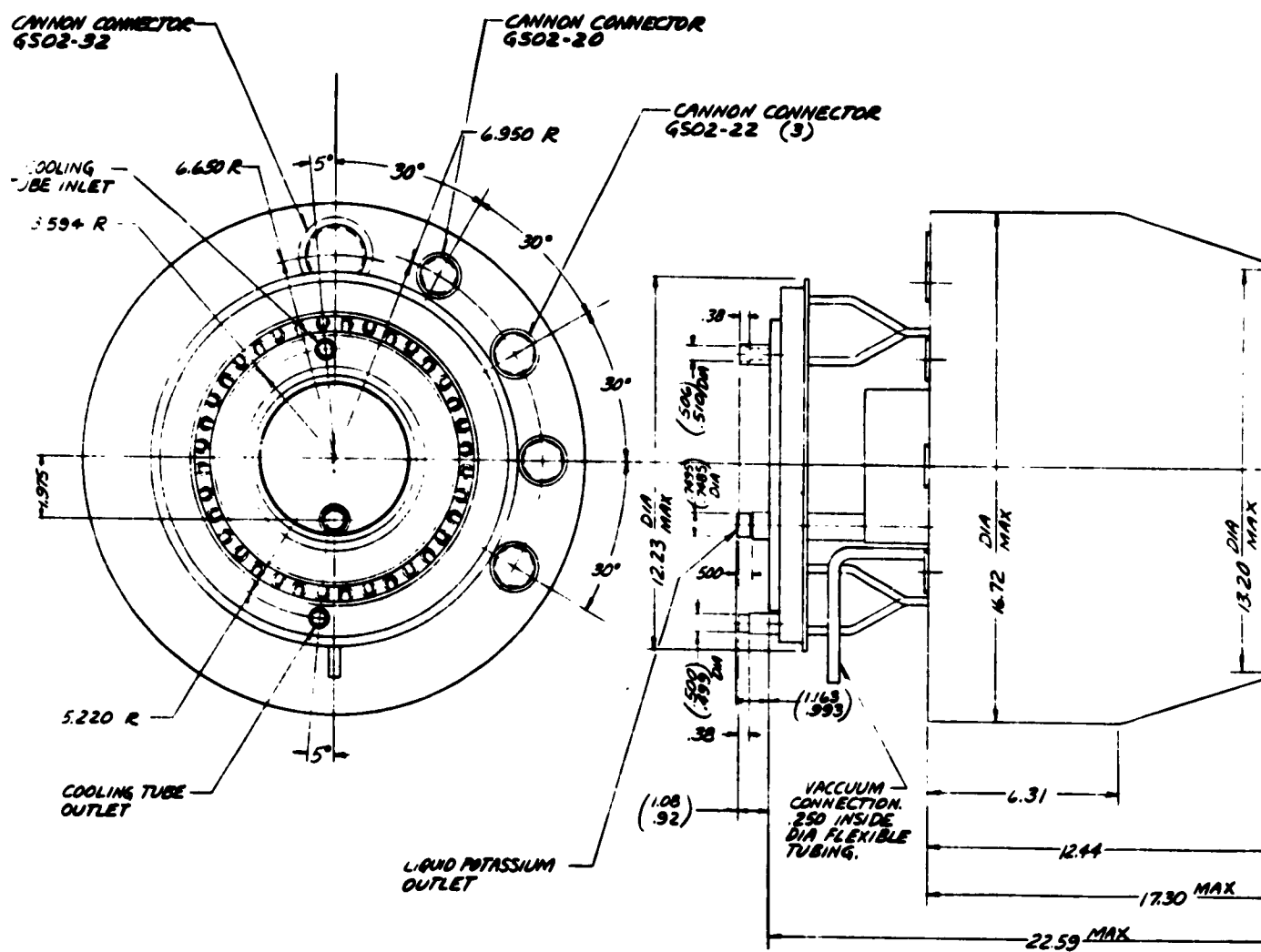


FIGURE 55

CROSS-SECTION OF LIQUID POTASSIUM COOLED MODEL GENERATOR

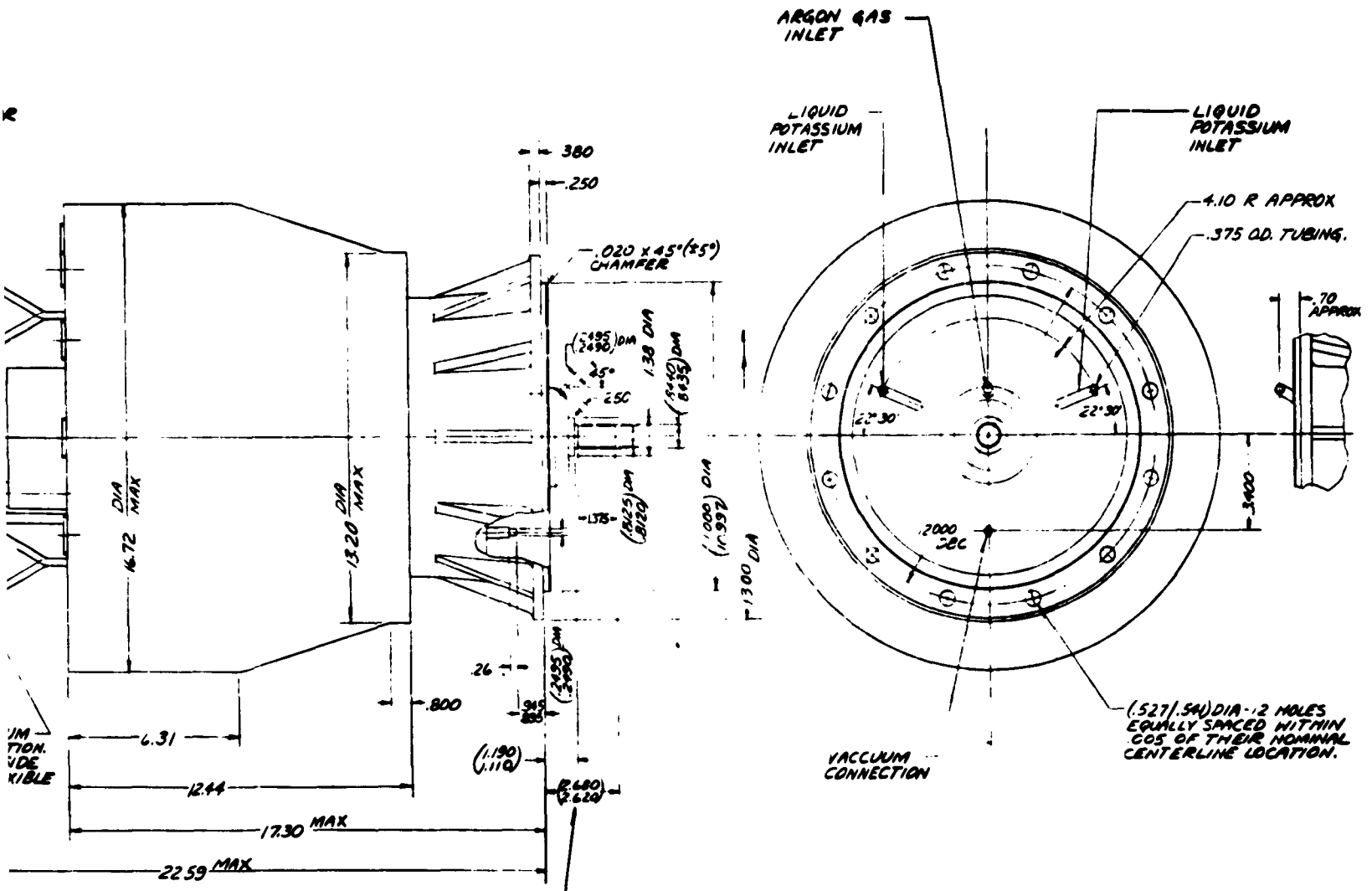
2



ROTOR TO BE A.
BY MATING UN.
DIMENSION.

FIGURE 56
OUTLINE DRAWING
50-KW LIQUID METAL
COOLED MODEL GENERATOR

1



POTDOR TO BE AXIALLY LOCKED BY MAT. 7 UNIT TO THIS DIMENSION.

FIGURE 56
 OUTLINE DRAWING
 50-KW LIQUID METAL
 COOLED MODEL GENERATOR

2



F. Alternate Turbogenerator Design, Task 2.2.4.4

Generator Design

Analysis of the rotor pole face losses, including the load component, has been completed. These losses were higher than expected, and changes in the previously optimized electromagnetic design are being made to minimize them. The mechanical design has been optimized, and the machine speed and the rotor tooth inner and outer diameters have been defined. Rotor tooth cooling is being incorporated.

Alternate armature conductor and conductor insulation designs are being studied, and an auxiliary method of stator conductor cooling involving end turn cooling is being considered. Analysis of electromagnetic stability has results in an equivalent circuit for the inductor alternator which is distinct from that for conventional synchronous machines.

Turbine Design

Detail loss and moisture extraction analyses have been initiated, and mechanical design of the discs, shaft extension, bearings, and seals is under way. Critical speed, stress analysis, and weight calculations for six-stage and five-stage configurations have been completed. A vortex hydrodynamic seal between the turbine and generator has been designed, permitting a large-diameter shaft between the turbine and generator rotors and increasing the critical speeds. (Critical speed calculations include the entire turbogenerator rotor-bearing support structure.)



The flow annulus layout and the computation of stage vector diagrams has been completed. The analytical evaluation of alternate turbine-stage "aerodynamic" designs is continuing, and alternate stage designs with varying values of work coefficient, velocity ratio, nozzle angle, aspect ratio, and axial velocity ratio are being compared on the basis of wet and dry operation.

Development Program Planning

Design of a generator statorette test facility is under way, and work on the air-turbine-driven-generator test rig is continuing.



G. Heat-Transfer Development

1. Single-Tube Boiling-Potassium Test, Task 2.2.5.1

Component fabrication was completed during this period, and loop assembly was initiated. A successful development of the test element resistance heating wire-to-conductor termination design was achieved. Electrical and instrumentation installation is 40 percent completed, and component installation is 50 percent completed.

A test series was conducted to verify the integrity of a new resistance heating wire-to-conductor termination design. Sheath-type Thermocoax heating wire was brazed to a 3.0-inch-diameter by 4.0-inch-long nickel billet. Nickel straps, shaped to permit freedom for thermal expansion, were attached to each end of the bare Nichrome heating wire. The test element was placed in a vacuum tank and electric power applied. During the first test, a maximum of 120 volts was applied across the heating element. When the element temperature reached 2150°F a failure occurred. The failure was attributed to a breakdown of the MgO insulation at high temperature. The electrical wiring was revised to permit a maximum potential of 50 volts between the heating wire and ground



with 120 volts across the heating element. The first test procedure was repeated and the test element heaters remained intact after 200 hours' continuous operation at 2100°F. For a second, and more severe, type of test, the area surrounding the termination was covered with 2 inches of microquartz insulation to reduce heat loss and thereby increase the temperature at this particular location. With this installation, 500 hours of operation at the maximum conditions expected during potassium testing were accumulated. The present termination design is considered acceptable for use on the test rig.

Sheath-type Geminol N-P thermocouples will be used to measure test section and potassium temperatures. For comparison purposes, a series of platinum - 6% rhodium/platinum - 30% rhodium thermocouples will also be installed at selected locations on the boiler test section. Noble metal thermocouples of this type are considered to represent the highest accuracy obtainable with the present state of the art. The rhodium percentages were selected to minimize drift due to diffusion effects. A sheath-type construction was selected to provide mechanical integrity and to protect the thermocouple wires from environment impurities. Experiments



have shown that the use of base-metal sheaths, such as Inconel, can lead to thermocouple drift due to diffusion of nickel from the sheath to the platinum. Therefore, a pure platinum sheath will be used to provide the required protection. The first test series should reveal if the accuracy and drift characteristics of a noble metal thermocouple assembly are sufficient to justify its greatly increased cost.

During the next quarter the loop will be assembled and filled, and testing will be initiated.

2. Vapor - Liquid Separator, Task 2.2.5.2

Modifications of the vapor-liquid separator assembly are essentially complete. The changes include heavier flanges with fairings to reduce stresses and an improved scroll design to increase the liquid collection efficiency. Figure 57 shows the separator before joining of the parts. Installation and testing of the separator are scheduled, and operational facilities have been expanded so that the separator can be operated either horizontally or vertically.

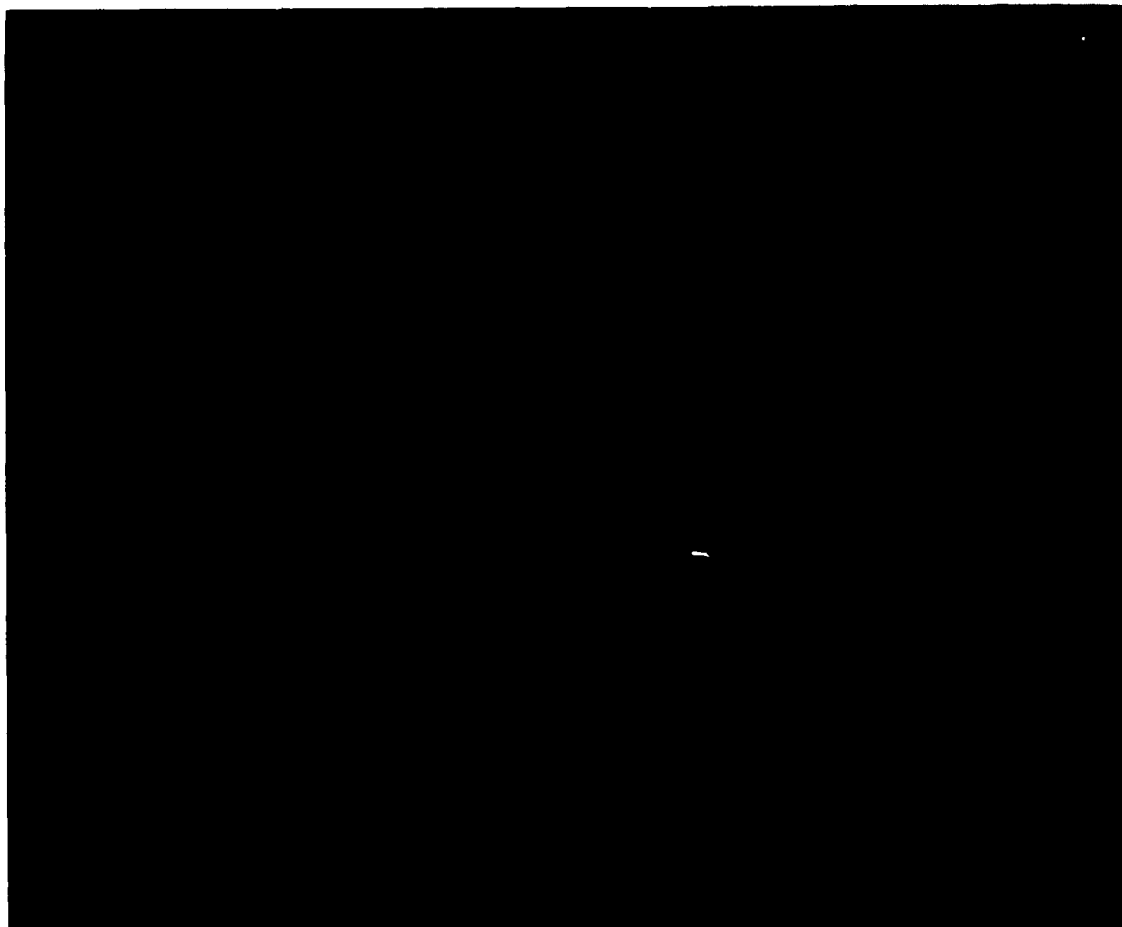


FIGURE 57
VAPOR-LIQUID SEPARATOR COMPONENTS



3. Multitube Water Boiler, Task 2.2.5.2

A series of tests were run on the 10-tube water boiler, to visually observe boiling in parallel tubes. The unit was instrumented to measure inlet temperature, pressure, and flow rate of both water and steam. There was no provision to measure outlet quality of either stream or flow variation in individual tubes. Instability was determined by visual observation of the time change in liquid volume fraction leaving each tube.

Subcooling of the boiler feed stream was varied between 16°F and 157°F. The greater the degree of subcooling, the more pronounced were the instabilities at the tube outlet. The water flow rate was varied from 0.3 to 10 pounds per minute, with instabilities increasing at the high flow rate. It is not known whether these latter instabilities were due to high flow rate or to the low exit quality that corresponded to the high flow rate. Differences in quality from tube to tube were noted at the exit from the boiler. Tubes that were running wet did not continue to run wet; instead, the flow oscillated, with first some tubes running wet, then others running wet, with the first ones going dry.

Further stability testing will be done on the large Freon loop and on the single-tube Freon loop. Both of these loops will provide quantitative information on vapor quality and flow oscillations in individual tubes. No further testing will be performed on the multitube water boiler.



4. Flow Visualization Studies, Task 2.2.5.2

A Freon blow-down loop was assembled and tested to develop instrumentation techniques and photographic methods and to confirm the feasibility of obtaining heat fluxes of 20,000 to 30,000 Btu per hr-ft² with hot air as the heat source. The techniques developed are being incorporated into the design of a large Freon loop that simulates many of the SPUR system characteristics.

The blow-down test loop is shown in Figure 58, and a close-up of the boiling test section in Figure 59. Freon passes through the inner tube, shown in Figure 59, with 800°F air passing through the rectangular quartz tube.

Flow oscillations were measured with a differential pressure transducer, with exit quality obtained by means of a heat balance on the air side. The first motion pictures showed poor resolution between liquid Freon and vapor. As a result, TRACE, a Freon coloring agent, was added to the Freon supply. Subsequent pictures showed excellent resolution and detail of the boiling process. A Fastax camera with 7000 frames per second was used to photograph the boiling action.

The tests to date have been highly successful and enlightening. Observation of the motion pictures has led to a better understanding of the mechanism of "dry-wall" or forced-convection "burnout."

Design of the large Freon loop was started in this quarter, and major components and long-lead-time items were purchased. The test boiler has progressed through detail drawings, and the test-condenser design drawings were started.



FIGURE 58
FREON BLOW-DOWN TEST LOOP

THE BARRITT CORPORATION
AirResearch Manufacturing Division
Phoenix, Arizona

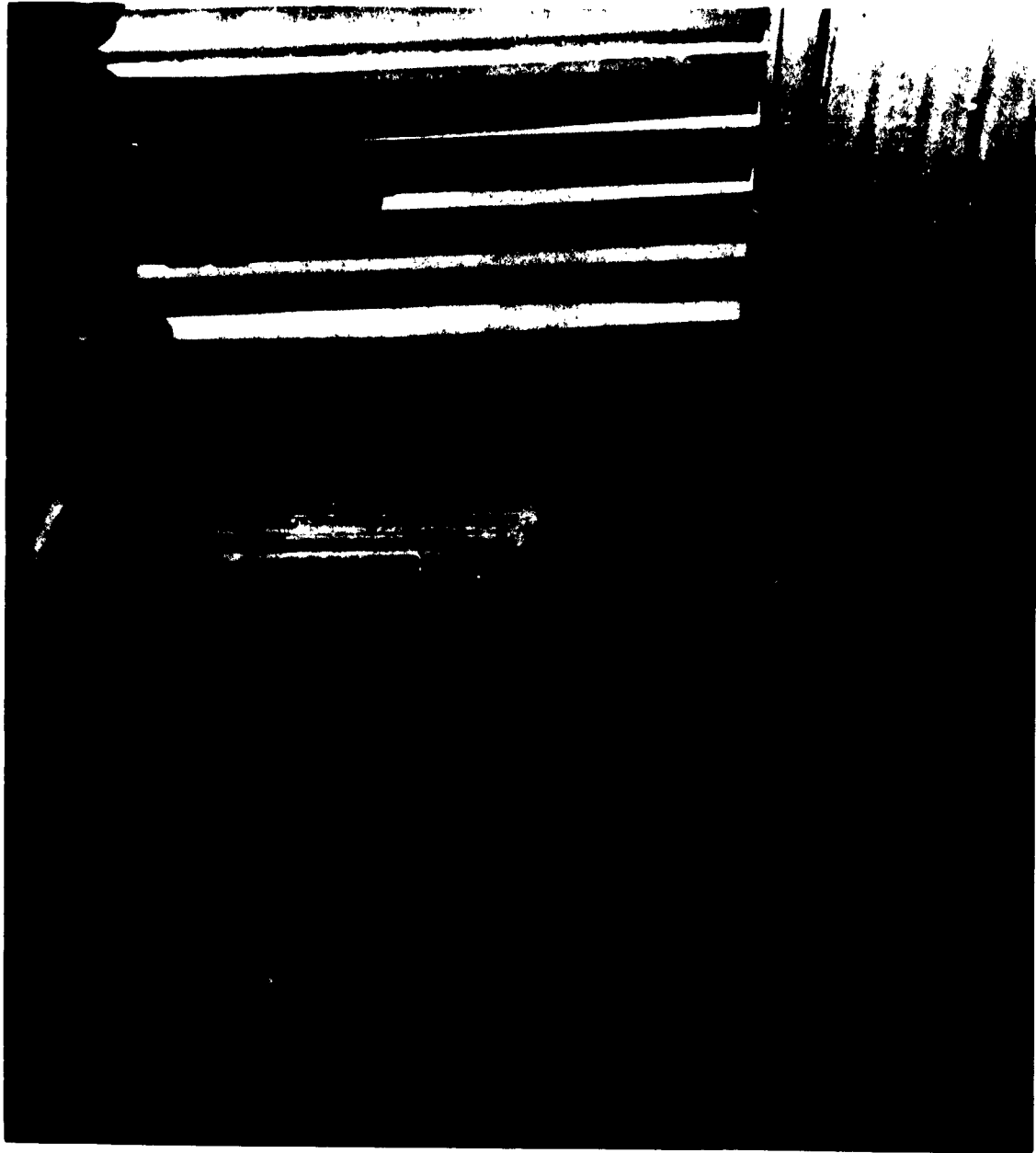


FIGURE 59
QUARTZ TUBE FREON BOILING SECTION



The loop design will be completed in January, with construction scheduled for completion in February. Experiments with the single-tube boiler will continue, with the objective of improving instrumentation techniques and obtaining further information on the forced-convection boiling process.

5. Stainless Steel Heat-Transfer Components, Task 2.2.5.3

Radiator

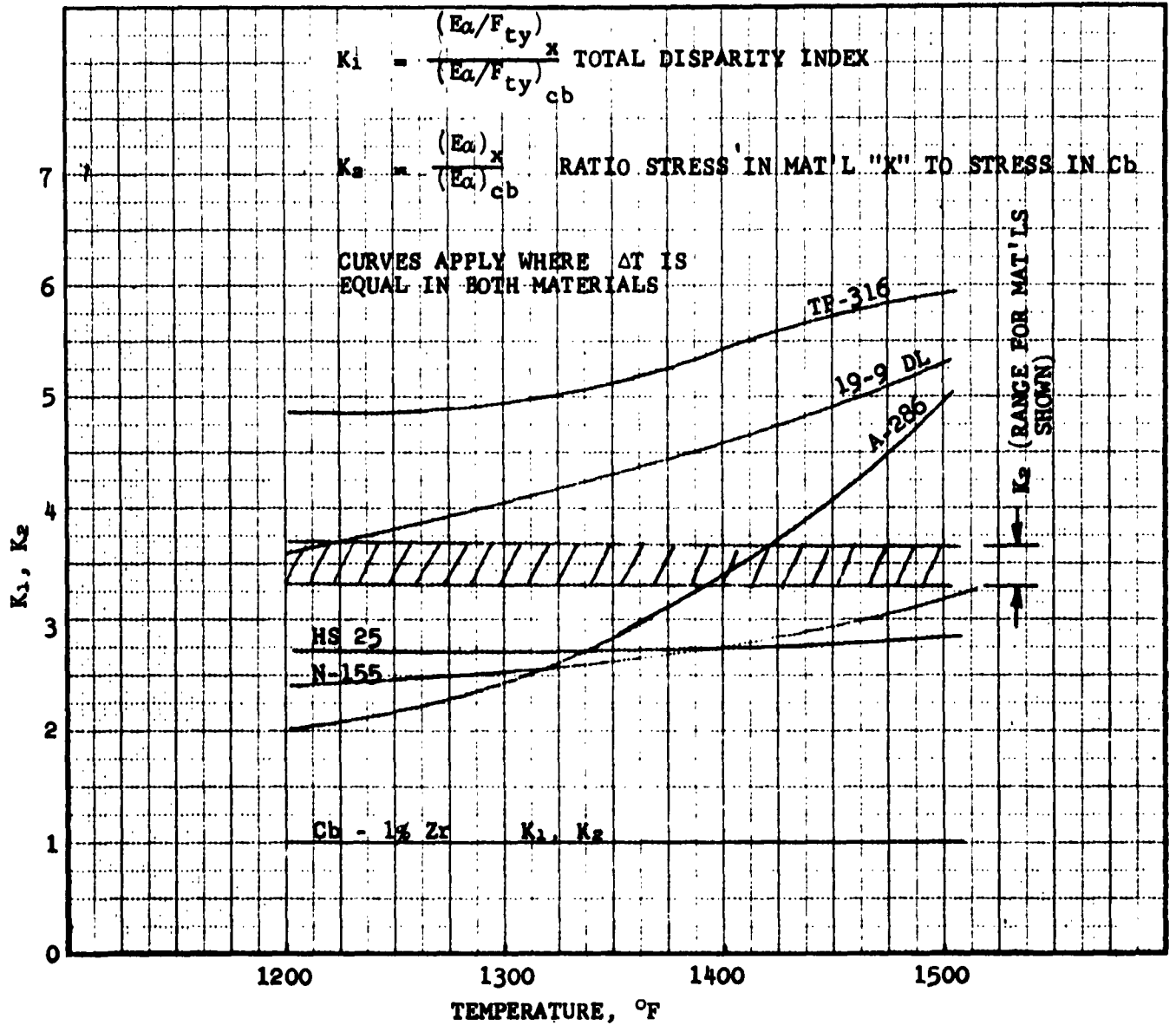
The thermal stress analysis of the full-size radiator was completed, and design was started on a conventional alloy radiator to be tested in the stainless steel heat-transfer loop. This radiator will be a flat panel, approximately 10 feet in width and 5-1/2 feet long. Stress analysis showed that stress simulation of the full-size columbium radiator was difficult because of the low coefficient of thermal expansion and elastic modulus, and high strength, and thermal conductivity of Cb + 1 W/o Zr compared to stainless steel and other conventional materials. Figure 60 shows a comparison of the relevant physical properties of several candidate materials with those of Cb + 1 W/o Zr. The total disparity index, K_1 , is the ratio of thermal stress to yield stress in the candidate material divided by that ratio in Cb + 1 W/o Zr, given the same temperature distribution. Another meaning of K_1 is the ratio of thermal stress safety margin in columbium to the safety margin in the candidate material. Also shown on Figure 60 is K_2 , the ratio of stress level in the candidate material to stress in Cb + 1 W/o Zr.



It is seen from Figure 60 that at the operating level of the SPUR radiator, Haynes Stellite No. 25 (HS 25) and N-155 are the two best materials for simulating Cb + w/o Zr. Of these two, HS 25 was chosen for (1), the greater fabrication and operating experience with it; (2), its more general availability; and (3), the doubtful mass-transfer characteristics of N-155 resulting from its high (20 percent) nickel content.

The test panel radiator will have the same detail configuration as the SPUR unit in respect to tube, fin, manifolds, and structural support. It will be essentially a 10-foot-wide section cut from the cylinder, with details full size. The fin effectiveness (temperature distribution) will be maintained the same as in the columbium fin by a 0.004-inch layer of copper covering the fin. The thin copper layer should have little or no effect on the radiator structure. The panel will be tested horizontally to simulate the effects of zero-gravity operation.

Other accomplishments in the last quarter include analysis of radiator transient and off-design characteristics, and analysis of the test-radiator operating environment required to simulate space operation.



PREPARED		ORVELL 10-62	PHYSICAL PROPERTIES OF CANDIDATE RADIATOR MATERIALS	FIGURE 60
WRITTEN				
APPROVED				
			AiResearch Manufacturing Company of Arizona	



Boiler

Stress analysis of the full-size Cb + 1 w/o Zr boiler and of the HS 25 boiler were made, and a layout drawing of the HS 25 boiler was initiated. Studies of the stability of liquid annular flow were continued. A boiler transient analysis was performed to determine start-up characteristics and the effect of perturbations about the design points.

Recuperator

An analysis of the effects of reduced flow and temperature on recuperator performance was made. The test conditions for the test unit were specified. A stress analysis will be performed in the next report period.

Separator

In the next report period an analysis of the effect of reduced-temperature operation on separator performance will be made, together with stress analysis.

6. Stainless Steel Heat-Transfer Loop, Task 2.2.5.4

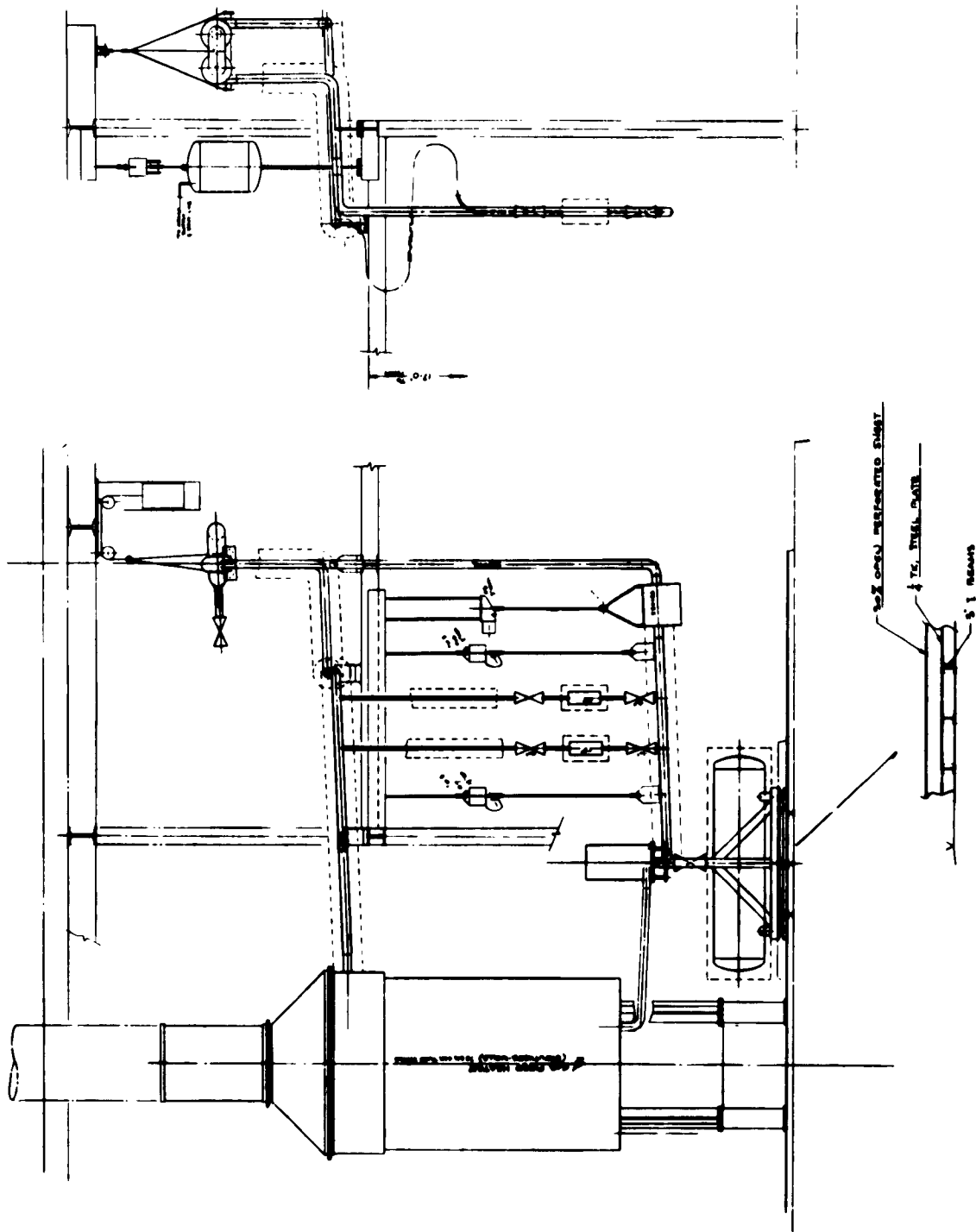
The principal effort during this quarter has been concentrated on primary-loop (sodium side) detail design. Stress analysis has been accomplished on the entire loop. Considerable communication with prospective vendors has



been carried out in an effort to make final selection of pumps, valves, and heat-exchanger equipment. Test requirements for SPUR heat-transfer components have been reviewed in an effort to reduce complexity and cost wherever possible. Instrumentation requirements have been reviewed and a comprehensive instrumentation list has been prepared. Controls requirements for loop operation have been studied, with decisions made in conjunction with test objectives.

Loop Design

Loop layout has been completed, with emphasis on stress and accessibility considerations. Design information on facility components has been obtained from prospective vendors and integrated into the design layout. Detailing of the primary loop has been carried to near completion, including the supporting structure. Figure 61 shows an elevation of the primary sodium loop showing constant-load hangers and supporting members. Final detailing of the secondary loop with the support structure has been deferred pending completion of test-component layout drawings to be completed under Task 2.2.5.3. An elevation of the potassium loop is shown in Figure 62. A plan view of the loop (Figure 63) shows the arrangement of the entire loop in the building projected to house the loop. Electrical design and control system layouts have been initiated and are scheduled for completion during the next report period.



HEAT TRANSFER LOOP - SODIUM PIPING ELEVATION

FIGURE 61

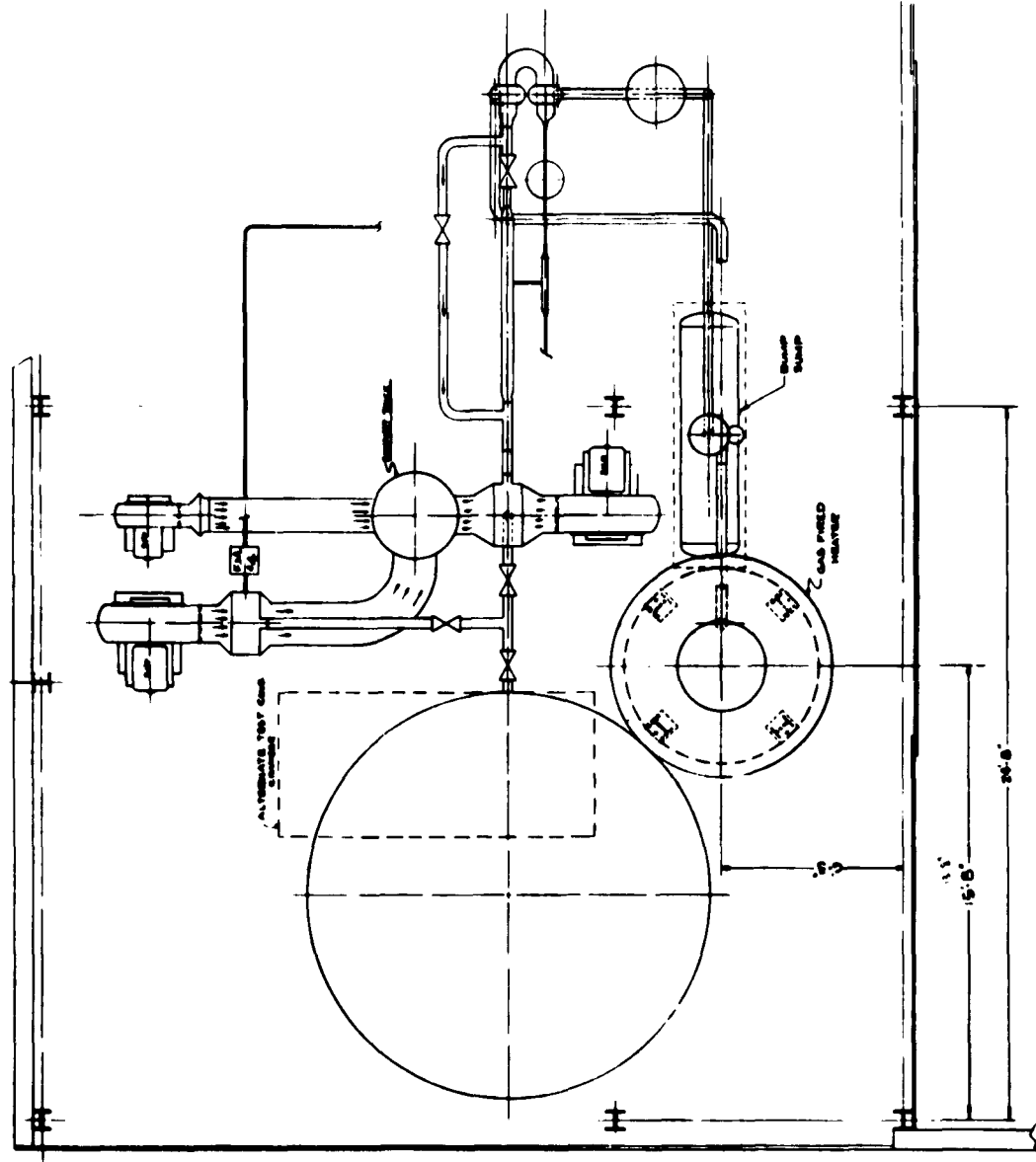
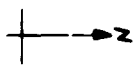


FIGURE 63
HEAT TRANSFER LOOP - PLAN VIEW





Stress Analysis

The piping flexibility analysis of the primary and secondary loops has been completed, and stress levels and reactions appear to be reasonable. Points of stress approaching or exceeding allowable tolerances based on stress-rupture life criteria can be relieved by cold-springing techniques or relatively minor design changes in all cases. Based upon the results of this analysis, detailed design of loop plumbing is being carried out. Detail thermal stress analysis of components subject to severe thermal shock or temperature transients is being carried out. Computer techniques developed for the above-mentioned analysis are readily adaptable to similar liquid-metal loops. The programming of this analysis will also facilitate stress evaluation of future loop modifications with minimum cost expenditure.

Controls

The following is a summary of operating controls for facility components.

The turbine simulator consists of a heat exchanger combined with a throttling valve to simulate energy extraction of the turbine. The heat exchanger effects a constant pressure change in enthalpy from 1600°F saturated vapor condition to 1600°F and 83.8 percent quality. The throttling valve in turn provides a constant enthalpy reduction in temperature and pressure to the desired condenser inlet conditions of 1420°F and 85 percent quality.



Control of the heat-exchanger performance by a self-regulating control device is impractical in that the potassium experiences no measurable change in temperature or pressure in passing through the unit. Assuming that potassium inlet conditions may be maintained at some predetermined quality, the air blower must be programmed to remove a definite quantity of heat corresponding to the desired change in enthalpy. Air-side temperature is the most readily measurable quantity and is considered the most logical control reference. Further, the heat exchanger has a performance characteristic based on inlet air temperature and mass flow, making inlet air temperature a logical choice. Blower air flow may be held constant, controlling inlet temperature by means of recirculating exit air.

Throttling to the 85 percent quality condition will be accomplished by means of a modulating throttling valve sensing the condenser inlet temperature.

The work horse condenser must operate in parallel with the test radiator panel and have the capability of condensing the full potassium mass flow of 1.0 pound per second. The normal flow split for radiator test will provide 0.28 pound per second to the radiator, and the remainder to the workhorse unit. The workhorse condenser with associated valving will be capable of operating within a pressure drop range of 1.0 to 6.0 psi to gain flexibility and accommodate future changes in SPUR radiator design.



Blower air flow and, hence, condensing rate will be controlled by condenser outlet temperature. The controller will take a temperature signal from the potassium discharge and actuate a damper in the air duct regulating air flow to the desired value.

The air blast subcooler reduces the temperature level for the recuperator test and provides positive control of the EM pump inlet temperature. Control of the heat-rejection rate will be provided by a device similar to that described for the condenser.

Pumps

Pumps on both the sodium and the potassium loops will use EMF output from the associated EM flowmeter as a control point. The sodium pump will be controlled by varying pump speed through a variable-frequency electric motor drive. The potassium loop EM pump is controlled from zero to maximum flow by a variable auto-transformer. The sodium mechanical pump speed will be variable from 3600 rpm at 60 cps power to 60 rpm at 10 cps power.

Sodium Heater

Positive control of the gas-fired heater will be provided by a proportional recording controller device sensing and controlling the heater outlet sodium temperature.



Instrumentation

A detailed instrumentation list has been prepared including range, accuracy, instrument environment, and data-collection requirements. It is anticipated that a digital voltmeter tape recorder system will be used for all data acquisition. This data logger system is capable of recording up to 200 data points every 67 seconds.

Studies have been initiated to improve measuring accuracy at the higher temperature levels. Techniques such as argon efflux pressure measurement with potential accuracies of 1/4 percent of full scale are under investigation. Critical temperature measurements will be made with platinum - platinum rhodium thermocouples with provisions for frequent removal and calibration to maintain the desired accuracies of $\pm 5^{\circ}\text{F}$.

Layout of the data acquisition system and control panels has been initiated.



H. Controls Development

1. Steady State Controls Analysis, Task 2.2.6.1

The off-design characteristics of the power-conversion system were secured and the various necessary coefficients were evaluated for full power and the 10 percent power level. The boiler analysis has reduced these characteristics such that the heat rejection and turbine inlet pressure may be derived only as functions of the primary inlet temperature and the secondary inlet flow.

The linearized power conversion system representation was simulated on the analog computer. The purpose of the evaluation of the dynamic characteristics on the analog computer was to verify the hand analysis and to establish accurate simulation as a basis for other studies.

The dynamic characteristics of each major component of the power-conversion system were determined by observing the transient response of the various system parameters to preselected disturbances for the same conditions considered in the hand analysis. The form and numerical identifying characteristics of the recorded transient response were compared with the transfer functions of the hand analysis.



Using the same procedure, an evaluation of the over-all system characteristics, plus other appropriate transfer functions, was made to synthesize the control function for the throttling valve control. This evaluation was made on the basis of alternator frequency specifications and assumed magnitude and frequency characteristics of external disturbances.

The system characteristics for 10 percent power plus the final evaluation of the system with the throttling valve control will be completed in the next quarter.

2. System Start-Up Analysis, Task 2.2.6.2

The preceding Quarterly Progress Report subdivided the start-up sequence study into three phases:

- (a) 400°F to initial boiling
- (b) Boiling to self-sustaining
- (c) Self-sustaining to 10 percent or idle power

The first phase was essentially completed in the previous quarter. The remaining two phases were completed during this quarter.



The other technique evaluated and subsequently determined to be the preferred technique involved preheating both primary and secondary loop fluids. At some scheduled temperature the secondary loop flow would be reduced to create an 80° to 100°F temperature difference between the boiler primary inlet and secondary outlet, while the back pressure on the turbine is reduced by resetting the accumulator reference. This change in conditions would cause the secondary fluid to boil off at essentially 100 percent quality. Turbine flow and accumulator pressure reference would then follow an acceleration schedule compatible with reactor discharge temperature, primary boiler temperature drop, and temperature difference between the boiler primary inlet and secondary outlet temperatures.

The graphical integration program for the third phase to 10 percent power level was completed for shielding removal rates of 1/22, 1/11, 33 percent and 50 percent of total shielding on the radiator removed essentially instantaneously. Shielding removal was based upon holding the radiator discharge temperature at 700°F, the maximum allowable pump inlet temperature, and at 290°F at the radiator outlet when stabilized at 10 percent power.



Two techniques to negotiate the transition from liquid to vapor were evaluated. The evaluation revealed that the bypass turbine technique would impose excessive weight and space considerations due to the additional hardware required. The additional valving would add unnecessary complexity to the system. Shock to the turbine wheel was found to be a serious disadvantage.

The system start-up analysis has been completed.

3. Controls Experiment, Task 2.2.6.3

During the past quarter, tests were conducted on the water loop to supplement the analytical work being conducted on SPUR start-up. The tests consisted of simulating an all-liquid startup technique similar to the start-up proposed for SPUR. Tests verified the predicted liquid inventory change during transition between all liquid and boiling. Also, a means of establishing a smooth transition from zero-quality steam to 100-percent-quality steam was tested, which correlated with the scheme proposed in the analytical phase of the start-up study.

1
A
B
C
D
E
F
G
H
I
J
K
L
M
N
O
P
Q
R
S
T
U
V
W
X
Y
Z





I. Reactor Loop

1. Reactor Loop Pump Bearing Test and Loop Simulation, Task 2.3.1.2 and Task 2.3.1.3

During the previous report period the pump was modified to prevent lithium from escaping through the gas seal during operation. It was operated at 1000 rpm; whereupon, the shaft seized and could not be rotated. The pump was removed from the loop, disassembled, and cleaned of lithium deposits. The shaft was then reinstalled, the impeller housing plate welded in place, and the pump made ready for welding into the loop.

Pump Installation

The pump was welded into the loop. A different drive motor was procured. The new motor was rated at 10 hp, and it was estimated it would develop enough torque to continuously shear a band of frozen lithium should a frozen seal develop in the cooling jacket region.

Pump and Loop Operation

The loop was heated and charged with lithium that had been purified by hot trapping with zirconium and titanium. The lithium was forced into the loop until thermocouples, installed on the pump housing at the bearing, indicated that lithium had reached that point.



During the time required to install the drive motor and clutch, a sudden and large increase in the chamber pressure occurred. The chamber was then filled with argon to prevent oxidation of the loop. No leak could be found in the chamber so an attempt was made to re-evacuate the chamber. When the diffusion pump gate valve was opened, the chamber pressure quickly returned to the normal operating level. Since everything else appeared normal, it was concluded that the vacuum instrumentation had malfunctioned.

The motor installation was completed and the motor started. It ran about 5 to 10 seconds and stopped, tripping the circuit breaker to the motor power. The shaft had seized and could not be turned by hand. The drive motor was then removed.

Upon opening the chamber it was found that a rupture had occurred in the loop and a fairly large quantity of lithium had been released at the exit of the thermionic converter (see Figure 64). The lithium had permeated the thermal insulation and dissolved some of the ceramic insulators on the trace heater leads in this area. Deposition of some reaction products on the foil insulation in unaffected areas can also be seen in the figure.



FIGURE 64
EXTERNAL APPEARANCE OF LOOP RUPTURE

NP-1590

SY-5396-R3
Page 161



The leak and the accompanying reactions with the insulation had apparently been the cause of the rise in chamber pressure reported above. The pump shaft seizure thus appeared to have been caused by running the bearing dry when the upper portion of the loop was drained by the leak.

It was decided, at this point, to analyze the loop and pump to determine the cause of failure and the condition of the bearing and journal. The amount of funds remaining in the program were not sufficient to consider re-running the pump.

Loop and Pump Analysis

The loop rupture was found to be a transverse crack in a 90° bend at the outlet of the thermionic unit (see Figure 65).

The pump was removed from the loop, washed out with water, and the shaft was pressed out. The journal had suffered fairly extensive visible damage (Figure 66). Part of the tungsten carbide coating was removed around the top of the journal and there were a number of fine cracks in the coating that remained on the journal. There was also a smeared, metallic coating over portions of the tungsten carbide coating remaining on the shaft. This was probably metal removed from the bearing. Figure 67 is a reference photograph of the bearing immediately following fabrication.

THE BARRITT CORPORATION
AirResearch Manufacturing Division
Phoenix, Arizona

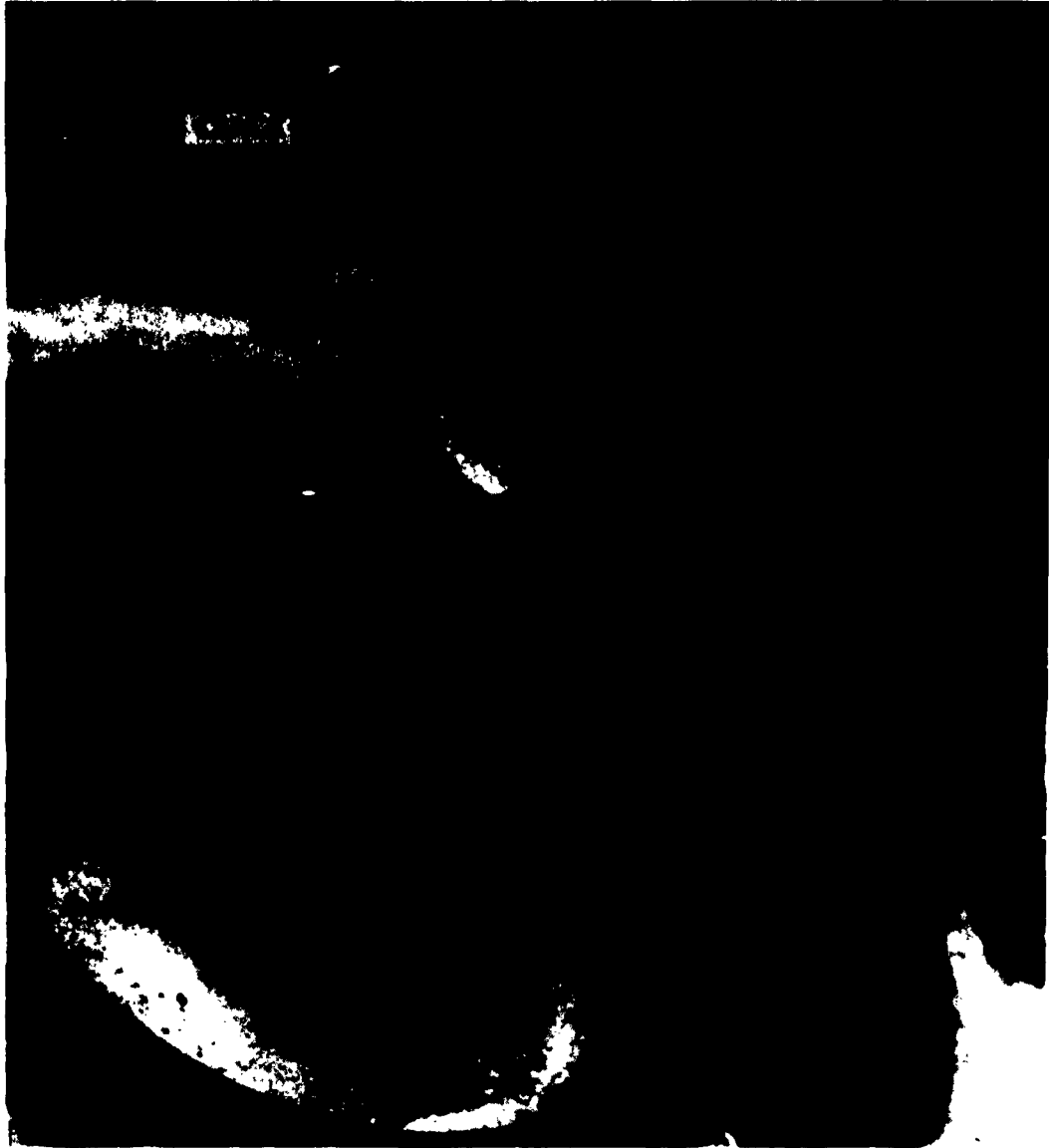


FIGURE 65

LOOP RUPTURE - OUTLET OF THERMIONIC CONVERTER

SY-5396-R3
Page 163

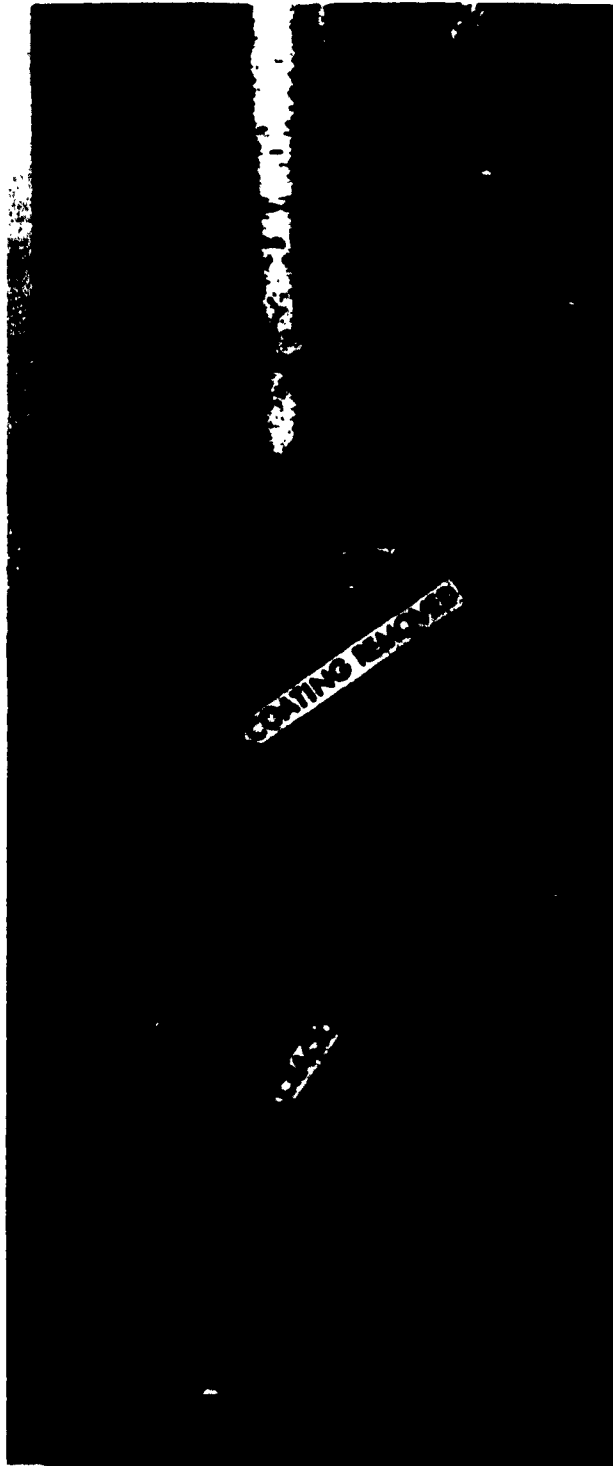


FIGURE 66
JOURNAL BEARING - POST TEST

MP-1001

SY-5396-R3
Page 164

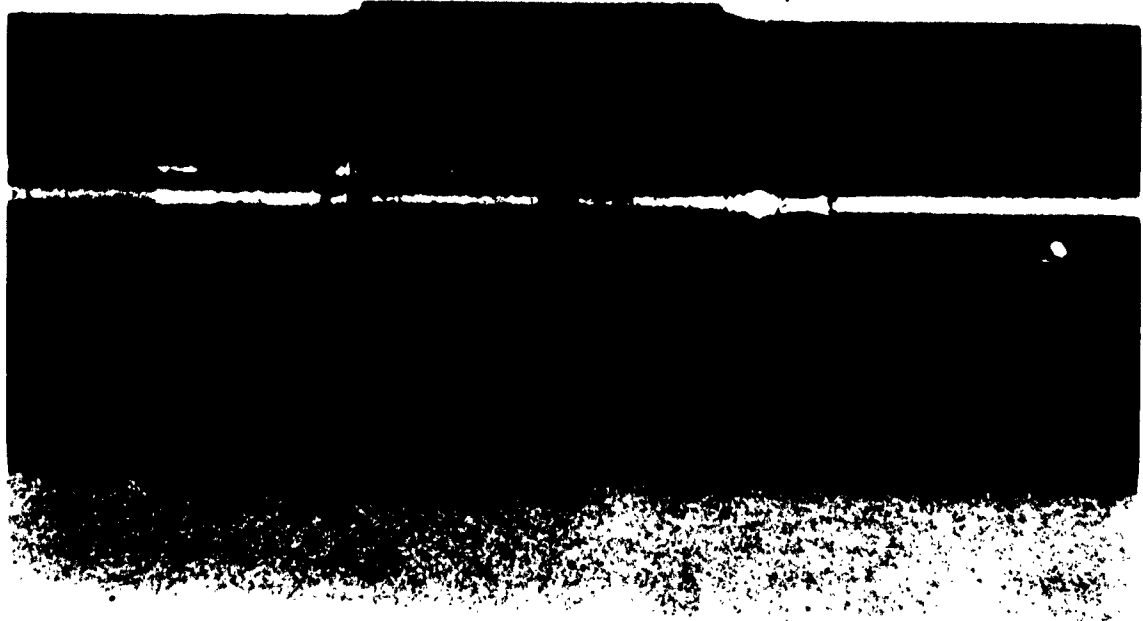


FIGURE 67
JOURNAL BEARING AS FABRICATED



When the pump housing was cut open, the bearing was found to be displaced axially upward with respect to the journal (see Figure 68). This was caused by two things: (1) the bearing had not been pressed all the way into the housing at assembly, (2) there appeared to have been an error made in either design or fabrication in locating the two bearing members with respect to each other. This is the reason that all of the wear marks on the journal are confined to its upper half.

Other immediately apparent items of interest included:

- (a) The welds joining the loop and pump at the inlet and outlet of the pump were extremely brittle and broke in handling.
- (b) A crack had developed in the weld zone at the point where the lower shaft housing joins onto the expansion tank of the pump (see Figure 69). It is believed that this fracture occurred when the shaft was pressed out of the pump.

A number of chemical and metallurgical tests were then specified. As of the end of this report period these tests were not complete and final analysis will await compilation of all data.

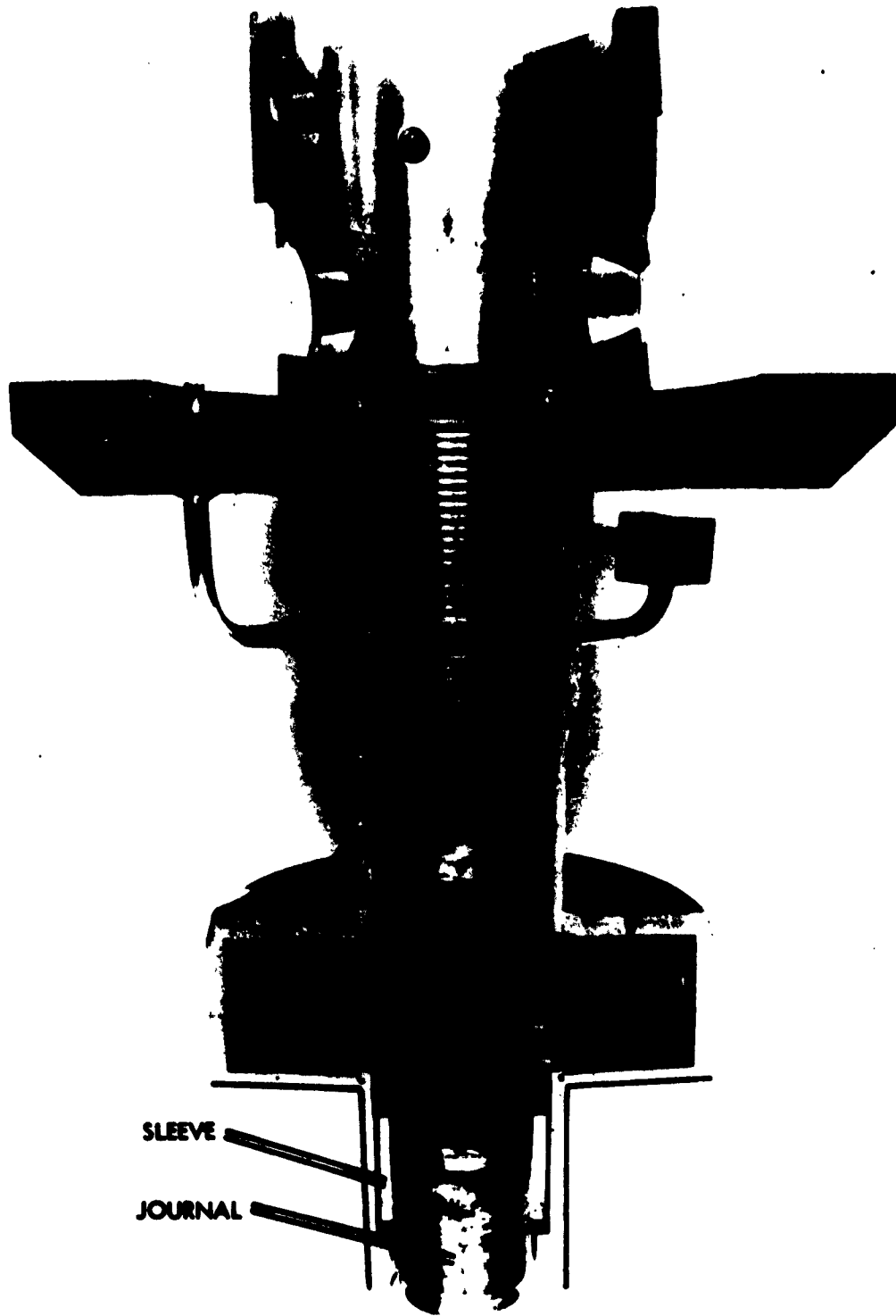


FIGURE 68

UPPER PUMP SECTION - POST TEST

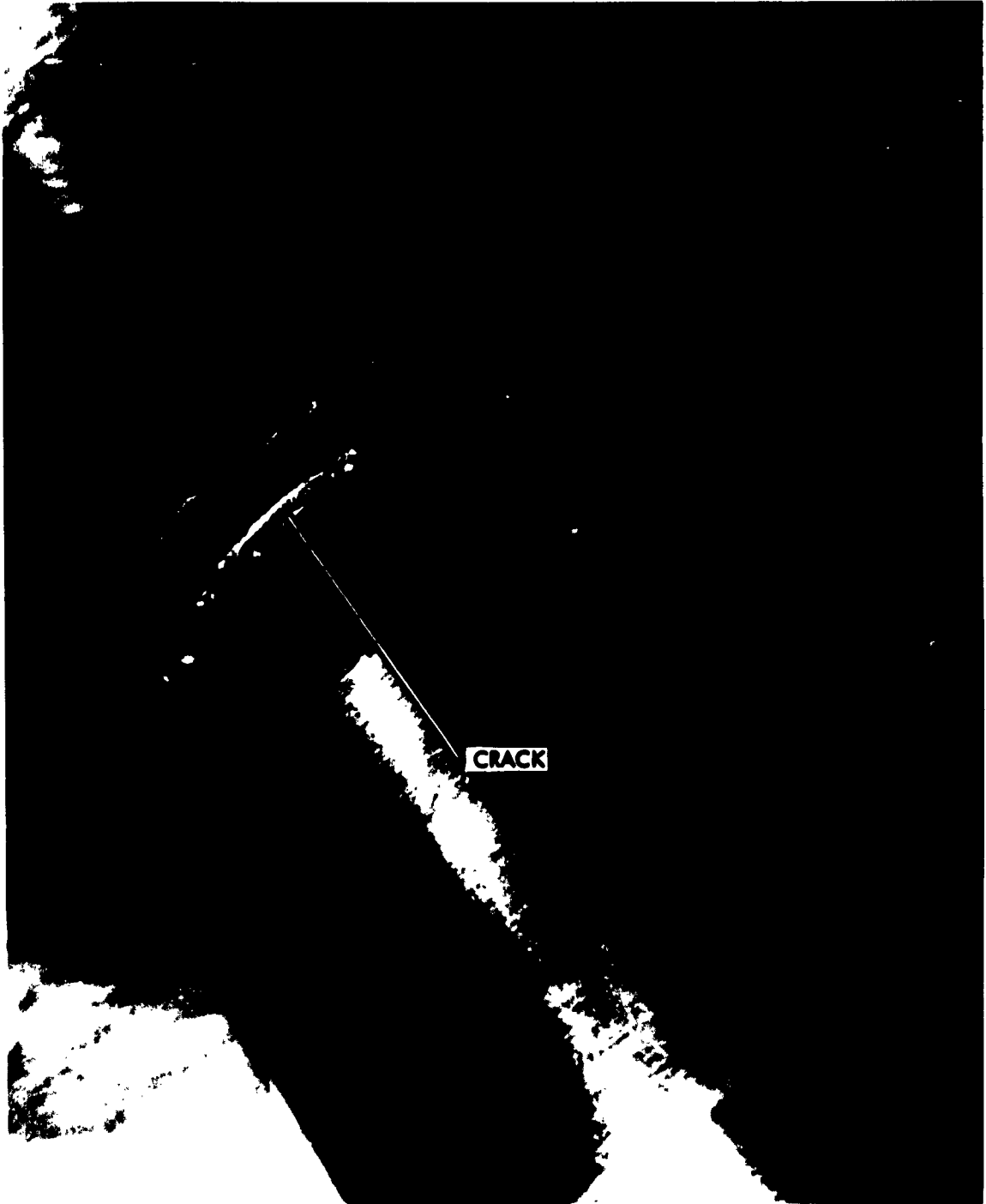


FIGURE 69
CRACKS IN WELD ZONE - LOWER
HOUSING TO EXPANSION TANK

SY-5396-R3
Page 168



2. Reactor Loop Controls, Task 2.3.2

Technical work on this task was essentially complete at the end of the report period. The dynamic behavior of the SPUR reactor loop was investigated for both normal operation and start-up. After completing these studies on the SPUR reactor loop, the analog simulator was modified for normal operation studies on the SNAP-50 reactor loop.

Control System Optimization

The control schemes for the SPUR reactor loop were developed as a part of the SPUR - Phase I effort under Contract AF33(616)-7379. These control schemes were reviewed and optimized early in the past quarter in preparation for a dynamic performance analysis of the SPUR reactor loop. Both linear and nonlinear analysis techniques were used in this effort.

The three different signals are available for providing the measure of thermal power across the boiler. These are neutron flux level, lithium temperature drop across the boiler (assuming constant flow), and a demand signal originating from the control programmer of the secondary loop. Control functions representing those three signal sources were investigated using both linearized techniques and analog simulation.



The third control function, i.e., the one that uses an external signal to generate the setpoint for reactor outlet temperature, was selected for SPUR for the following reasons.

- (1) The selected system is inherently stable whereas the other two require compensating networks.
- (2) The primary system temperatures are least sensitive to disturbances in the secondary loop.
- (3) An electrical signal indicating power demand is available from the controls of the power conversion system. Hence, a temperature sensor at the boiler outlet which is in addition to that at the boiler inlet, or a high level neutron flux detector will not be required.
- (4) The reliability potential of the power level detector in the selected system is greater than that in the other two.

The only disadvantage of the selected control function is that it increases the dependence of the primary loop on performance of the secondary loop. In the other two control functions, the only coupling between the primary and secondary loops is through the boiler.



Performance Analysis

The dynamic performance of the reactor loop was determined by an analysis of the analog computer response under various operating conditions. Detailed results will be presented in a topical report. These include the step response of the SPUR and SNAP-50 reactor loops, start-up modes for the SPUR reactor loop, and a Bode diagram for the SPUR reactor loop as obtained from the analog computer.

Start-Up

The programming of the start-up equations was completed during this report period.

Start-up of the SPUR reactor loop can be divided into the three phases of attainment of criticality, transition of the neutron level from source level to warm-up power level, and warm-up of the power plant to achieve the self-sustaining conditions. Since the first phase, attainment of criticality, involves only the monotonic addition of reactivity, its simulation on the computer produces no interesting results. Hence, in start-up studies, the initial conditions were a critical reactor with neutron level set at about 9 decades below full power. Two start-up schemes for the SPUR reactor



loop were examined. In both cases the objective was to warm-up the entire power plant at a rate near $1^{\circ}\text{F}/\text{sec}$. while providing for the thermal power requirements of the radiator, using a relation for boiler power vs time for a warm-up rate of $1^{\circ}\text{F}/\text{sec}$. derived from the conversion loop studies.

The first scheme, based on a three control mode system, uses reactor period control, rate-of-change of temperature control, and temperature control. The second start-up scheme involves use of only the period control and temperature control circuits. Control of the rate-of-change of temperature is achieved by setting appropriate limits on shim rod speed. This is the preferred start-up scheme since development of a suitable sensor for determining the rate-of-change temperature with a wide dynamic range is extremely difficult. The penalty in inadequate control of the rate-of-change of temperature does not appear to be a serious problem.

Analysis of the two schemes has been accomplished and both appear suitable. Consequently, the second, simpler scheme has been tentatively selected.



Bode Diagram for SPUR Reactor Loop

A Bode diagram was generated for the SPUR reactor loop in order to determine its sensitivity to disturbances originating in the secondary loop. The objective was to determine the amplitude of sine wave disturbances as a function of the frequency which results in intolerable temperature transients in the reactor loop. Since acceptable temperature transients for the reactor loop have not been established, the results are presented in parametric form. The disturbance amplitude is plotted as a function of frequency in Figure 70, for 10°, 30°, and 50°F transients in reactor coolant outlet temperature. Data for these curves were obtained by oscillating the boiler output power on the analog simulator to obtain the required amplitude response in reactor outlet temperature. It is evident from this Bode diagram that the reactor loop is most sensitive to disturbance frequencies near 0.01 cycles per second. At this frequency 30°F transients in reactor loop temperatures are produced by boiler power oscillations which have amplitudes near 16 percent of full power. Therefore, the general conclusion of this study is that the reactor loop is rather insensitive to disturbances occurring in the secondary loop.

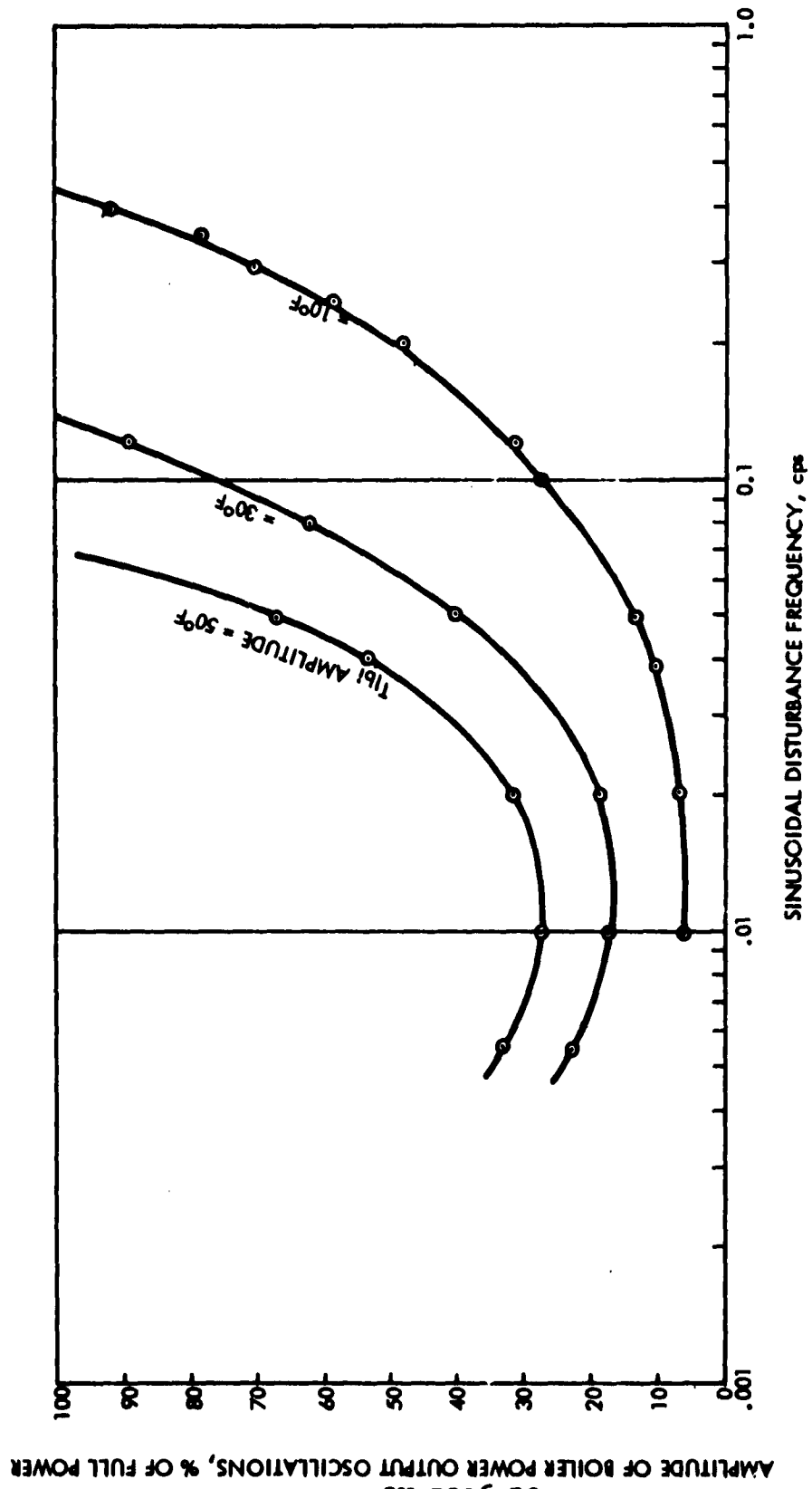


FIGURE 70
 TEMPERATURE PERTURBATIONS IN PRIMARY LOOP DUE TO
 POWER OSCILLATIONS ACROSS BOILER



3. Properties of Reactor Clad and Structural Materials,
Task 2.3.3

The objective of this task is to obtain creep data on Cb + 1w/o Zr (and other suitable advanced alloys) in contact with lithium at SPUR temperatures. Generally, creep strength of metals is determined by loading a machined specimen in simple tension at a desired stress and temperature. In the present effort, it is planned to obtain creep data using cylindrical capsules filled with pressurized Li at the desired temperature. Proper sizing of the capsule wall and selection of the pressure will result in a selected biaxial stress in the wall. It was shown in the previous Quarterly Progress Report, that the capsule will not significantly elongate (or shorten) but instead, will increase in diameter as creep occurs. Thus, creep data can be obtained by measuring the capsule diameter at selected time intervals.

During the present report period the detailed operation of the test apparatus was given a further study. It was concluded that a modified design would be easier to operate. Therefore, the design of the experimental apparatus was changed.

It will be necessary to conduct a short preliminary run to obtain experimental primary creep data on the particular lot of material on which data are desired.



Two stresses, bracketing the stress range that can be investigated in a single capsule, appear to be adequate for such a preliminary run. It will be necessary to start the preliminary run at a pressure below that estimated to produce the desired creep rate to allow for the possibility of a high initial creep rate and a large error in the estimated rupture strength. The test will then be stopped after the first hour or two and the strains measured. These can be compared with the estimated strains and a suitable adjustment of the pressure made.

A second step for another adjustment may also be required. Once the creep rate is in the range desired, the test can be allowed to run for a few tens of hours with 2 or 3 stops to obtain strain vs time data. These data should then be suitable for designing the final run so that it can be run with no pressure adjustment.

Apparatus Design

The conceptual furnace design described in the previous quarterly report was changed when detailed design and close study of filling procedures were undertaken. It was found that the filling procedures would be unduly complex. The advantages of the original design appeared to be outweighed by the



disadvantages when this complexity was added to the operation complexity. The revised design allows much simpler procedures to be used and the gain in reliability is believed to more than compensate for the disadvantages, as outlined below. The major difference from the previous design is that the capsule will hang down from the top rather than be supported from the bottom.

The main advantage of the bottom support was that the lithium drained from the capsule at each shutdown. Therefore, there was no change of capsule deformation due to melting of the Li in a closed volume. Also, the amount of Li loaded did not have to be accurate nor did Li contact the gas line valves. Offsetting these advantages were the following.

More cumbersome and unreliable loading procedure.

Longer furnace.

More complex capsule assembly, increasing probability of a leak.

More complex capsule support structure.

More complex and hazardous shutdown and measuring procedure.



To overcome disadvantages of the top support method, careful heating from the top of the furnace will be required so that the Li melts from the top surface down. Also, a loading procedure was derived to fill the capsules with Li within the desired limits. It is necessary that Li cover all gauge sections, but that it not extend into the fill tube where a large temperature gradient exists. If Li did extend into the gradient, thermal convection could occur since the top is cooler. This could lead to significant heat loss and a poor temperature uniformity in the capsule zone.

The apparatus is divided into assemblies to facilitate discussion. These are:

Capsule assembly - It includes the capsule, the gas lines, the 3 inch top flange, the liquid metal valves, and the thermocouples.

Furnace tube assembly - It includes the furnace tube, top tee, all parts internal to the furnace tube, and the capsule assembly.

Furnace assembly - It includes the furnace, furnace support, and furnace tube assembly.

Inert gas pressurizing system.

Purification system.

Lithium purification and filling system.

Vacuum system



The capsule assembly is shown in Figure 71 included with the furnace tube assembly. It consists of the capsules, the gas tubes, the liquid metal valves, the end flange, the Conax gland, and the thermocouples. The transition from refractory alloy to stainless steel is made with the Swagelok near the end of the furnace tube.

The assembly is designed to be lifted as a unit (including the top insulating plug) from the furnace tube when a strain measurement is made.

The capsule consists of a body and two end plugs. The body is machined from tubing and the end plugs from barstock of the same material. Furnace size will allow only 4 capsules having maximum dimensions of 7/8 inch diameter x 11 inches long.

Eleven inch long capsules with 5 one-inch long gauge lengths machined into each were originally planned. However, an 11 inch capsule proved to be quite expensive to machine in one piece to the tolerances desired. Therefore, capsule bodies will be made from rough machined body blanks, each of which contains two gauge lengths. Completed capsules will consist either of a single 2-stress body or a 4-stress body made by welding two 2-stress body blanks together.



Since tubing usually contains residual stresses from the straightening operation, a capsule machined to such thin walls would be expected to warp when heated. To minimize this, the following set of operations is planned.

- (1) Rough machine all parts.
- (2) Inspect and radiograph for hidden flaws.
- (3) Heat treat to relieve stresses or obtain some desired metallurgical structure.
- (4) Final machine all parts.
- (5) Inspect and measure final dimensions.
- (6) Assemble and weld.
- (7) Inspect and radiograph.

Warpage is expected during the welding operation; however, this should lead only to eccentricity of the capsule. The wall thickness will remain the same and once the capsule is stressed at temperature, the residual stresses will soon be relieved.

Final proof test of the capsules will be a helium leak check while at temperature in the furnace. This will come at the conclusion of a bake-out period and will be done by bleeding He into the capsule to a pressure of a few mm Hg and opening the leak detector to the furnace tube atmosphere.

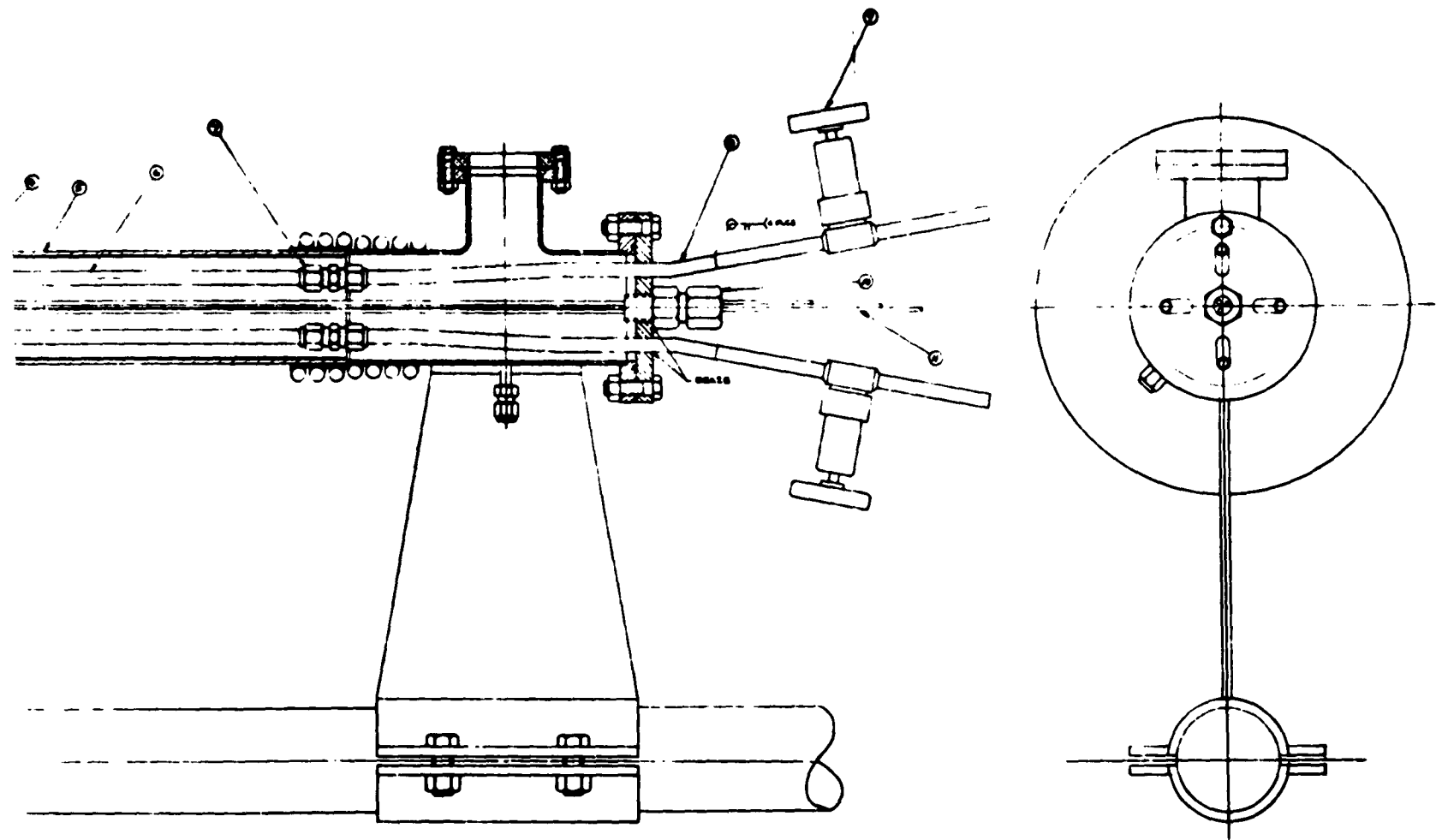


FIGURE 71. FURNACE TUBE ASSEMBLY

2



Details on the exact dimensions and design of the capsules will be included in a subsequent report.

Procurement and Fabrication

(a) Capsule Assembly

A 10-inch length of B-66 barstock will be supplied by Westinghouse. The Cb + 1 w/o Zr tubing is a month behind schedule but is expected to be received in January. The tantalum sheathed, platinum, platinum-rhodium thermocouples are scheduled for delivery at the end of January. These are the pacing items.

Other materials are on hand or will be received in January. The stainless steel capsule will be fabricated in January. Fabrication of the refractory metal capsules will start in January if the Cb + 1 w/o Zr tubing is received.

(b) Furnace Tube Assembly

The furnace tube is being attached to the adapter by Coors. Other parts are being fabricated. Final assembly and leak testing is expected in January without the thermocouples.



(c) Furnace Assembly

The facility has been completed with water and power installed. The furnace was received. All AGN furnished equipment (controller, stand, powerstats, regulators) was received except the Heise gauges. These are expected late in January. Installation of the furnace is scheduled to start the second week in January.

(d) Argon System

The purification system is being fabricated and the principal tanks have been completed. Most of the plumbing parts have been received. Final assembly will proceed concurrently with the furnace installation.

(e) Lithium Filling System

The purification system was cleaned and is being re-assembled. All materials are on hand

(f) Vacuum System

The 2 inch vacuum system, furnished by AGN, was completed and is being checked out by the manufacturer.